UNIVERSITEIT GENT

FACULTEIT **INGENIEURSWETENSCHAPPEN EN ARCHITECTUUR**

Vakgroep Chemische Proceskunde & Technische Chemie
Laboratorium voor Chemische Technologie
Directeur: Prof. Dr. Ir. Guy B. Marin

VERTROUWELIJK TOT EN MET 31/ 12 /9999
BELANGRIJK

Oligomerization of Ethylene to Liquid Fuels and Chemicals

Julie Timmerman

Promotor: prof. dr. ir. Joris Thybaut
Begeleider: Kenneth Toch

Masterproef ingediend tot het behalen van de academische graad van
Master in de ingenieurswetenschappen: chemische technologie

Vakgroep Chemische Proceskunde en Technische Chemie
Voorzitter: prof. dr. ir. Guy Marin
Faculteit Ingenieurswetenschappen en Architectuur
Academiejaar 2012-2013

UNIVERSITEIT GENT

UNIVERSITEIT GENT

FACULTEIT **INGENIEURSWETENSCHAPPEN EN ARCHITECTUUR**

Vakgroep Chemische Proceskunde en Technische Chemie
Laboratorium voor Chemische Technologie
Directeur: Prof. Dr. Ir. Guy B. Marin

Laboratorium voor Chemische Technologie

Verklaring in verband met de toegankelijkheid van de scriptie

Ondergetekende, Julie Timmerman

afgestudeerd aan de UGent in het academiejaar 2012-2013 en auteur van de scriptie met als titel: Oligomerization of Ethylene to Liquid Fuels and Chemicals

De auteur(s) geeft(geven) de toelating deze masterproef voor consultatie beschikbaar te stellen en delen van de masterproef te kopiëren voor persoonlijk gebruik.
Elk ander gebruik valt onder de beperkingen van het auteursrecht, in het bijzonder met betrekking tot de verplichting de bron uitdrukkelijk te vermelden bij het aanhalen van resultaten uit deze masterproef.

Dankwoord

Naarmate het einde van mijn studies en deze thesis nadert, wil ik nog even de tijd nemen iedereen te bedanken die heeft bijgedragen tot het tot stand komen van deze thesis, en/of mij gesteund heeft de afgelopen jaren gedurende mijn opleiding.

Mijn eerste woord van dank gaat uiteraard naar prof. dr. ir. J. W. Thybaut voor de begeleiding doorheen dit thesis jaar. Niet alleen kon ik bij u terecht om raad voor mijn thesis, ook daarbuiten kon ik steeds op uw steun rekenen. Zo denk ik maar aan mijn stage bij Johnson Matthey en de MaChT-activiteiten waar we steeds op u hulp konden rekenen. Daarnaast wil ik uiteraard prof. dr. ir. G. B. Marin bedanken voor het mogelijk maken van deze thesis, dit in een boeiende onderzoeksomgeving.

Een grote 'bedankt' moet zeker ook gegeven worden aan mijn begeleider Kenneth Toch. Je stond steeds voor me klaar als ik er weer eens niet uitgeraakte. Dit dan zowel op theoretisch vlak, voor de opstelling van mijn model, als op praktisch vlak, wanneer de High-Throughput me weer al eens in de steek liet. De tijd die je gespendeerd hebt aan het controleren van mijn model of het lezen van mijn thesis werd ten zeerste geapprecieerd. Bedankt hiervoor!

Verder wil ik ook mijn collega's van 914 bedanken. Mijn toekomstige collega Pieter, tevens meest optimistische persoonlijkheid uit mijn omgeving, kritische Thomas en de immer lachende begeleider Bart maakten het aangenaam werken in 914. Uiteraard ook een dankjewel voor mijn medestudenten van de richting Chemische technologie en de mede bestuursleden van MaChT. Onze activiteiten waren steeds een schot in de roos en een ideale ontspanning. Pieter, ook de gezellige fietstochten naar Zwijnaarde mogen zeker niet vergeten worden. Deze zorgden er niet alleen voor dat ik steeds op tijd in Zwijnaarde was, maar dat ik ook vol goede moed aan mijn dag kon beginnen.

Mijn thesisjaar en tevens mijn volledige studiejaren zouden me veel zwaarder gevallen zijn mocht ik de steun niet gehad hebben van mijn ouders, broer en zus. Jullie stonden steeds klaar om mij te verwennen en de nodige oppeppende raad te geven waardoor ik er weer met frisse moed kon invliegen. Jullie steun was zeker van onschatbare waarde. Joke, de laatste drie jaar *'thuis'* komen op het gezelligste appartement van Gent was steeds een leuk vooruitzicht na een lange dag in die grauwe universiteitsgebouwen.

Als laatste gaat mijn dankwoord uit naar mijn fantastische vriend!! Thomas, ik wil je bedanken voor alle steun en je oneindig geduld. Ook al had je het zelf heel druk met je thesis, toch wist je steeds nog tijd te maken voor mij en voor de ideale ontspanning te zorgen. Ik kijk er naar uit samen met jou aan het échte leven te beginnen.

Oligomerization of ethylene to liquid fuels and chemicals

Julie Timmerman*

Coach: ir. Kenneth Toch

Promoter: Prof. dr. ir. J.W. Thybaut

Abstract: **The oligomerization of ethylene over a bifunctional heterogeneous catalyst was experimentally investigated. The main focus was to describe the acid catalyzed reaction steps adequately. The kinetic model for oligomerization of ethylene, consisting of the metal ion based reaction mechanism, has been expanded with carbenium involved reactions, i.e., (de)-protonation, β-scission, alkylation, 1,2-alkyl shift and PCP-branching. By applying the principles of single event microkinetic modeling, together with thermodynamic consistency, the number of kinetic parameters was successfully reduced. Regression and simulation were performed with the model. This allowed to obtain significant values for both kinetic and catalytic descriptors. The model was capable of describing most effects of variations of the reactions conditions.**

Keywords: Ethylene oligomerization, bifunctional catalyst, SEMK model, β-scission

I. Introduction

The oligomerization of ethylene is a conversion process in which higher olefins and chemicals are produced. These compounds are considered to be valuable products for detergents, fuels, plasticizers, etc. Due to the increasing global demand for fuels and chemicals and the increment of the corresponding prices, this process is becoming more viable. Industrially, this process is already implemented using homogeneous catalysis. To improve the product flexibility and environmental friendliness, the use of heterogeneous catalysts is investigated. These heterogeneous catalysts are bifunctional, i.e., containing two type of active sites, i.e., transition metal ions, e.g., nickel-ions, deposited on an acid carrier. Zeolites are best suited for this application since they provide an acid framework and a prospective for product distribution tuning via the shape selectivity effect due to their specific geometry.

Protonation of ethylene leads to a primary carbenium ion, which is not stable at the relative mild reaction conditions applied for oligomerization. Therefore, dimerization of ethylene takes place on the metal ion sites. It is assumed that oligomerization on these sites occurs through an insertion-termination mechanism analogous to homogeneous catalysis. Further oligomerization of the butenes produced takes place on the acid sites through a carbenium ion mechanism.

The importance of these acid sites is their major influence on the product distribution. Oligomerization of ethylene on the metal ion sites solely leads to the production of even numbered linear α-olefins. However, acid catalysis can disrupt this product composition via additional oligomerization, i.e., so-called alkylation, isomerization reactions and cracking. This leads to a product mixture which can be more easily used as a transport fuel. In previous work, the metal ion kinetics were already described extensively.

In this work, the acid catalyzed reactions are studied. By performing an experimental study on a Ni-β catalyst, known to be an active acidic catalyst, the kinetic model is expanded with the acid reactions, i.e., β-scission, alkylation, 1,2-alkyl shift and PCP-branching. The kinetic model is then regressed to the experimental dataset obtained to determine the kinetic and catalytic descriptors.

II. Procedures

A. Experimental work

An experimental study was performed on a 4.89wt%Ni-β catalyst in a plug flow reactor, i.e., the HTK-1. The range of reaction conditions is given in Table 1. For this range of conditions it was verified that intrinsic kinetics are observed. In order to eliminate condensation of the reaction mixture in the set-up to facilitate the experimentation, dilution with nitrogen was necessary.

Table 1: Experimental reaction conditions

Reaction condition	Experimental range
Temperature [K]	443-503
Partial pressure C_2H_4 [MPa]	0.17-0.40
Space time [kg_{cat} s mol^{-1}]	4.0-12.0
Nitrogen dilution [mol%]	88.0

XRD studies showed that NiO clusters were present on the catalyst, in contrast with the reference catalyst tested in previous work, i.e., a 1.80wt%Ni-SiO_2-Al_2O_3. The properties of the Ni-β and reference catalyst is given in Table 2.

Table 2: Catalysts properties

	4.89wt%Ni-β	**1.80wt%Ni-SiO_2-Al_2O_3**
Nickel content [wt%]	4.89	1.80
BET-surface area [m^2 g^{-1}]	458.32	199.11
Acid site conc. [mmol g^{-1}]	0.634 (strong)	0.79 (weak)

B. Modeling

Since experiments were performed in a plug flow reactor, the reactor is modeled using a set of differential equations:

$$\frac{dF_i}{dW} = R_i \qquad (1)$$

*E-mail:Julie.Timmerman@UGent.be

with F_i [mol s^{-1}] the molar flow rate of component *i*, *W* [kg_{cat}] the mass of the catalyst and R_i the net production rate of component *i* [mol s^{-1} kg_{cat}^{-1}]. The kinetic model is implemented by means of the single-event concept.

By determining the elementary reaction steps and lumping them into several reaction families, a significant reduction of the number of kinetic parameters is obtained. This is because for every reaction family only one single event reaction rate coefficient has to be considered. The rate coefficient of an elementary step is calculated as the product of the single event reaction rate coefficient, $\tilde{k}$, and the number of single events:

$$k = n_e.\tilde{k} \quad (2)$$

The number of single events represents the number of geometrically independent ways in which the transition state can be formed from the reactant[1]. Hence, the structural differences between the elementary steps of one reaction family are taken into account.

III. RESULTS

A. Experimental results

With increasing partial pressure, temperature and space time, the ethylene conversion is increased. However, a maximum value of 15% was obtained within this range of reaction conditions. At higher temperature, an increase in activity of acid sites occurs, e.g., dimerization of butene to octene and cracking of octene to propylene and pentene. For all conditions tested, mainly the production of even-numbered olefins was observed (>95%) and only small amounts of propylene and pentene were detected, indicating that β-scission occurred.

Compared to the reference catalyst, the Ni-β showed lower activity, despite the higher amount of nickel present. Most probably, clustering of the nickel into NiO is causing this behavior. The high nickel content and the relatively high acid site concentration leads to pore blocking, hence the low ethylene conversion[2]. During the experiments, also quick deactivation was observed, which is in correspondence with the blocking of the active sites. No regeneration method could be found. Based upon the experimental observations, a reaction network was proposed, see ***Figure 1***.

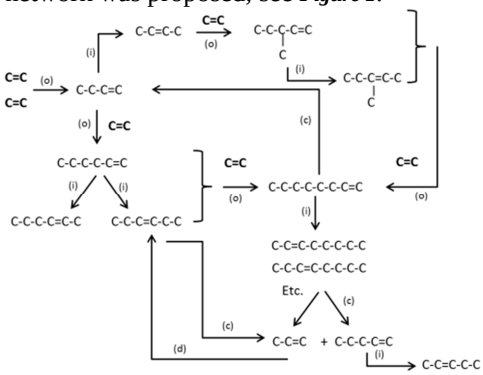

Figure 1: Proposition of reaction network on Ni-β catalyst

Ethylene is dimerized on the nickel-ion sites to butene. This butene then mainly oligomerize further to hexene and octene via consecutive insertions of ethylene on the nickel-ion sites. However, a small fraction of the butenes can dimerize on the acid sites to octene which subsequently is cracked to propylene and pentene.

B. Kinetic model expansion

A SEMK model describing the metal ion kinetic in detail was already available. The acid catalyzed reactions are implemented to be able to describe the experimental observations, i.e., via alkylation and β-scission, 1,2-alkyl shift and PCP-branching. The ease of protonation depends on the type of carbenium ion, in particular its stability. Thermodynamic constraints were introduced to limit the number of kinetic parameter describing (de)-protonation and isomerization. For alkylation and its reverse reaction, i.e., β-scission, thermodynamic consistency was accounted for by means of a Born-Haber cycle. This way, the activation energies of the alkylation and β-scission are coupled.

C. Regression and simulation

The expanded kinetic model was regressed to the experimental data in order to estimate the kinetic and catalyst descriptors. By using values for the kinetic descriptors from literature, see Table 3, the number of kinetic parameters to be estimated could be limited. After a significant regression, i.e., F_{cal}=234.0 > F_{tab}=3.1, a set of significant parameters was obtained, see Table 4.

Table 3: Kinetic descriptors from literature used during regression of the kinetic model to the experimental data

Kinetic descriptor	Value (kJ mol^{-1})
$E_{a,ins(Ni)}$	76 [3]
$E_{a,ter(Ni)}$	68 [3]
$E_{a,1,2as}$	76 to 105 [4]
$E_{a,PCP}$	92 to125 [4]

Table 4: Kinetic parameters estimated by regression of the kinetic model to the experimental data

Kinetic parameter	Value (kJ mol^{-1})
$\Delta H_{chem,C2(Ni)}$	-107±0
$\Delta H_{phys(C2)}$	-10±2
$\Delta\Delta H_{phys(2C)}$	-31±0
$\Delta H_{pr}(s)$	-32±6
$\Delta H_{pr}(t)$	-31± 6
$E_{a,alk}$	41±1 to 61±1
» $E_{a,\beta s}$:	150 to 160

The model was able to predict the experimental data adequately, as shown by the performance figure and parity diagram, see resp. Figure 2, 3 and 4. The model is capable to describe the effect of temperature and space-time but can be improved concerning the effect of the partial pressure of ethylene.

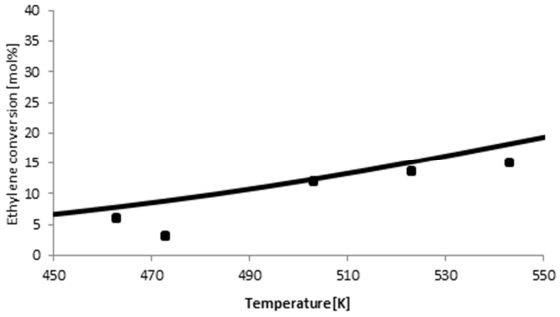

Figure 2: Comparison between simulated, i.e., full line, and experimentally (■) obtained ethylene conversion in function of temperature

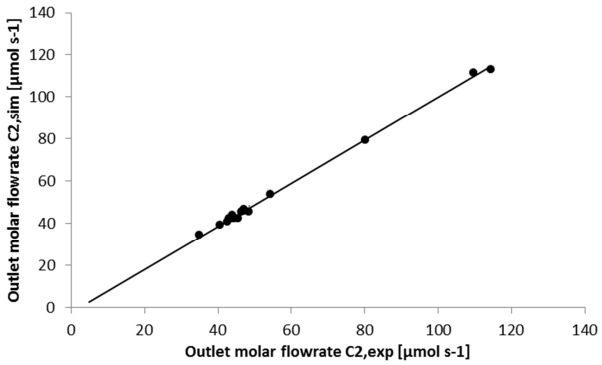

Figure 3: Parity diagram of the outlet molar flow rate of ethylene.

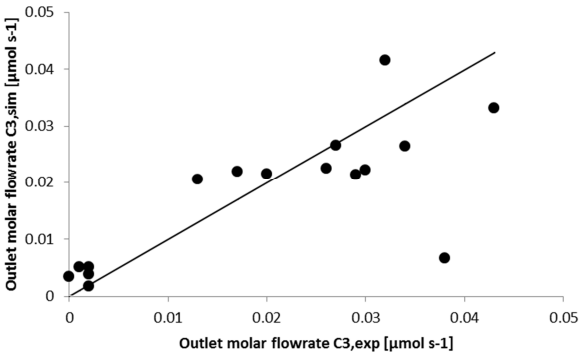

Figure 4: Parity diagram of the outlet molar flow rate of propylene.

By performing a reaction path analysis, it can be concluded that mainly metal ion oligomerization and isomerization are responsible for the production of olefins.

IV. CONCLUSION

An experimental study of oligomerization of ethylene on a Ni-β catalyst was performed. Additionally, the kinetic model was adapted to describe the acid catalyzed reactions. By using the dataset, the adequate performance of the kinetic model could be verified.

V. FUTURE WORK

In order to obtain a more interesting experimental dataset for the modeling of the cracking reactions, a bifunctional catalyst with more stable and active behavior should be tested. In literature, the Ni-AlMCM-41 catalyst is stated as an active catalyst for acid oligomerization of ethylene[2].

REFERENCES

[1] Toch, K., et al., A Single-Event Micro Kinetic model for "ethylbenzene dealkylation/xylene isomerization" on Pt/H-ZSM-5 zeolite catalyst. Applied Catalysis a-General, 2012. **425**: p. 130-144.

[2] Hulea, V. and F. Fajula, Ni-exchanged AlMCM-41—An efficient bifunctional catalyst for ethylene oligomerization. Journal of Catalysis, 2004. 225(1): p. 213-222.

[3] Toch, K., J. W. Thybaut, et al. (2013). Ethylene Oligomerization on Bifunctional Heterogeneous Catalysts: Model Development and Catalyst Optimization. Netherlands' Catalysis and Chemistry Conference (NCCC XIV).

[4] Vandegehuchte, B.D., et al., n-Hexadecane hydrocracking Single-Event MicroKinetics on Pt/H-beta. Applied Catalysis A: General, 2012. 441–442(0): p. 10-20.

Oligomerisatie van ethyleen tot vloeibare brandstoffen en chemicaliën

Julie Timmerman*

Begeleider: ir. Kenneth Toch

Promotor: Prof. dr. ir. J.W. Thybaut

Abstract: **De oligomerisatie van ethyleen over een bifunctionele katalysator is experimenteel onderzocht. De focus van het onderzoek was de adequate beschrijving van de zuur gekatalyseerde stappen. Het kinetische model voor ethyleen oligomerisatie, waarin reeds de metaal ion gebaseerde kinetiek is opgenomen, is uitgebreid met de carbenium ion gerelateerde reactiestappen, d.z., (de)-protonatie, β-scissie, alkylering, 1,2-alkyl shift en PCP-vertakkingen. Door toepassing van het Single Event MicroKinetisch (SEMK) concept en thermodynamische consistentie, is het aantal (te schatten) parameters verminderd. Het model is geregresseerd naar de experimentele data. De regressie is significant getest en de geschatte parameters hebben een relatief klein betrouwbaarheidsinterval. Uit simulaties blijkt dat het model in staat is om de meeste invloeden van de reactiecondities op de kinetiek te beschrijven.**

Kernwoorden: ethyleen oligomerisatie, bifunctionele katalysator, SEMK model, β-scissie

I. Inleiding

Oligomerisatie van ethyleen is een conversie proces waarbij langere olefines en chemicaliën worden geproduceerd. Deze componenten worden beschouwd als waardevolle producten voor detergenten, vloeibare brandstoffen, weekmakers, enz. Door de wereldwijde stijgende vraag naar brandstoffen en chemicaliën en de overeenkomstige stijging in prijs, neemt dit proces steeds meer in belang toe. Op industriële schaal wordt dit proces reeds toegepast met behulp van homogene katalyse. Om de product flexibiliteit en milieuvriendelijkheid te verhogen wordt het gebruik van heterogene katalysatoren onderzocht. Deze heterogene katalysatoren zijn over het algemeen bifunctioneel, met twee types actieve katalytische centra, d.i., transitiemetaal ionen, bvb. nikkel, aangebracht op een zure drager. Steeds meer worden zeolieten beschouwd als interessante zure dragers voor deze toepassing. Door in te spelen op hun morfologie, en, dus gebruik makend van vorm selectieve effecten, kan de product distributie worden beïnvloed.

Daar protonatie van ethyleen aanleiding geeft tot productie van een primair carbenium ion, wat onstabiel is onder de geteste reactiecondities, vindt initiatie plaats via het metaal ion center. Er wordt verondersteld dat oligomerisatie via deze route verloopt volgens een insertie-terminatie mechanisme op de nikkel-ion centra. Op de zure centra kan dan verdere oligomerisatie plaatsvinden via een carbenium mechanisme. Het belang van de aanwezigheid van de zure centra ligt in hun invloed op de product-samenstelling. Mocht alleen oligomerisatie op metaalionen beschouwd worden, dan zouden enkel α-olefinen worden geproduceerd met een even aantal koolstofatomen. Echter, door de aanwezigheid van de zure centra, die de primair gevormde lineaire producten omzetten naar vertakte, oneven koolwaterstoffen, wordt een uitgebreider productmengsel bekomen wat beter inzetbaar is als brandstof. In vorig werk zijn vooral de metaal ion reactie stappen uitgebreid beschreven.

In dit werk is de aandacht gevestigd op de secundaire zuur gekatalyseerde reacties. Door het uitvoeren van een experimentele studie op een Ni-β katalysator, gekend wegens zijn zure activiteit, kan het kinetisch model uitgebreid worden met de zure reacties. Eenmaal het model is opgesteld kunnen zowel de kinetische als de katalytische descriptoren bepaald worden door regressie naar de experimentele data.

II. Procedures

A. Experimenteel werk

Een experimentele studie werd uitgevoerd op een 4.89m% Ni-β katalysator in een propstroomreactor, d.i., HTK-1. Het bereik van reactiecondities is gegeven in Tabel 1. Bij deze reactiecondities wordt intrinsieke kinetiek opgemeten. Om te voorkomen dat condensatie van het reactie mengsel plaatsvindt en het bedrijf van de reactor te vergemakkelijken, is verdunning met stikstof noodzakelijk.

Tabel 1: Experimentele reactie condities

Reactieconditie	Experimenteel bereik
Temperatuur [K]	443-503
Partieeldruk C_2H_4 [MPa]	0.17-0.40
Ruimtetijd [kg_{cat} s mol^{-1}]	4.0-12.0
Verdunning met stikstof [mol%]	88.0

XRD heeft aangetoond dat er NiO clusters aanwezig zijn op de Ni-β katalysator. Dit is in tegenstelling met de referentie katalysator, d.i., 1.80wt%Ni-SiO_2-Al_2O_3, getest tijdens vorig werk. De eigenschappen van de Ni-β katalysator en de referentie katalysator zijn gegeven in Tabel 2.

Tabel 2: Eigenschappen van de katalysatoren

	4.89wt%Ni-β	**1.80wt%Ni-SiO_2-Al_2O_3**
Nickel inhoud [wt%]	4.89	1.80
BET-oppervlakte [m^2 g^{-1}]	458.32	199.11
Concentratie zure centra [mmol g^{-1}]	0.634 (sterk)	0.79 (zwak)

B. Modeling

Daar experimenten werden uitgevoerd op een propstroom reactor, wordt het reactormodel geschreven als:

$$\frac{dF_i}{dW} = R_i \qquad (1)$$

*E-mail:Julie.Timmerman@UGent.be

met F_i [mol s^{-1}] het molaire debiet van component *i*, *W* [kg_{kat}] de katalysatormassa en R_i de netto productiesnelheid van component *i* [mol s^{-1} kg_{kat}^{-1}]. Het kinetisch model is opgebouwd via het single-event principe. Door het bepalen van de elementaire reactiestappen en deze te groeperen in verschillende reactiefamilies, wordt een significante reductie van het aantal kinetische parameters verkregen. Daar er nu voor elke reactiefamilie slechts één single-event reactie snelheidscoëfficiënt moet worden bepaald.

De snelheidscoëfficiënt voor elke elementaire stap wordt berekend als het product van de single-event reactiesnelheid coëfficiënt en het single-event getal:

$$k = n_e.\tilde{k} \qquad (2)$$

Het single-event getal stelt het aantal geometrisch onafhankelijke manieren voor waarop de transitie toestand kan gevormd worden startend van het reactant[1]. Dit zorgt voor een opdeling binnen de reactiefamilies.

III. RESULTATEN

A. Experimentele resultaten

Met toenemende partieeldruk, temperatuur en ruimtetijd, neemt de ethyleen conversie toe. Echter, een maximum waarde van 15% werd opgemeten binnen het bereik aan experimentele reactie condities. Bij hogere temperatuur vindt een toename in activiteit van de zure centra plaats, zoals dimerisatie van buteen naar octeen en kraking van octeen naar propyleen en penteen. Voor het volledige experimentele gebied was de selectiviteit naar olefinen met een even koolstofgetal hoog (>95%) terwijl maar kleine hoeveelheden aan propyleen en penteen zijn gedetecteerd. Dit laatste duidt het optreden van β-scissie aan.

In vergelijking met de referentie katalysator is de Ni-β minder actief, ondanks de grote hoeveelheid aan nikkel aanwezig op de katalysator. Hoogst waarschijnlijk heeft deze grote hoeveelheid aanleiding gegeven voor de vorming van NiO clusters. De hoge nikkel lading en de relatief hoge concentratie aan zure sites leidt tot blokkering van de poriën vandaar de lage ethyleen conversie[2]. Een snelle deactivering werd waargenomen gedurende experimenten, wat ook in verband kan worden gebracht met de blokkering van de poriën. Een regenereringsprocedure is niet gevonden. Op basis van de experimentele waarnemingen is een reactie netwerk opgesteld, zie Figuur 1.

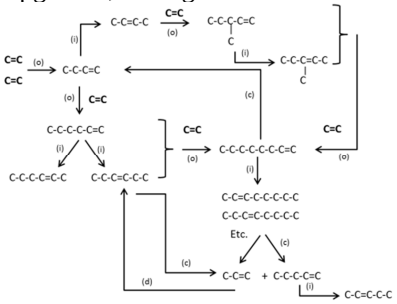

Figuur 1: Voorstelling reactie netwerk op Ni-β katalysator

Ethyleen dimeriseert op de nikkel-ion centra ter vorming van buteen. Dit buteen zal vervolgens vooral verder oligomeriseren tot hexene en octene via opeenvolgende inserties van ethyleen op de nikkel-ion centra. Echter, een beperkte buteen fractie dimeriseert naar octeen op de zure centra wat onmiddellijk kan kraken ter vorming van propyleen en penteen.

B. Uitbreiding van het kinetische model

Een SEMK model welke de metaal ion kinetiek beschrijft was voorhanden. De zuur gekatalyseerde reacties zijn geïmplementeerd om de experimentele waarnemingen te kunnen beschrijven, d.z., alkylatie, kraking, 1,2-alkyl shift en PCP-vertakking. Het gemak van protonatie is afhankelijk van het type carbenium ion dat wordt gevormd, met name zijn stabiliteit. Thermodynamische voorwaarden zijn opgelegd om het aantal te schatten parameters te bepreken, met name de (de)-protonatie en isomerisatiereacties. Voor de alkylatie en zijn terugwaartse reactie, zijnde kraking, is thermodynamische consistentie geïmplementeerd gebruik makend van een Born-Haber cyclus. Op deze manier, konden beide activeringsenergieën met elkaar in verband worden gebracht.

C. Regressie en simulatie

Het uitgebreide kinetische model is geregresseerd naar de experimentele data om de kinetische en katalytische descriptoren te schatten. Voor enkele kinetische descriptoren waren waarden gekend uit de literatuur, zie Tabel 3. Op deze manier is het aantal te schatten parameters nog afgenomen. Na een significante regressie, d.i., F_{ber}=234.0 > F_{tab}=3.1, is een set van significante parameters verkregen, zie Tabel 4.

Tabel 3: Kinetische descriptoren uit literatuur werden gebruikt tijdens regressie van het kinetisch model naar de experimentele data

Kinetische descriptor	Waarde (kJ mol^{-1})
$E_{a,ins(Ni)}$	76 [3]
$E_{a,ter(Ni)}$	68 [3]
$E_{a,1,2as}$	76 tot 105 [4]
$E_{a,PCP}$	92 tot125 [4]

Tabel 4: Geschatte parameter waarden bekomen via regressie van het kinetisch model naar de experimentele data

Kinetische parameter	Waarde (kJ mol^{-1})
$\Delta H_{chem,C2(Ni)}$	-107±0
$\Delta H_{fys(C2)}$	-10±2
$\Delta\Delta H_{phys(2C)}$	-31±0
$\Delta H_{pr}(s)$	-32±6
$\Delta H_{pr}(t)$	-31± 6
$E_{a,alk}$	41±1 tot 61±1
» $E_{a,\beta s}$:	150 tot 160

Het model is in staat om de experimentele data adequaat te beschrijven, zoals te zien is op de performantie figuur en pariteitsdiagramma, zie resp. Figuur 2, 3 en 4. Het model is in staat het effect van de temperatuur en ruimtetijd te beschrijven. Echter, het kan nog worden verbeterd worden op vlak van de beschrijving van de partieeldruk-effecten van ethyleen.

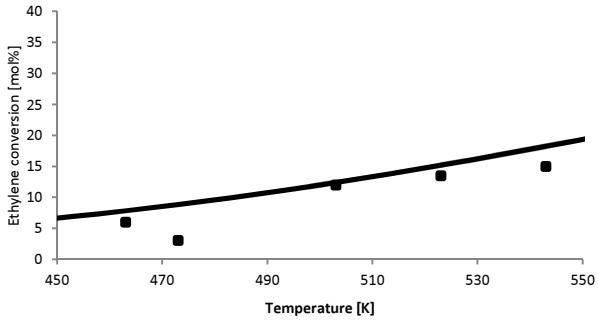

Figuur 2: Performatiecurve voor de conversie van ethyleen als functie van temperatuur. Volle lijn: simulatie, ■: experimenteel.

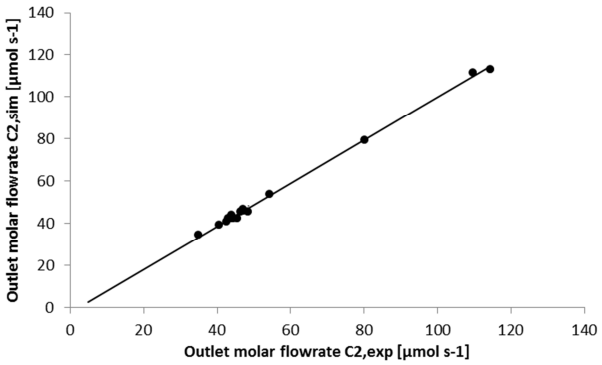

Figuur 3: Pariteitsdiagramma voor de molaire uitlaatstroom van ethyleen.

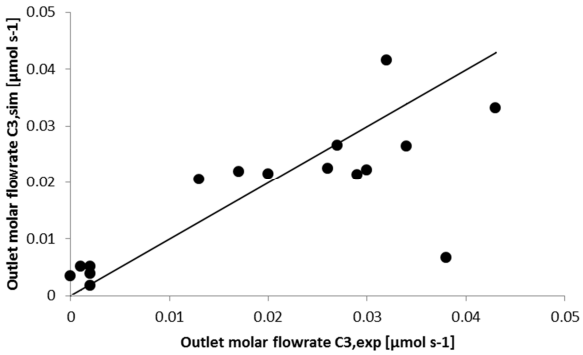

Figuur 4: Pariteitsdiagramma voor de molaire uitlaatstroom van propyleen.

Via een reactiepadanalyse is bepaald dat voornamelijk metaal oligomerisatie en isomerisatie verantwoordelijk zijn voor de product verdeling.

IV. CONCLUSIE

Een experimentele studie van ethyleen oligomerisatie op Ni-β werd uitgevoerd, evenals een uitbreiding van het kinetisch model met de zuur gekatalyseerde reacties. Via de experimentele data kon de adequaatheid van de performantie van het kinetisch model worden gecontroleerd.

V. TOEKOMST PERSPECTIEVEN

Experimenteel onderzoek moet worden uitgevoerd op een katalysator met een meer stabiel en actief gedrag, specifiek voor de modellering van de kraking. In literatuur wordt Ni-AlMCM-41 katalysator vermeld als actieve katalysator voor zure oligomerisatie[2].

REFERENTIES

[1] Toch, K., et al., A Single-Event Micro Kinetic model for "ethylbenzene dealkylation/xylene isomerization" on Pt/H-ZSM-5 zeolite catalyst. Applied Catalysis a-General, 2012. **425**: p. 130-144.

[2] Hulea, V. and F. Fajula, Ni-exchanged AlMCM-41—An efficient bifunctional catalyst for ethylene oligomerization. Journal of Catalysis, 2004. 225(1): p. 213-222.

[3] Toch, K., J. W. Thybaut, et al. (2013). Ethylene Oligomerization on Bifunctional Heterogeneous Catalysts: Model Development and Catalyst Optimization. Netherlands' Catalysis and Chemistry Conference (NCCC XIV).

[4] Vandegehuchte, B.D., et al., n-Hexadecane hydrocracking Single-Event MicroKinetics on Pt/H-beta. Applied Catalysis A: General, 2012. 441–442(0): p. 10-20.

TABLE OF CONTENT

List of symbols

Abbreviations

AS	Alkyl Shift
ASF	Anderson Schultz Flory distribution
GTL	Gas To Liquids
HTK-1	High-Throughput Kinetic setup
LNG	Liquefaction of Natural Gas
LPG	Liquified Petroleum Gas
MCM	Mobil Crystalline Material
NGL	Natural Gas Liquid
PCP	Protonated Cyclo Propane
SEMK	Single-Event MicroKinetic
SHOP	Shell Higher Olefin Process

Symbols

A_i	Peak surface area of component *i* in the gas chromatograph
$A_{i,corr}$	Corrected peak area of component *i*
a_v	Heat specific external surface area of one pellet [$m^2\,m^{-3}$]
b_i	Estimation value of the parameter β_i
Bi	Biot number [-]
Bo	Bodenstein number [-]
$C_{A,b}$	Bulk concentration of reactant *A* [mol m^{-3}]
$C_{A,s}$	Surface concentration of reactant *A* [mol m^{-3}]
CF	Conversion factor
$C_{sat,i}$	Saturation concentration for physisorption of olefine *i* [mol g_{cat}^{-1}]
E_a	Activation energy [J mol^{-1}]
F_1	Real flow rate through the controller [mol s^{-1}]
F_2	Flow rate that has to be set in the LabVIEW® interface [mol s^{-1}]
F_A	Molar flow rate of component *A* [mol s^{-1}]

F_{calc}	Calculated value for *F* test [-]
f_f	Fanning friction factor[-]
$F_{i,j}$	Experimental molar outlet flow rate of experiment *j* and component *i* [mol s^{-1}]
F_{IS}^{0}	Inlet flow rate of Internal Standard [mol s^{-1}]
f_m	Modified Fanning friction factor[-]
F_{tab}	Tabulated value for F test [-]
$F_{wt,i}$	Mass flow rate [kg s^{-1}]
h	Planck constant [J s]
k_B	Boltzmann constant [J K^{-1}]
k_f	Mass transfer coefficient between pellet and fluidum [m s^{-1}]
K_{iso}	Isomerization equilibrium coefficient [dependent on reaction]
L	Length of reactor tube [m]
MW_A	Molecular weight [g mol^{-1}]
n_e	Number of single events [-]
n_{exp}	Number of experiments [-]
n_{par}	Number of parameters [-]
n_{resp}	Number of responses [-]
P^0	Normal pressure [Pa]
R	Multiple correlation coefficient [-]
R	Gas constant [J mol^{-1} K^{-1}]
R_3^+	Carbenium ion corresponding with olefin O_3
R_i	Production rate of component *i* [mol g_{cat}^{-1} s^{-1}]
S	Entropy [kJ mol^{-1} K^{-1}]
$S_{B,A}$	Selectivity to component *B* towards component *A* [-]
sigma	Symmetry number of molecule [-]
T	Temperature [K]
TR_i	Thermal respons factor
t_{tab}	Tabulated value for t test [-]
V(b)	Variance-covariance matrix
W	Catalyst weight [g_{cat}]
WF_i	Weight factor Dietz
WHSV	Weight hourly space time [kg s^{-1} kg $_{cat}^{-1}$]
w_i	Weight factor of response *i* [-]
X_A	Conversion of component *A* [-]

$X_{mol,i}$	Mol fraction of component *i* [-]
$x_{wt,i}$	Massfraction of component *i* [-]
$Y_{B,A}$	Yield to component *B* [-]
α	Significance treshold
$\Delta G^{0,\ddagger}$	Standard Gibbs free energy between transition state and reactants [J mol^{-1}]
$\Delta H^{0,\ddagger}$	Standard enthalpy difference between transition state and reactants [J mol^{-1}]
ΔH_r	Enthalpy of reaction [J mol^{-1}]
$\Delta S^{0,\ddagger}$	Standard entropy difference between transition state and reactants [J mol^{-1} K^{-1}]
ε_b	Bed porosity [m^3_{space} m^{-3}_{bed}]
η	Efficiency [-]
τ	Space time [kg_{cat} s mol^{-1}]
Φ	Weisz-Modulus [-]
ϕ	Thiele modulus [-]
$\lambda_{\varepsilon\rho}$	Effective radial bed thermal conductivity [W m^{-1} K^{-1}]
$\widehat{F_{i,J}}$	Calculated molar outlet flow rate of experiment *j* and component *i* [mol s^{-1}]
$\tilde{k}$	Single-event reaction rate coefficient [dependent on reaction]
$\rho_{i,j}$	Correlation coefficient between parameters b_i and b_j [-]

Superscripts and subscripts

0	Reactor inlet
alk	Alkylation
chir	Chiral
cr	Cracking
depr	Deprotonation
ext	External
gl	Global
int	Internal
IS	Internal Standard
isom	Isomerization
phys	physisorption
pr	Protonation
rot	Rotation
s	Secondary
t	Tertiary

trans	Translational
vib	Vibrational

Chapter 1

Literature survey

Nowadays, the world is fully dependent on the crude oil markets by having so many daily needs that require fossil fuels and chemicals. But with the increasing oil prices and increasing world-demand, scientists are looking for alternatives, e.g., fuels synthesized in a non-conventional way. One such alternative process is the *OCMOL* process, funded by the European Commission, comprising the transformation of natural gas or biogas to chemicals and fuels [1]. This is done via an oxidative coupling step, leading to ethylene which is subsequently oligomerized to chemicals and fuels, depending on the reaction conditions applied. The unreacted methane is reformed to syngas which is used to produce oxygenates and hydrocarbons. It is the oligomerization step which is subject of this thesis. In this chapter, an overview of the available literature on ethylene oligomerization will be discussed. First, a brief description of the *OCMOL* process and the properties of ethylene will be given. This is followed by an elaboration on the oligomerization step and the types of catalysts which can be used. Both the reaction conditions as the catalyst properties have a significant influence on the product distribution. Concerning diesel and gasoline fuels, the appropriate catalyst properties will be discussed. Finally, the influence of the catalyst framework and the different types of frameworks for ethylene oligomerization will be mentioned.

1.1 OCMOL

This master thesis is situated within the European *OCMOL* project, which stands for the *Oxidative Coupling of Methane followed by the Oligomerization to Liquids*. This methane conversion process is especially designed for small reservoirs, i.e., so-called stranded gas, or biogas. The project aims at developing a complete and chemical route to valorize this methane. Since nowadays, one third of the world's natural gas reservoirs are stranded and remain unexploited.

1.1.1 Natural gas valorization

Natural gas contains approximately 95% methane, but its composition varies within origin [2]. Using methane as a combustion source is not reaching up to its potential due to the low energy efficiency of the combustion processes, i.e., less than 30%.

Two main conversion, c.q., valorization, processes used nowadays are:

1. Chemical liquefaction process (GTL or Gas To Liquids)

   By chemical liquefaction, the methane can be converted into syngas. This syngas can further react using processes like Fisher-Tropsch. Syngas exists out of carbon monoxide and hydrogen. With Fisher-Tropsch, this syngas is converted into liquid fuels. Other technologies are able to convert syngas into methanol, dimethyl ether, …

2. Natural gas liquefaction (LNG)

   Liquefaction of the natural gas is used especially for the transport of the gas. The liquefaction increases the energy density of the gas, which makes it possible to transport the natural gas more easily. Liquefaction is performed at atmospheric pressure and low temperature, condensing the gas into a liquid. For the liquefaction process, cryogenic cooling is required.

The greatest disadvantage of these two conversion processes is their great investment and production cost, especially for the small natural gas reserves that are spread out all across the world. This is the strength and opportunity of *OCMOL*: this process uses this natural gas that cannot be economically exploited by the conventional routes, to produce more valuable liquid fuels and chemicals.

1.1.2 Biogas

One renewable methane source of the future is biogas. Every year, natural biodegradation of organic material under anaerobic conditions is estimated to release 590-800 million tons of methane in the atmosphere [3]. Therefore, it can be used as an important and environmental-friendly methane source for the *OCMOL* process.

Biogas is produced during the bio-degradation of organic material with the use of bacteria. This natural production of methane is one step of the biogeochemical carbon cycle. Biogas is a mixture of methane (40-70vol%), carbon dioxide (60-30vol%) and other gases such as hydrogen and hydrogen sulfide. Biogas has a calorific value of 6kWh/m³, which is comparable with 0.5dm^3 of diesel oil [4].

The production of biogas can be divided into three stages, i.e. hydrolysis, acidification and methane formation, see Figure 1-1. In every step, different bacteria are necessary.

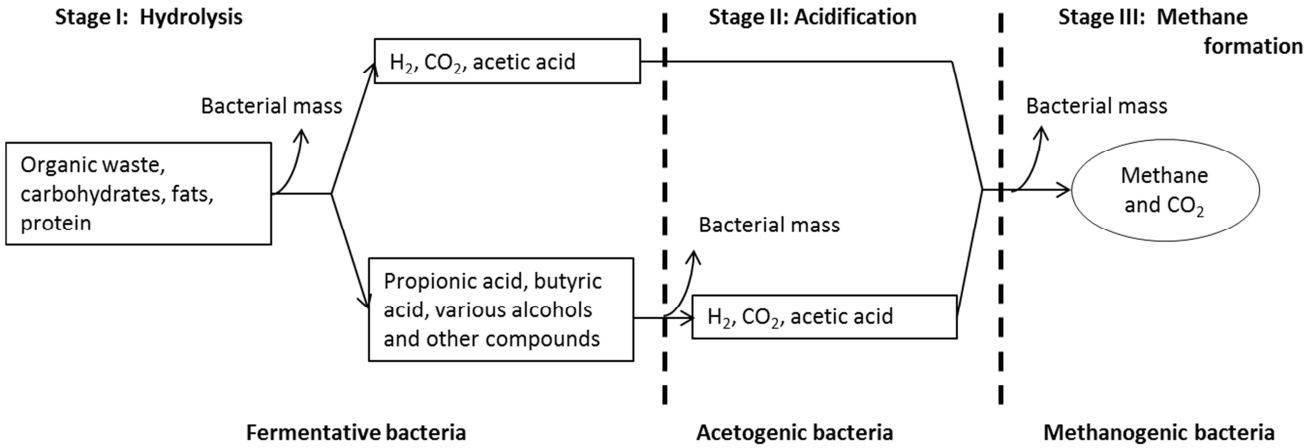

Figure 1-1 :The three stage anaerobic fermentation of biomass [5]

Currently, in several development countries like India, China, etc. this method is used to obtain methane that can be used to increase the life standards.

1.1.3 *OCMOL* process [1]

The *OCMOL* process starts with pure methane and oxygen. The first step is the oxidative coupling of methane, i.e., *OCM*. In this exothermic reaction, two methane molecules are coupled to ethylene and other byproducts such as C_2H_6, CO, CO_2, H_2O and H_2 are formed. The second step is the separation, c.q., purification of the ethylene, from the other products. The heat generated during the *OCM* reaction is used in the endothermic reformer reactor. In the reformer, syngas is produced out of methane and other compounds like CO_2, CO, H_2O.

After step two, the purified ethylene is oligomerized, i.e., step 4 in Figure 1-2. The syngas reacts further to liquid fuels by the oxygenate synthesis, i.e., step 3. In this synthesis, methanol and dimethyl ether are the two main products. These are converted into oligomers in the oxygenates-to-liquid reactor. *OCMOL* aims at producing both chemicals, e.g., alpha-olefins, and liquid fuels. Off-course, a hydrogenation step has to be performed to convert the olefins to saturated hydrocarbons or liquid fuels. Figure 1-2 shows the *OCMOL* process and its different steps.

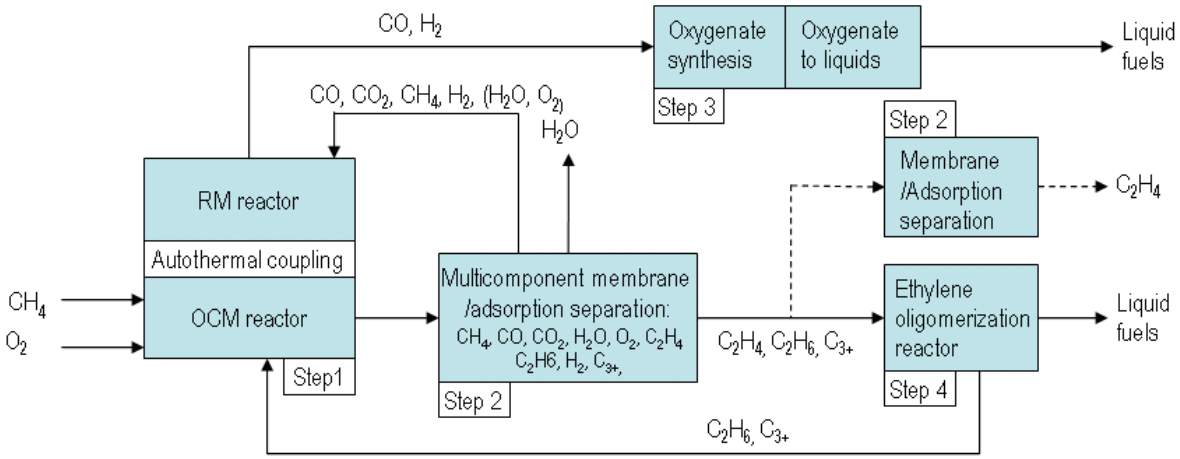

Figure 1-2: Schematic overview of the *OCMOL* process [6]

The advantage of *OCMOL* is the *environmental friendly* way of producing liquid fuels and chemicals, i.e., without any CO_2-emission. Moreover, the liquid fuels don't contain any hetero-atoms, such as nitrogen and sulphur, or aromatics, so no further purifications have to be performed. The fuels that are produced range from gasoline to diesel. Concerning the chemicals, especially high valuable alpha olefins are targeted. These olefins can be added as a co-monomer for the production of poly-ethylene and polypropylene, which makes it possible to change the properties, i.e., strength, molecular weight, density…, of the polymers.

This thesis will focus on one specific step of the process, i.e., ethylene oligomerization. With this step, both liquid fuels and chemicals can be produced, depending on the reaction conditions applied.

1.2 ETHYLENE

1.2.1 Properties of ethylene

Ethylene, C_2H_4, is the organic chemical with worldwide the largest consumption. This molecule is mostly used as a raw material for the manufacturing of plastics, fibers and other chemicals. Since 1940, ethylene slowly replaced the use of acetylene for different kind of synthesis. Ethylene is produced mostly by thermal cracking of hydrocarbons in the presence of steam or recovery of refinery cracked gas [7].

Ethylene is a colorless, flammable gas with a sweet odor and is the lightest olefin. Ethylene is a very reactive molecule due to the presence of a double bond. The electrons in the *Pi*-bond are less strongly bond and more polarizable than electrons in a *σ*-bond. This is the main reason of its numerous uses in the chemical industry. Chemical reactions of ethylene with commercial importance

are: addition, alkylation, halogenation, hydration, oligomerization and polymerization. In Table 1-1, the most interesting physical properties of ethylene are summarized.

Table 1-1: Physical properties of ethylene [8]

Property	Value
Molecular mass [g mol^{-1}]	28.0
Boiling point [K]	169
Vapor pressure, at 288K[kPa]	8100
Relative vapor density	0.98
Explosive limits [vol% in air]	2.7-36.0

1.2.2 Applications of ethylene

The production of polyethylene is the largest consumer of ethylene. Polymerization of ethylene occurs through a cationic reaction mechanism, e.g., the production of HDPE with Ziegler-Natta catalysts, or a radical reaction mechanism, e.g., the production of LDPE. The ethylene polymer can have different forms, e.g., LDPE, HDPE…, dependent of the applications. Due to the growing use of polyethylene, the world ethylene market is projected to reach 160.55 million tons by the year 2015 [9]. Within the polyethylene industry, a big variety of products are made. For example, High Density Poly Ethylene(HDPE), Low Density Poly Ethylene(LDPE), Linear Low Density Poly Ethylene(LLDPE), etc. Besides the polymers, ethylene can also be used for the production of ethylene oxide (EO), ethyl benzene (EB), etc. This ethyl benzene can further be hydrated to styrene. The percentages of ethylene consumption for every derivate is given in Figure 1-3 [10].

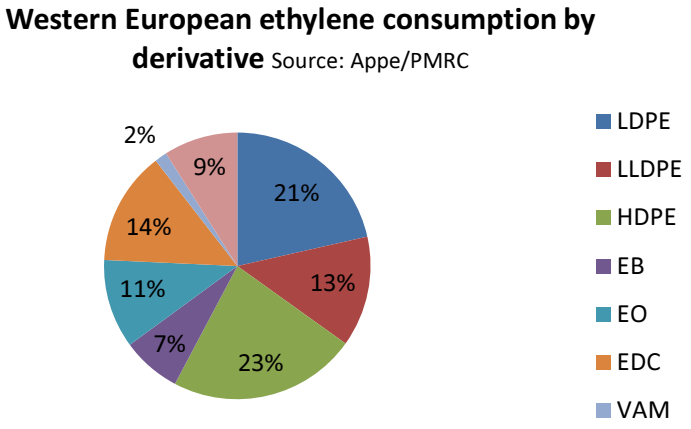

Figure 1-3: Western European ethylene consumption by derivative [10]

1.2.3 Production methods for ethylene

Several raw materials can be used for the production of ethylene, the most conventional one is naphtha, which is a liquid hydrocarbon stream derived from the refining of crude oil. Naphthas are mixtures of hydrocarbons in a boiling range of 303-473K. Besides naphtha, also refinery gas, containing C_4- hydrocarbons, nitrogen and carbon oxides are considered as usable raw material for ethylene. These gasses are becoming more and more important for the production of ethylene. But the material with the biggest evolution is *LPG* and *NGL*. These Natural Gas Liquids, e.g., like ethane, propane and butane, and Liquefied Petroleum Gas containing propane and butane are becoming more popular. Table 1-2 indicated this shift of raw materials from the eighties to the nineties.

Table 1-2: Relative indication of raw materials used for the production of ethylene [4]

Raw material	USA 1979	USA 1995	Western Europe 1981	Western Europe 1995	Japan 1981	Japan 1995
Refinery gas	1	4		3		
LPG,NGL	65	76	4*	17	10*	3*
Naphtha	14	11	80	71	90	97
Gas oil	20	9	16	9	0	0

*Including refinery gas

The bulk of the worldwide annual commercial production of ethylene is based on thermal cracking of petroleum hydrocarbons with steam: commonly called pyrolysis or steam cracking, see Figure 1-4 [7]. During a short residence time, the hydrocarbons of the feedstock are cracked into smaller molecules. Ethylene, other olefins, and di-olefins are the major products. Since the conversion of saturated hydrocarbons to olefins in the radiant section is highly endothermic, high energy input is needed.

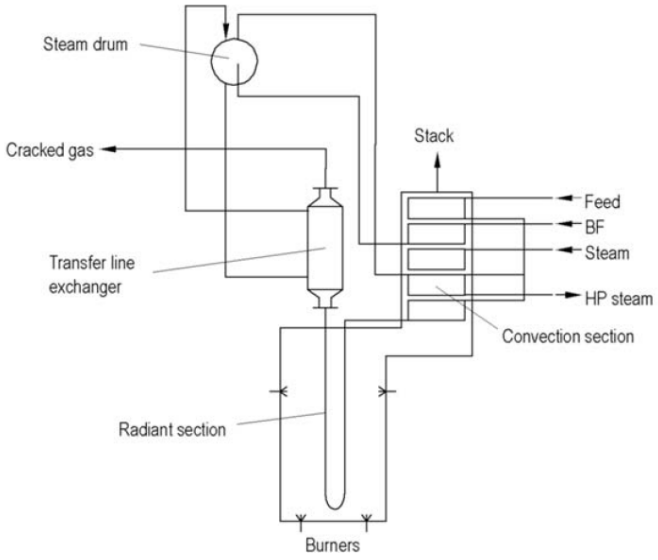

Figure 1-4: Principal arrangement of steam cracker of naphta [7]

The feed enters the convection section, where the inlet flow is preheated. In the radiant section, the actual cracking occurs and a lot of heat is required for this endothermic cracking. The cracked products are then sent to the transfer line exchanger, where immediate cooling of the products happens. This cooling is very necessary to overcome re-addition of the cracked products. The resulting product mixture, which can vary widely, depending on feedstock and severity of the cracking operation, is then separated into the desired products by using a complex sequence of separation and chemical-treatment steps [11].

Besides pyrolysis, other, more ecological ways of ethylene production, exist. With the increasing oil prices, the production of ethylene out of bio-ethanol gains more attention. This bio-ethanol is produced by fermentation of mainly starches, sugar crops and lignocellulose. Production of ethylene from ethanol occurs by a dehydration reaction. More than 65% of the worldwide bio-ethanol supply is used for the production of fuels out of ethylene [7].

1.3 ETHYLENE OLIGOMERIZATION

The oligomerization of ethylene is of considerable interest for the synthesis of higher olefins, which are valuable products used in the manufacturing of detergents, plasticizers, oil additives, fatty acids, etc. Moreover, as a consequence of environmental concerns, there is an increasing interest in the production of aromatics and sulfur-free transportation fuels via lower olefins oligomerization [12].

Nowadays, ethylene oligomerization can occur through three different kinds of synthesis: through organo-aluminum compounds, transition metal catalyzed oligomerization or acid catalyzed processes. The first process for the industrial oligomerization of ethylene was discovered by Ziegler in

the early 1950's. The reaction proceeded in two steps: a growth step, followed by an elimination step. The second type uses a transition metal as catalyst for the oligomerization. The most common used metals are nickel, cobalt, titanium and zirconium. The last synthesis type is based on acid catalysts, mainly zeolite structures, the oligomerization reaction can lead to isomerization of the primary products which encourages the production of branched olefins [11]. The main property of every synthesis is given in Table 1-3.

Table 1-3: Different types of synthesis with their main properties [11]

Type of synthesis	Main properties
Organo-aluminum catalyzed oligomerization	-Discovered by Ziegler in 1950. -Reaction in two steps: first a growth step [T=373K and p=10Mpa], followed by an elimination step [T=573K and p=1Mpa] $AlEt_3 + 3n\ CH_2 = CH_2 \rightarrow Al[(CH_2CH_2)_nEt]_3$ $Al[(CH_2CH_2)_nEt]_3 + 3CH_2 = CH_2 \rightarrow AlEt_3 + 3CH_2 = CH(CH_2CH_2)_{n-1}Et$ -Two industrially developed applications: Gulf Oil process and Ethyl process
Transition metal catalyzed oligomerization	-Transition metals: nickel, cobalt, titanium and zirconium -Combination of 3 reactions: oligomerization, isomerization and methathesis -Commercial process: Shell Higher Olefin Process (SHOP) -Complete control of product distribution
Acid catalyzed oligomerization	-Product distribution: mainly branched olefins

Oligomerization is significantly different from polymerization by the lengths of the formed products. The amount of basic units of ethylene is much lower after oligomerization than polymerization, which ensures that the product is still a liquid under standard conditions. In a first oligomerization step, mainly C_4-C_{14} alpha-olefins are made. Sometimes further transformation steps, e.g., isomerization, occur. When producing liquid fuels, additional hydrogenation is required. Oligomerization is also an exothermic reaction. This makes it necessary to remove the generated heat during the oligomerization.

1.3.1 Industrial oligomerization processes

The first oligomerization processes used homogeneous catalysts. This kind of oligomerization is the conventional one and already has several industrial applications. Ni complexes are the most widely used as homogeneous catalyst. Other homogeneous catalysts are AlR_3 (Ziegler Type) and $Me(OR)_4$-AlR_3 (Ziegler-Natta type) [12].

Industrial production of alpha-olefins out of ethylene is based on homogeneously catalyzed oligomerization. Here, the catalyst is dissolved in a liquid, through which the gaseous ethylene is sent. Four main technologies with homogeneous catalysts are used commercially [11]:

- The Albemarle-process
- The Chevron-Gulf process: with Ziegler catalyst
- The Shell Higher Olefin process (SHOP): uses a nickel salt as catalyst
- The Idemitsu process

A more detailed description of each process can be found in the master thesis of W. De Wilde [6].

The biggest disadvantage of this oligomerization method is the separation of the finished products from the liquid catalyst after synthesis. This separation is both a technological and an economical challenge. Moreover, some of these processes, like SHOP, generate a mathematical product distribution, i.e., *Anderson Schultz Flory* distribution, that does not correspond with the world demand. This type of non-selective production method has to be overcome with other oligomerization technologies, e.g., using heterogeneous catalysis. Using this type of catalysts avoids the catalyst separation issues. Ni-containing porous solids, like nickel-sulfated alumina or Ni-exchanged amorphous silica-alumina, Ni-AlMCM-41 and Ni-dealuminated Y zeolite are known as efficient heterogeneous oligomerization catalysts [13].

1.4 BIFUNCTIONAL HETEROGENEOUS CATALYSIS FOR ETHYLENE OLIGOMERIZATION

As indicated before, most of the industrial processes for the oligomerization of ethylene are based on homogeneous catalysis. However, for *OCMOL*, heterogeneous catalysis is favored. By using this type of catalysts, the selectivity and the environmental aspect can be controlled. The homogeneous catalysts consist of organo metallic complexes, into which heavy metals are incorporated. Some of the industrially applied heavy metals are zirconium, titanium and nickel. This catalyst is dissolved in a liquid and after reaction, the products have to be separated from the catalyst. This separation step is

cost inefficient due to the high energy consumption. With heterogeneous catalysis, this separation step can be avoided and moreover, less waste is generated, i.e., the solvents required for dissolving the catalysts are eliminated. In the following sections, the main aspects of the heterogeneous catalysts are discussed.

1.4.1 Bifunctional heterogeneous catalysis for oligomerization of ethylene

The mechanism for oligomerization of olefins goes through a carbenium ion mechanism. These carbenium ions are formed by acid catalysts. The necessity to form carbenium ions is the main raison why an oligomerization catalyst always contains acid sites. However very low conversion of ethylene is obtained on acidic catalysts containing no other active sites at moderate reaction conditions. This is due to the very low stability of the primary carbenium ion formed in the first reaction step under the reaction conditions applied. Propylene molecules are the shortest hydrocarbons that are able to produce stable carbenium ions through protonation, see Figure 1-5. Because of the stability of these higher carbenium-ions they can react further with other olefins available in the mixture.

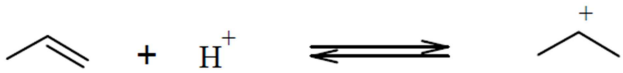

Figure 1-5: protonation of propylene

To overcome this activation problem, more advanced catalytic systems were prepared. Transition metals are known for their high activity concerning ethylene dimerization and oligomerization. A combination of acid sites and metal ion sites can give an optimal catalyst, e.g., nickel on silica, nickel on silica-alumina and nickel on zeolites [14]. In these catalyst systems, the metal ion activates the first dimerization step from ethylene to butylene with a coordinated mechanism. The acid sites can further catalyze oligomerization to octene or longer hydrocarbons. But other reactions, such as isomerization, alkyl shifts, PCP-branching are catalyzed too by these acid sites.

1.4.2 Overall reaction network

In this section, an overview of the reactions triggered by the bifunctional catalyst is given. Ethylene oligomerization occurs with the support of two interacting types of mechanisms: one based on coordination chemistry on nickel-ion sites and the second based on a carbenium mechanism on the acid sites, see Figure 1-6. Bifunctional catalysts contain two types of functional groups: metal ions and acid sites. The metal ions are responsible for the initiation of the oligomerization reaction. The acid sites have a significant influence on the stability and the activity of the catalyst and are mainly

responsible for the further oligomerization [12]. The acid character of the catalysts also influences the product distribution, by allowing isomerization and cracking. Figure 1-6 indicates that both active sites are desired to obtain a high enough yield to relative high molecular mass components.

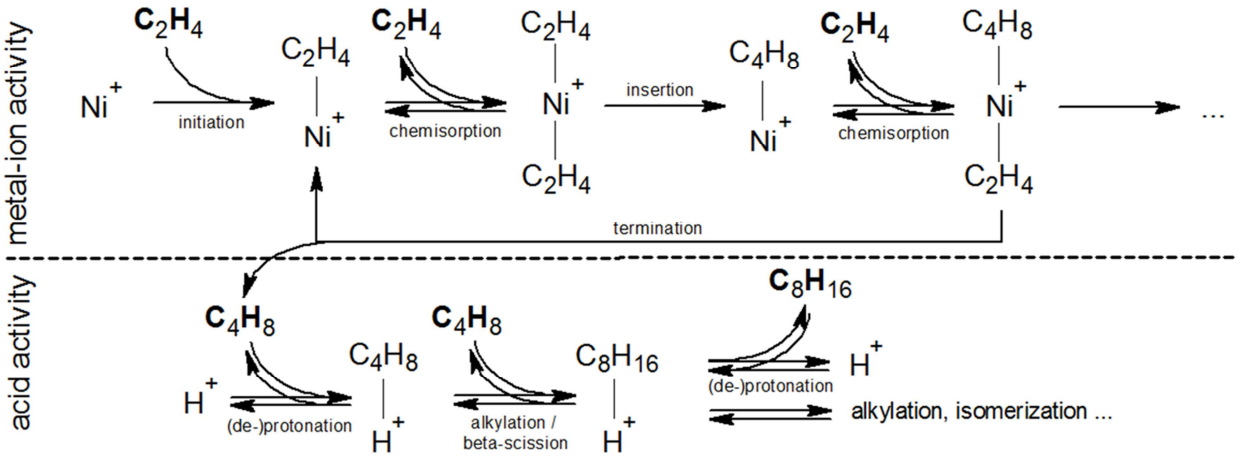

Figure 1-6: Reaction mechanism ethylene oligomerization [15]

1.4.2.1 Metal ion sites based reactions

The oligomerization on a metal ion center involves an insertion mechanism [16]. In the initial step, an ethylene unit approaches the coordinately unsaturated metal ion to form a *Pi*-complex, which is then followed by an insertion of the ethylene into the Ni-H bond, with Ni the metal ion. When the insertion is completed, a vacant coordination site is released and a new insertion is possible. Repeating this cycle several times, generates even numbered alpha-olefins, see Figure 1-7. Metal ion initiated oligomerization is called "*true oligomerization*", because in each step an new ethylene molecule is added to the chain[16].

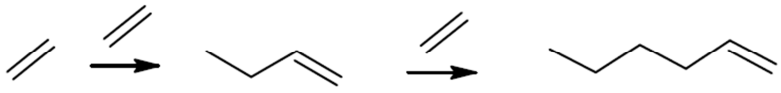

Figure 1-7: Schematic overview of the oligomerization of ethylene on metal ion site

Experiments have shown that with increasing chain length, the activation for further oligomerization is decreasing, which explains the rather low overall conversion of ethylene with the only metal based catalysts[17].

The most conventional metal used for the oligomerization is nickel. Besides nickel, other heavy transition metals like zirconium, chromium and titanium can be used.

One aspect is the amount of metal ion sites present on the catalyst. Nicolaides et al. [18] have performed experiments that investigate the influence of the amount of nickel on a silica-alumina

catalyst. Figure 1-8 indicates that a maximum conversion of ethylene is obtained with a nickel content around 1.5 wt%.

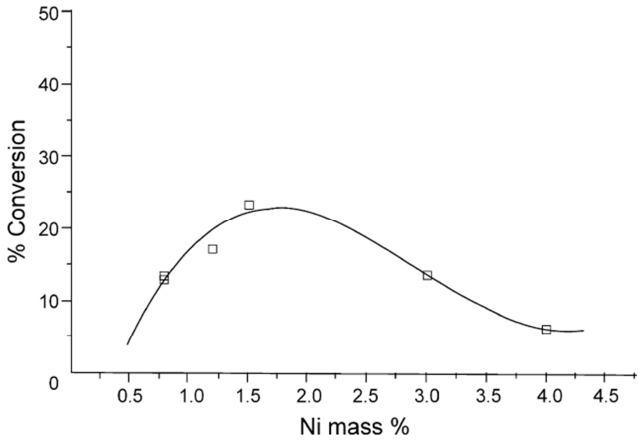

Figure 1-8: Conversion of ethylene as a function of Ni mass% (T=373K, P=1.5MPa, MHSV=4h^{-1} and time on stream=280min) [18]

Two different methods are used for adding Ni-atoms to the catalyst framework: impregnation and ion-exchange. The most effective use of the nickel ions is found on catalysts prepared by ion-exchange. This method produces highly active isolated nickel species that are associated with the ion-exchangeable sites of the silica-alumina supports. Whereas, for the impregnated catalysts most of the nickel is not associated and these catalysts are therefore less active [17].

1.4.2.2 Acid site based reactions

The acid site has a significant role in the stabilization of the catalyst and the product distribution. High- temperature acid catalyzed oligomerization is less selective, due to the wide range of reactions catalyzed by the acid sites. With increasing temperature, the acid sites become more active due to the increasing stability of the carbenium ions [17].

When olefins come in contact with an acid site, protonation of the double bond occurs resulting in the formation of a carbenium ion. As already mentioned before, due to stabilization, the real dimerization of ethylene occurs on a metal ion. From the instant a dimer, i.e., butylene, is formed, protonation can occur to form stable secondary ions which can react with other olefins. This mechanism leads to the formation of branched oligomers. These olefins can be protonated again and lead to further isomerization.

Besides this isomerization mechanism, also double bond isomerization can occur. This kind of isomerization can go through a sequence of protonations and deprotonations or by an hydride-shift.

The carbenium ions can undergo other reactions as well, like alkyl shifts, PCP-branching (Protonated CycloPropane branching), PCB-branching (Protonated CycloButane branching) and beta-scission. Results of this kind of reactions are resp. the branching on the olefins and the formation of odd numbered carbon olefins.

It can be concluded that due to the presence of acid sites, many different reactions can take place, which is the main reason of the big variety on the product distribution. The substituents on the carbenium ion define the stability. This stability increases with the degree of substitution: tertiary>secondary>primary and the lowest stability is for the ethylene carbenium ion. Therefore, the reaction rate is dependent of the stability of the compounds [19].

The role of the acid sites also increases with increasing temperature. The combination of all the acid catalyzed reactions leads to the term "*hetero oligomerization*". This refers to the wide product distribution, containing more than only the even numbered carbon olefins. The distribution also contains branched olefins, olefins with an odd carbon number and olefins with non-terminal double bonds.

Most catalysts contain both weak and strong acid sites. Besides this difference, another distinction is made, i.e. Lewis acids sites and Brönsted acid sites. The Brönsted sites are associated with framework aluminium atoms and react as proton donor for unsaturated hydrocarbons, while the Lewis sites are associated with the extra framework aluminium atoms and react as electron acceptor where a hydrid-ion is removed from the hydrocarbon [13]. The number of Brönsted acid sites on the catalyst active sites is vital in the olefin conversion to liquid hydrocarbons [20]. As the number of the Brönsted sites increases, the oligomerization rate of olefins will also increase.

The source of the acid sites on the catalysts can be a zeolite framework, like Y-zeolites, ZSM-5 zeolites or MCM-frameworks. By modifying the Si/Al ratio of the framework, the concentration of the acid sites can be adjusted.

Heveling et al. used the ratio of C_6/C_5 to indicate the occurrence of *hetero oligomerization*. The formation of C_5 occurs by a secondary reaction on the acid sites. Which means than an increase of the ratio corresponds to change in the dominating mechanism for ethylene oligomerization from nickel catalyzed coordination to the acid catalyzed carbenium mechanism [17].

1.4.2.3 Influence of the reaction temperature

The reaction temperature plays a decisive role in determining the activity, stability and selectivity of the catalysts [21]. Figure 1-9 shows the ethylene conversion as function of the reaction temperature. On this figure, three different temperature regions can be indicated:

- Low temperature region: increased ethylene conversion with the production of mainly linear olefins by coordinated ethylene oligomerization on a Ni ion
- Intermediate temperature region: irreversible transformation of the Ni-ions which lowers the ethylene conversion
- High temperature region: increased acid (and metal ion) activity which leads to the production of a broad distribution of products.

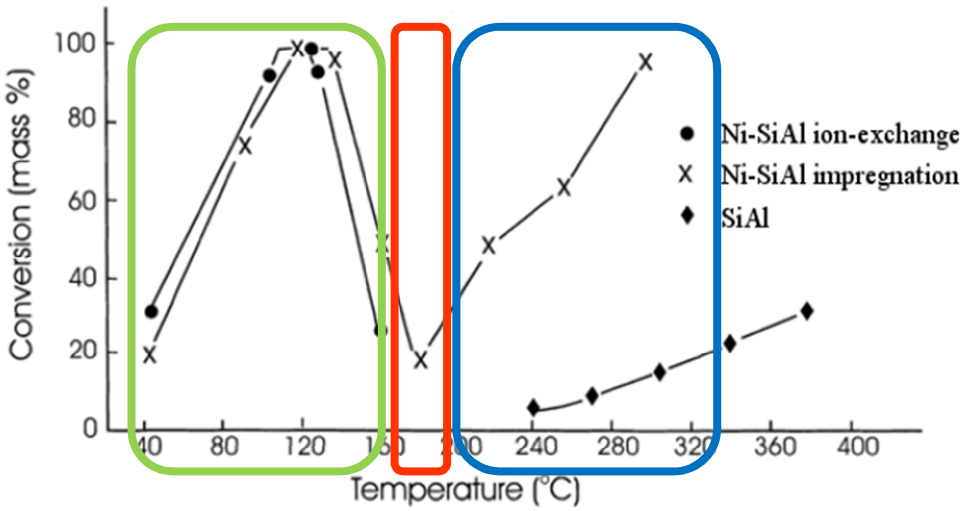

Figure 1-9: Temperature dependence of the ethylene conversion [14]

The irreversible transformation of the Ni-ions could explain the volcano-curve detected in the low temperature region. However, no fundamental explanation has already been provided. The results also show that the contribution of the nickel ions to ethylene conversion in both temperature regions is necessary to obtain significant conversions [14].

1.4.2.4 Influence of the reaction pressure

In this oligomerization case, the pressure dependency could not be assigned to the Principle of Le Chatelier. Since this states that with increasing partial pressure of ethylene, the reaction rate for the larger hydrocarbons is increasing, which is only applicable for equilibrium reactions[22]. However, the reaction is still favored with increasing pressure. This observation is in agreement with results obtained from experiments performed by Nicolaides et al[18]. Figure 1-10 shows the effect of increasing pressure on the amount of oligomers produced. A clear increase of production is obtained when the pressure is increased and the reason is probably due to the increasing oligomerization rate with this increasing partial pressure of the reactants.

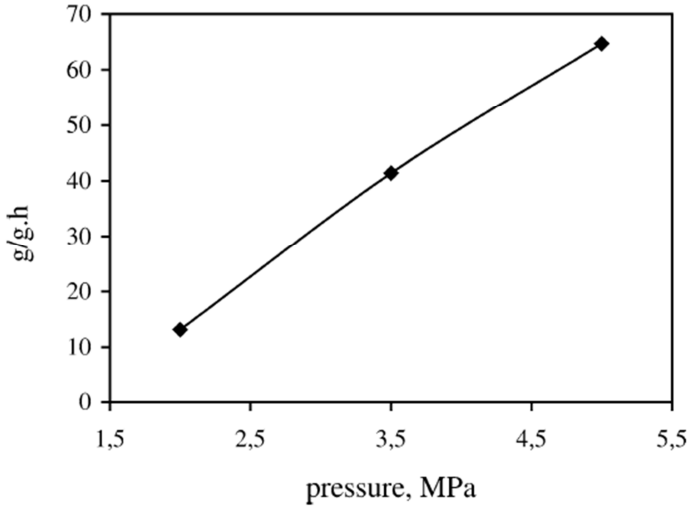

Figure 1-10: Influence pressure on conversion ethylene [22]

This increase of conversion is the main reason why ethylene oligomerization is performed at an ethylene partial pressure as high as possible [12].

1.4.3 Conclusion

Ethylene oligomerization can only result in the desired products by using a bifunctional catalyst. Every site type, i.e., metal ion or acid, lead both to different kind of reaction types. By changing their concentrations on the catalyst, the product distribution can be adjusted. Besides the catalyst properties, the reaction conditions, e.g., pressure and temperature, can have a significant influence on the product yield.

1.5 PRODUCT DISTRIBUTION

Paragraph 1.4 has shown that, depending on what kind of reactions occur, a completely different mixture of oligomers can be produced. Some reactions are more favored than others and this is influenced by the catalyst properties and the reaction conditions[21].

During ethylene oligomerization, chemicals and liquid fuels can be produced. The chemicals contain olefins from 1-butene to 1-octene. Otherwise liquid fuels can be produced in a range from gasoline to diesel.

1.5.1 Statistical distribution: *Anderson Schultz Flory* distribution

When only *true oligomerization* occurs, the product distribution is similar to the ASF-distribution with only even carbon numbered hydrocarbons. Starting from ethylene, especially butene, hexene and octene are produced by insertion. This can be seen in Figure 1-11 where the weight fraction of butene is the biggest one, and an increasing carbon number leads to a decreasing weight fraction. A deviation of this product distribution can be assigned to the acid catalyzed reactions by isomerization and beta-scission of carbenium ions. This way, the number of different products becomes larger. By allowing these acid reactions, also odd numbered alpha olefins are generated.

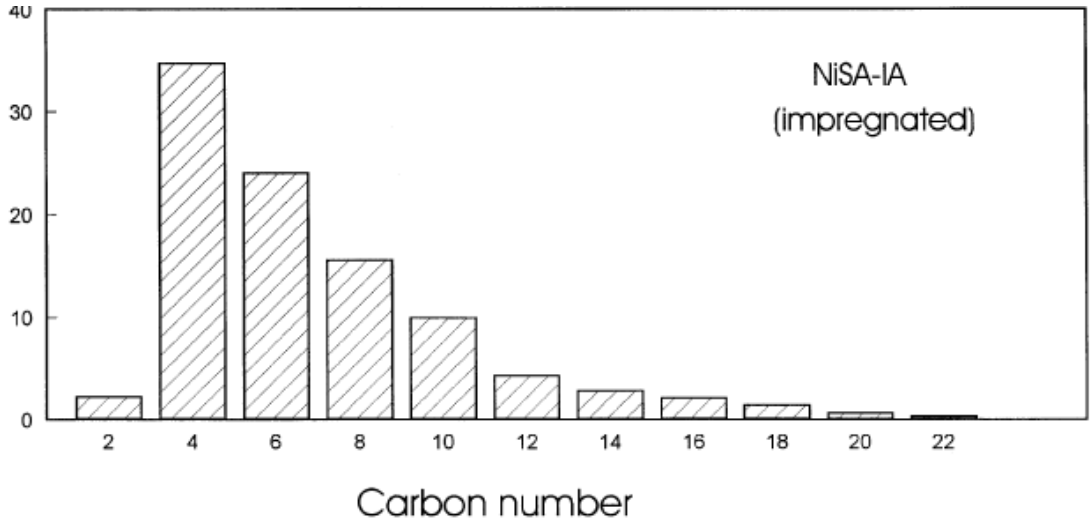

Figure 1-11: *Anderson Schultz Flory* distribution [14]

As an example, a deviation of this *ASF* distribution is given. The major deviation is the occurrence of dimerization of butene. This lowers the fraction of butene and increases the fraction of octene, meaning that the octene fraction is significantly greater than the hexene fraction, see Figure 1-12.This dimerization of butene goes through a carbenium reaction, caused by the presence of acid sites.

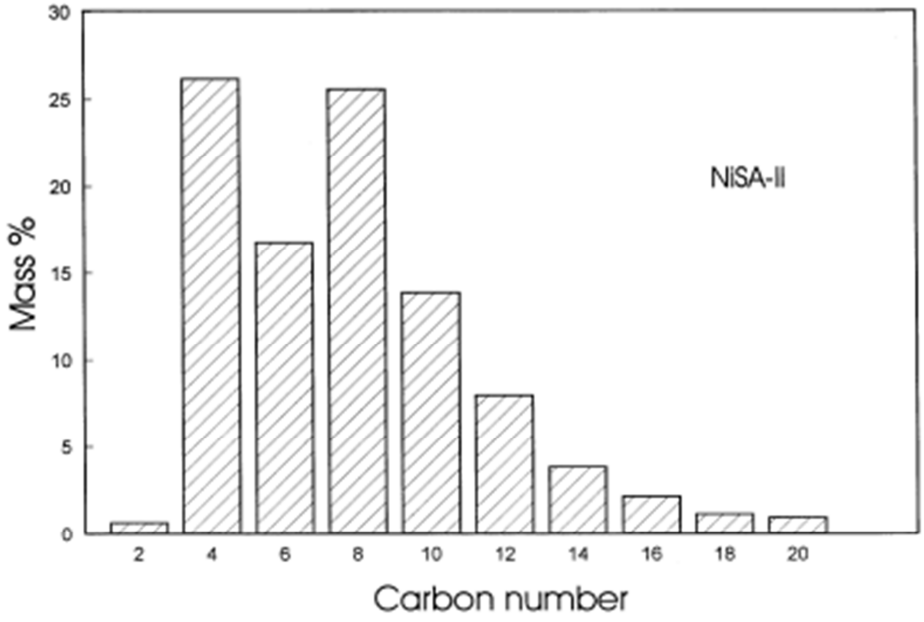

Figure 1-12: product distribution with deviation of ASF-distribution [14]

In Figure 1-13 the C_n distribution is plotted against similar catalysts with a different acid concentration and varying reaction temperature. For all the catalysts, C_4 olefins are the main oligomerization products at low temperature. NiY3, containing the lowest acid concentrations, obtains a near *Anderson Schultz Flory* type distribution. Over NiY1, a higher oligomerization towards C_6, C_8 and C_{10} was observed. However, at higher temperatures NiY3 also produces these longer olefins. This suggests the occurrence of secondary acid catalyzed reactions. This means that deviation of the ASF-distribution can occur by a higher temperature or an increase in acid site concentrations. Both aspects are substantiating the occurrence of secondary acid catalyzed reactions [21].

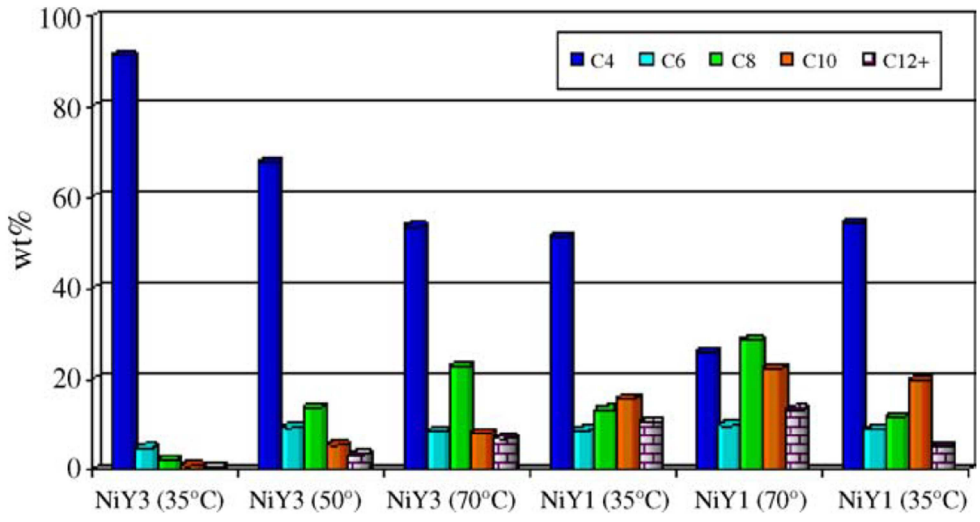

Figure 1-13: Oligomers distribution per carbon atom number [21]

1.5.2 Product types

In this thesis, besides alpha-olefins, a distinction between two main product groups will be made: gasoline and diesel. Starting from ethylene oligomerization, olefins are produced. To generate fuels for combustion engines, first hydrogenation should be performed to convert the olefins.

The easiest way to tell one kind of alkane from another, is by its boiling point. A boiling point represents the strength between the different molecules. It is a rough measure of the amount of energy needed to separate a liquid molecule from its nearest neighbor to form a gas molecule [23]. Conventionally, the boiling temperature increases with increasing chain length of the hydrocarbon. Short molecules have only weak interactions between each other, corresponding with a low boiling temperature, instead of longer chain molecules that can be wrapped in each other.

1.5.2.1 Characterization of products oligomerization

Besides high activity and no deactivation of the catalyst, also a desirable selectivity has to be obtained. With this selectivity, the weight fraction of the compounds in the output flow is considered. The number of carbon atoms of the products has to be high enough to be useable as fuel, e.g., gasoline, diesel or kerosene. Apart from fuel production, also chemicals can be produced. These chemicals can be used as additives in the petrochemical industry and for this, mainly alpha-olefins are obtained.

In this chapter, a brief description of each group of hydrocarbons will be given and their main properties will be elaborated. Two valuable indication numbers are used: the *cetane* and the *octane number*. These numbers classify the fuel in terms of its ignition quality. Cetane number for diesel describe the tendency to ignite spontaneously, and the octane number describes the resistance to auto-ignition of a gasoline fuel. Higher cetane numbered fuels generally give better performance in aspects such as emissions, noise and cold white smoke generations for the diesel engines. The higher the octane number, the more compression the fuel can withstand before detonating which is required for a gasoline engine. When this value would be too low, engine knocking could occur, which damages the engine.

Table 1-4 gives the properties of the some fueltypes.

Table 1-4: Properties of different fuels [24]

Fuel	Carbon atoms	Research octane number (RON)	Cetane number	Boiling point (°C)	Energy Content (MJ/litre)
Gasoline	C_5-C_{12}	92-98	0-5	37-205	34.6

Diesel	C_{12}-C_{22}	25	45-55	140-360	38.6
Kerosene	C_{10}-C_{18}			175-325	

- Diesel range products

Diesel range products have primarily a linear-chain structure and the specification of the cetane number is one of the important properties to be met. For a high performance diesel fuel, the cetane number should be higher than 50 [17].

Table 1-5: Cetane numbers of diesel range products obtained from oligomerization of ethylene, propene or 1-butene under different reaction conditions [17]

Test	Feed	T(K)	P(MPa)	MHSV (h^{-1})	Bromine number (gBr/100g)	Mid-boiling point (K)	Density/20°C (g cm^{-3})	Cetane number
1	Ethylene	383	3.5	2	84.2	493	0.8	60
2	Ethylene	493-553	2.5-3.5	1-3	32.4	511	0.8	37
3	Propylene	373	3.5	1.6	6.5	472	0.77	<34
4	Propylene	393	3.5	1.6	9	477	0.77	<34
5	Propylene	473	3.5	1.6	8.2	487	0.78	<34
6	Propylene	513	3.5	1.6	27.7	490	0.78	<34
7	1-Butene	363-373	3.5	1.4	0.9	477	0.78	<34
8	1-Butene	<488	3.5-4.5	0.6-6	25.9	483	0.78	<34

Heveling et al. concluded that oligomerization of ethylene produced the highest mass percentage of C_{10+} products in comparison with propene and butene at a reaction temperature of 120°C and pressure of 3.5 MPa [17]. Table 1-5 gives an overview of the cetane numbers of the diesel products produced by oligomerization of different products, e.g. ethylene, propylene and 1-butene. Concerning the ethylene oligomerization, an optimal cetane number is detected at low temperature. Whereas high temperature oligomerization of ethylene produces diesel with a cetane number that is too low and corresponds with a strong formation of branched olefins. When the results of ethylene are compared with propylene and butene, one can conclude that longer olefins lead to formation of branched hydrocarbons and consequently to lower cetane numbers. This shows that any contribution of acid catalysis has an undesirable effect on the formation of good quality diesel fuels.

Another observation, based on Table 1-5, is the influence of the temperature and the MHSV. A temperature increase leads to a decrease in the cetane number, but the increase of the MHSV has a positive effect on the cetane number.

For the production of diesel range products, the presence of secondary acid catalyzed reactions has to be avoided. Which means that in reality, catalysts containing less acid sites will be used or oligomerization will be performed at low temperature.

- Gasoline range products

Gasoline is a complex mixture, comprising more than 500 different hydrocarbons, with 5 to 12 carbon atoms. Small amounts of aromatics and cyclic alkane compounds are present but virtually no olefins and alkynes are present. Gasoline is most often produced by fractional distillation of crude oil. A typical composition of gasoline is given in Table 1-6.

Table 1-6: Composition of gasoline [23]

General name	Example	Weight percentage
Aliphatic-straight chain	Heptane	
Aliphatic-branched chain	Isooctane	30-50
Aliphatic-cyclic	Cyclopentane	20-30
Aromatic	Ethylbenzene	20-30

As already mentioned, the octane number is a specific property measurement of gasoline and defines its resistance to knock. It can be determined by comparing its characteristics to iso-octane and heptane. Iso-octane has an octane number of 100, and is a highly branched compound that burns smoothly, with little knock. Whereas heptane is a straight, unbranched chain with an octane number of zero due to its bad knocking properties [17].

Straight run gasoline has an octane number of 70 and contains mostly straight chain alkanes. But cracking, isomerization and other refining processes can be used to increase the octane rating to about 90. By expanding this idea to oligomerization of ethylene, the secondary reactions have to be promoted to increase the cracking and isomerization reactions. For a high value gasoline product, a high temperature and a high concentration of acid sites is necessary. This is just the opposite of the requirements for a proper diesel range product.

1.5.3 Conclusion

Both the temperature and the catalyst properties have a significant influence on the acid catalyzed reactions. The occurrence of this type of reactions (isomerization, cracking, etc.) defines the product distribution of the oligomerization of ethylene. By modifying the temperature or the catalyst properties, one type of product can be favored. Catalysts containing only metal ion sites, have a product distribution that is similar to an *Anderson Schultz Flory*-like distribution which exists of

mostly linear olefins. This corresponds with a diesel rang product mixture. When more isomerization and cracking reactions are allowed, gasoline fuels are produced.

1.6 INFLUENCE OF ZEOLITE FRAMEWORK ON REACTION OUTPUT

Bifunctional heterogeneous catalysts are used for ethylene oligomerization. As already indicated, the reaction conditions together with the catalyst properties, i.e., structure, metal ion to acid ratio,… define the product spectrum of the reaction. In this chapter, different catalyst frameworks will be studied. First, a general structure of a zeolite framework will be given, together with its main aspects and properties. Then, the most conventional frameworks will be discussed separately.

1.6.1 General structure of frameworks

1.6.1.1 Zeolites

Zeolites can be considered as the most widely used catalysts in industry. They become extremely successful in petro chemistry, oil refining and production of fine chemicals. Six specific features form the main reasons why zeolites play a key role in catalysis [25]:

- they have a high surface area and adsorption capacity,
- their controllability of the adsorption properties and the ease to modify their hydrophobic behavior,
- the strength and concentration of the active sites can be adjusted,
- the size of the channels corresponds with the dimensions of some interesting molecules and within the micropores, strong electric fields together with the electric confinement of the molecule are responsible for the pre-activation of the molecules,
- the shape selectivity of the different channels can modify the reaction rate and the selectivity towards several products and
- the chemical and thermal stability of the zeolites can be adjusted.

Generally, zeolites are crystalline aluminosilicates with the formula, $M_{(2/n)}O.Al_2O_3.ySiO_2$ where *n* is the valance of the cation M and *y* may vary from 2 to infinite. Zeolites are crystalline polymers based on a three-dimensional arrangement of TO_4 tetrahedra (SiO_4 or AlO_4-) connected through their oxygen atoms to form subunits and finally large lattices by repeating identical building blocks or unit cells. The structural formula of zeolites (i.e. the chemical composition of the unit cells) is the following:

$$M_{(x/n)}(AlO_2)_x(SiO_2)_y$$

Where *x+y* is the total number of tetrahedral per unit cell and *y/x* the atomic Si/Al ratio varying from a minimal value of 1 to infinite [26].

The most essential aspect of the zeolites is their engineering availability, which is the ease to modify their properties like crystal size, composition, polarity, etc.. By playing with the Si/Al ratio, addition of specific metal compounds, etc. the zeolite properties can be adjusted.

Within the zeolite group, a wide range of different structures can be found. Every framework has its own framework type code, derived from the name of the material type and consists of three letters. Table 1-7 gives the type codes of the six most researched zeolite frameworks for ethylene oligomerization. The MCM-structure is invented by Mobil employees and stands for Mobil Crystalline Material. MCM-22 and MCM-36 come from the same template structure, i.e., the MWW. Whereas the MCM-41 is an ordered mesoporous type on its own.

Table 1-7: Zeolite frameworks and corresponding structure[27]

Name	Framework type code	Structure
Beta	BEA	12-Ring structured
ZSM-5	MFI	10-Ring structured
MCM-22	MWW	10-Ring structured
MCM-36	MWW	10- Ring structured
Y-zeolite	FAU	12-Ring structured
MCM-41	MCM-41	

These zeolite structures can be modified easily, dependent on their industrial applications. Important modification methods exist like steaming, dealumination, cation-exchange and metal loading.

1.6.2 Influence of the properties of the catalyst framework

The three main framework aspects that could influence the stability and activity are the texture of the catalyst (amorphous vs. crystalline), the porosity and the metal ion/ acid ratio. Every aspect will be investigated in more detail in this section.

1.6.2.1 Porosity

The microporous character of some zeolite materials can lead to diffusion limitations which results in a rapid enrichment of polymeric waxes in the micropores [21]. This emphasis the importance of the pore size of the catalysts as one of the crucial variables affecting the stability and the activity of the catalyst.

Concerning the pores of a zeolite framework, the following classification is applicable is done [25]:

- Microporous: diameter < 2.0 nm
- Mesoporous: 2.0 nm < diameter < 50 nm
- Macroporous: diameter > 50 nm

The larger pores are beneficial to the diffusion of the longer heavy products and avoids deactivation of the catalyst. This means that an active and stable framework should contain no pores that are too small compared with the dimensions of the produced molecules. However, large pores also allows production of larger molecules that can deactivate the framework. This indicates that the effects of the porosity is still a subject of discussion, especially for the oligomerization mechanism.

Confinement is another effect that is present in zeolites due to its small pores, which influence the acidity and selectivity. This occurs by interfering in the way that the reactants are adsorbed, or even limit the formation of bulky intermediates [28].

1.6.2.2 Texture: amorphous vs. crystalline

The influence of the framework texture can be directly related to the accessibility and mobility of different molecules inside pores of the solid catalyst [13].

Amin et al. [20] have showed that with increasing crystallinity of a ZSM-5 catalyst, the ethylene conversion increases similar. This is because high zeolite crystallinity implies a high surface area and a more active catalyst [20]. This ensures the high mobility of the molecules and the ease to get into contact with the active sites.

1.6.2.3 Metal ion/acid site ratio

By varying the amount of metal ions or the Si/Al ratio of the framework, the metal ion to acid site ratio of the catalyst can be modified. This ratio has an influence on the product selectivity, due to its influence on the acidity of the zeolite and on the thermal and chemical stability.

For a long time it is known that the aluminum content in a zeolite influence the acidity, as proposed by Weisz [28]. The framework Si/Al ratio is a reflection of the number of potential acid sites. For each particular zeolite structure the acidity per active site reached a maximum value at a particular Si/Al ratio, which determines the acidic strength of the zeolite. High acid strength as well as high thermal and chemical stability are desirable properties that could be improved by increasing the framework Si/Al ratio [20]. Post-synthesis dealumination treatment is the most effective way to increase the Si/Al ratio by removing Al from the framework. However a too high density of acid sites can be responsible for a high deactivation during the oligomerization reaction. A high acid/nickel ion site

ratio results in rapid surface deactivation of Ni-containing materials due to acid catalyzed reactions, which are responsible for the formation of strong adsorbed long-chain oligomers [12]. The production of these heavy products is made possible by the acid sites present on the catalyst. These acid sites are responsible for the further transformation of the primary oligomers. A lot of investigation is already done on the pore size and the acidity of the zeolites to overcome this kind of deactivation[29]. However, no real solution is already obtained.

1.6.3 Types of frameworks

The most investigated catalyst frameworks for ethylene oligomerization will be discussed. Their stability and activity will be the main aspects.

1.6.3.1 Amorphous Silica-alumina

Amorphous silica-alumina is commonly used as a solid acid catalyst in a wide range of chemical processes, such as hydrocracking, isomerization and alkylation. By modifying the silica-alumina with Ni-atoms, an interesting catalyst for ethylene oligomerization can be prepared. Hulea et al. [12] have reported that Ni-exchanged amorphous silica-alumina is a very active and stable catalyst for ethylene oligomerization [12]. Besides its activity and stability, it is also considered to be a highly selective catalyst at low temperatures and elevated pressures.

Experiments have shown that both the oligomerization activity and the molecular size of the products increases with increasing acid strength of the support. Espinoza et al.[30] investigated the influence of the acid strength on the activity of the catalyst. Lighter products were obtained with catalysts having a lower acid strength. This indicated that the acid strength of the support both influenced the activity and the selectivity of the catalyst the most [30].

1.6.3.2 MCM-41 type catalysts

Mobile Crystalline Material (MCM) is a silicate that is obtained by a templating mechanism. The MCM-41 displays an ordered structure with uniform mesopores arranged into a hexagonal, honeycomb-like lattice. Because MCM-41 contains mesopores, it can overcome the problem of diffusion limitations and provide access to large molecules, when compared with the conventional zeolites structures.

Production of MCM-41 needs just like other zeolites a template to start from. For the synthesis of MCM-41 the same quaternary ammonium ions are used for zeolites with one modification, i.e., at least one of the short alkyl groups is replaced by a long alkyl chain, like a hexadecyl group [31]. By changing the length of the template molecule, the width of the channels can be controlled to be within 2 to 10 nm. The walls of the channels are amorphous SiO_2. Together with the exceptional

porosity (up to 80%), this makes of MCM-41 the least mechanically stable compared to other porous silicas and zeolites[32].

The main property for the use of MCM-41 zeolites for the ethylene oligomerization is the mesoporous structure. As already mentioned, the deactivation by blocking off the active sites can be reduced by using this meso- structures.

The Ni-exchanged AlMCM-41, with Si/Al >30 and large pores (d> 3nm), containing a medium acid strength and density of the active sites was tested by Lallemand et al [13]. Their experiments revealed that although the fact that the AlMCM-41 has interesting properties for selective ethylene oligomerization, some aspects limit their practical applications. The low hydrothermal and mechanical stability of the mesoporous MCM-41 structures was considered as the main reasons [13].

1.6.3.3 NiMCM-36 and NiMCM-22

Both MCM-22 and MCM-36 have the same layered precursor and corresponds with the two-dimensional MWW structure. This MWW structure zeolites possess two independent pore systems, see Figure 1-14. One system consists of two-dimensional sinusoidal 10-membered ring channels and the other is composed of large 12-memberded ring super cages connected by 10-membered ring channels [33].

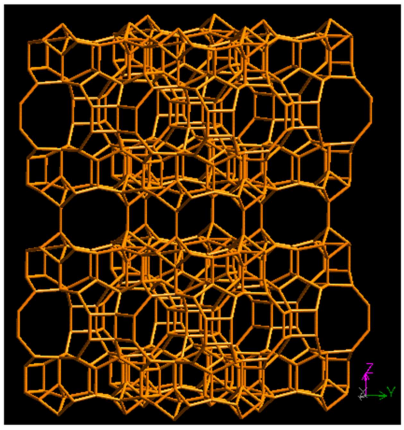

Figure 1-14: MWW zeolite structure [27]

Ni-exchanged MCM-36 has a dual-system of pores, with mesopores in the interlayer space. The mesoporous channels facilitate the diffusion of bulkier olefins obtained from the oligomerization process, which results in a lower deactivation rate and higher activity of this zeolite compared to the purely microporous NiMCM-22 catalyst [13]. MCM-36 zeolites have an acid site concentration that is significantly lower compared to MCM-22. Besides this dual porosity behavior and lower acidity, MCM-36 also consists of an amorphous structure, resulting from irregular arrangement of the pillars within the zeolite structure (dimensions and internal ordering) [13]. All these properties make of MCM-36 a more valuable zeolite for ethylene oligomerization than MCM-22.

1.6.3.4 Dealuminated ZSM-5

ZSM-5 is the most frequently used zeolite in the petroleum industry for hydrocarbon isomerization processes. It is a 10-membered sieve containing channel openings from 5.1 to 5.6 Angstroms, see Figure 1-15. ZSM-5 can also be used for oligomerization of ethylene. Increasing the ethylene conversion can be acquired by dealumination of ZSM-5. XRD-results have shown that dealumination of ZSM-5 affects the unit cell parameter and volume unit cells. These values decrease due to the removal of framework aluminium. This decrease can be attributed to the slight disorder of lattice structures and the increase in the crystallinity of the dealuminated ZSM-5 [20].

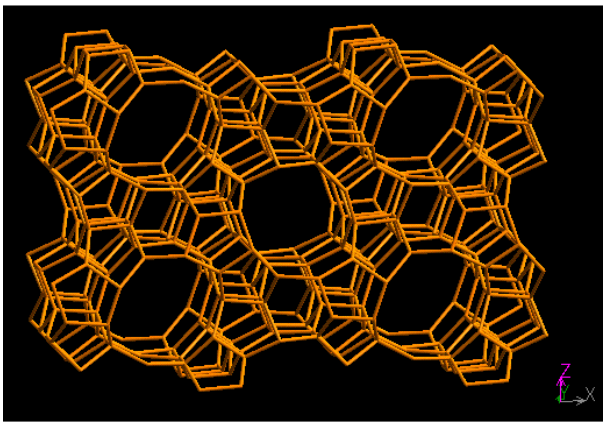

Figure 1-15: MFI zeolite structure [27]

For ethylene oligomerization over ZSM-5, both Brönsted and Lewis acid sites were observed to be active although lewis sites have a small advantage in suppressing the coke formation. The strong acid sites eliminated coke or aromatic formation and allowed only oligomerization to proceed. The amount of framework aluminium is related to the number of Brönsted acid sites.

1.6.3.5 Dealuminated Y-zeolite

The conventional Y-zeolite contains only micro pores within 12-membered structures. As already mentioned, for a good stability and activity, ethylene oligomerization prefers mesoporous materials. By dealumination of the Y-zeolite, a mesoporous structure can be obtained. This dealuminated Y-zeolite knows a lot of advantages in comparison with Y-zeolite: large supercages and pore volume, well controlled concentration and strength of the acid sites and high thermal and chemical stability [21]. However, due to the high density and strength of the acid sites, a significant deactivation during the reaction process could occur.

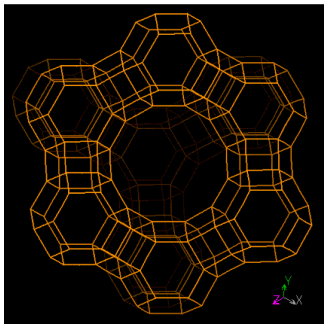

Figure 1-16: FAU zeolite structure [27]

Hulea et al. have done a comparison between a NiMCM-22, a dealuminated Y-zeolite and the mesoporous NiMCM-41. For the ethylene oligomerization the activity followed the order NiMCM-41>> NiUSY>>NiMCM-22. The main disadvantage of Ni-containing zeolites was the diffusion control of the oligomerization reactions what enhanced the blocking in the pores. The acid site concentration increases from NiMCM-22 to NiUSY and NiMCM-41 [34]. These results confirm the idea that the concentration of acid sites cannot be too high, due to blocking properties of the heavy waxes.

1.6.3.6 Ni-β catalyst

The Ni-β zeolite of the *BEA deviates from the other zeolites, because it doesn't consist of one pure crystal phase but of three polymorphs. It is a large pore zeolite (7.5 Å), with a three-dimensional interconnected channel system with 12-membered rings.

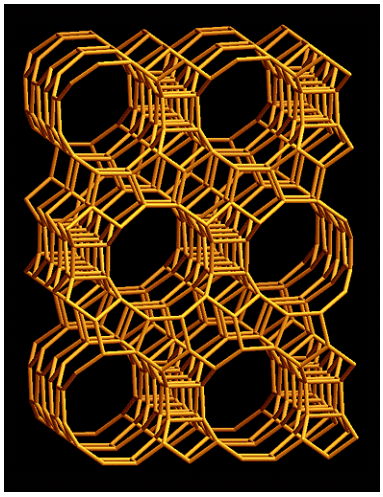

Figure 1-17: BEA zeolite structure[27]

No investigation is already been performed on the Ni-Beta catalyst for ethylene oligomerization.

1.6.4 Conclusion

Zeolites are the perfect catalysts for ethylene oligomerization. Their main advantage is their flexibility which makes it possible to modify the structure with properties desirable for the oligomerization reaction. For example addition of metal ion sites, modify the acid strength and concentration.

For ethylene oligomerization, the main aspects of the zeolite that have an influence on the product distribution are the porosity, the texture of the catalyst and the metal ion to acid site ratio. Every aspect has its specific way of influencing the activity and stability of the catalyst.

The most conventional zeolites that are used, were discussed. Al-MCM-41 seems to be the zeolite structure with the highest activity due to its mesoporous character. However, this framework also has the lowest thermal and chemical stability. Other frameworks, like dealuminated Y, have a high mechanical and chemical stability but will deactivate rather quickly.

1.7 CONCLUSION AND WORK SCOPE

Oligomerization of ethylene is an industrially valuable process and some investigation is already performed on this subject. This process can be catalyzed both by homogeneous and heterogeneous catalyst, but the latter is the most environmental friendly one. This heterogeneous catalyst is bifunctional, consisting of both acid sites and metal ion sites and which are equally important. Together with the reaction conditions, the catalyst has a significant influence on the product distribution. In this thesis, a difference is made between gasoline and diesel range products. The influence of the catalyst framework was also investigated. The most significant aspects of the framework, like porosity, texture and metal ion to acid site ratio were discussed. Finally, a collection of zeolite frameworks was mentioned. With this literature review, insight is gained in the reaction mechanism, properties of the catalysts and its frameworks.

The aim of this master thesis consists of two main aspects. First, an experimental study has to be performed with one specific catalyst, i.e., Ni-β catalyst. This experimental data will be used for the expansion of the kinetic model to estimate several catalytic and kinetic descriptors. Mainly the acid catalyzed reactions have to be implemented since in previous thesis the attention was put on the metal ion kinetics.

1.8 REFERENCES

1. *Oxidative coupling of methane followed by oligomerization to liquids: towards sustainable production of high quality fuels and petrochemicals*. Available from: www.ocmol.eu.
2. 2012; Available from: www.uniongas.com.
3. Bond, T. and M.R. Templeton, *History and future of domestic biogas plants in the developing world.* Energy for Sustainable Development, 2011. **15**(4): p. 347-354.
4. (ISAT), I.a.A.S.o.A.T. and D.G.f.T.Z. (GTZ), *Biogas Digest Volume I.* 1999.
5. Eggeling, G., G. Mackensen, and L. Sasse, *Production and utilization of biogas in rural areas of industrialized and developing countries*. 1985, Eschborn, Germany: Deutsche Gesellschaft für Technische Zusammenarbeit.

6. Wilde, W.D., *Oligomerisatie van Ethyleen naar Vloeibare Brandstoffen en Chemicaliën*, in *Laboratory for Chemical Technology*, 2009-2010, University of Ghent. p. 155.
7. Zimmermann, H. and R. Walzl, *Ethylene*, in *Ullmann's Encyclopedia of Industrial Chemistry*, 2000, Wiley-VCH Verlag GmbH & Co. KGaA.
8. *International chemical safety chards*. Available from: http://www.cdc.gov/niosh/ipcsndut/ndut0475.html.
9. *World Ethylene Market to Cross 160 Million Tons by 2015, According to New Report by Global Industry Analysts*. October 28, 2008 [cited 2012 3/10]; Available from: http://www.prweb.com/releases/ethylene/polyethylene/prweb1530734.htm.
10. Europe, A.o.p.p.i. *Western European market review*. [cited 2012 4/10]; Available from: http://www.petrochemistry.net/ethylene-production-consumption-and-trade-balance.html.
11. Griesbaum, K., et al., *Hydrocarbons*, in *Ullmann's Encyclopedia of Industrial Chemistry*, 2000, Wiley-VCH Verlag GmbH & Co. KGaA.
12. Hulea, V. and F. Fajula, *Ni-exchanged AlMCM-41—An efficient bifunctional catalyst for ethylene oligomerization.* Journal of Catalysis, 2004. **225**(1): p. 213-222.
13. Lallemand, M., et al., *NiMCM-36 and NiMCM-22 catalysts for the ethylene oligomerization: Effect of zeolite texture and nickel cations/acid sites ratio.* Applied Catalysis A: General, 2008. **338**(1–2): p. 37-43.
14. Heveling, J., C.P. Nicolaides, and M.S. Scurrell, *Catalysts and conditions for the highly efficient, selective and stable heterogeneous oligomerisation of ethylene.* Applied Catalysis A: General, 1998. **173**(1): p. 1-9.
15. K.Toch, J.W. Thybaut, and G.B. Marin, *Ethylene Oligomerization on Bifunctional Heterogeneous Catalysts: Model Development and Catalyst Optimization*, 2012: Laboratory for Chemical Technology, Ghent University, Krijgslaan 281-S5, B-9000 Gent, Belgium.
16. Fan, L., et al., *Theoretical Study of Ethylene Oligomerization by an Organometallic Nickel Catalyst.* Inorganic Chemistry, 1996. **35**(13): p. 4003-4006.
17. Heveling, J., C.P. Nicolaides, and M.S. Scurrell, *Activity and selectivity of nickel-exchanged silica-alumina catalysts for the oligomerization of propene and 1-butene into distillate-range products.* Applied Catalysis A: General, 2003. **248**(1–2): p. 239-248.
18. Nicolaides, C.P., M.S. Scurrell, and P.M. Semano, *Nickel silica-alumina catalysts for ethene oligomerization—control of the selectivity to 1-alkene products.* Applied Catalysis A: General, 2003. **245**(1): p. 43-53.
19. Caeiro, G., et al., *Activation of C2–C4 alkanes over acid and bifunctional zeolite catalysts.* Journal of Molecular Catalysis A: Chemical, 2006. **255**(1–2): p. 131-158.
20. Nor Aishah Saidina Amin, D.D.A., *Dealuminated ZSM-5 Zeolite Catalyst for Ethylene Oligomerization to Liquid Fuels* Journal of Natural Gas Chemistry, 2002: p. 79-86.
21. Lallemand, M., et al., *Catalytic oligomerization of ethylene over Ni-containing dealuminated Y zeolites.* Applied Catalysis A: General, 2006. **301**(2): p. 196-201.
22. Myers, R.L., *The basics of chemistry*, 2003, Greenwood. p. 392.
23. Ophardt, C.E. *Boiling points and structures of hydrocarbons*. 2003 [cited 2012 13/11]; Available from: http://www.elmhurst.edu/~chm/vchembook/501hcboilingpts.html.
24. association, E.A.m. *Main differences between petrol and diesel*. [cited 2012 6/11]; Available from: http://www.acea.be/news/news_detail/what_are_the_main_differences_between_diesel_and_petrol/.

25. Corma, A., *From Microporous to Mesoporous Molecular Sieve Materials and Their Use in Catalysis.* Chem. Rev., 1997: p. 2373-2419.
26. M. Guisnet, J.-P.G., *Zeolites for Cleaner Technologies (Catalytic Science Series, 3)*. 2002: World Scientific Publishing Company. 388.
27. Ch. Baerlocher, W.M.M., D.H. Olson, *Atlas of zeolite framework types*, 2001, Elsevier.
28. Oliveira, P., et al., *Light olefin transformation over ZSM-5 zeolites with different acid strengths – A kinetic model.* Applied Catalysis A: General, 2010. **384**(1–2): p. 177-185.
29. Heydenrych, M.D., C.P. Nicolaides, and M.S. Scurrell, *Oligomerization of Ethene In a Slurry Reactor Using a Nickel(II)-Exchanged Silica–Alumina Catalyst.* Journal of Catalysis, 2001. **197**(1): p. 49-57.
30. Espinoza, R.L., et al., *Catalytic oligomerization of ethene over nickel-exchanged amorphous silica-aluminas; effect of the acid strength of the support.* Applied Catalysis, 1987. **29**(2): p. 295-303.
31. Lensveld, D.J., et al., *Synthesis and characterisation of MCM-41 supported nickel oxide catalysts.* Microporous and Mesoporous Materials, 2001. **44–45**(0): p. 401-407.
32. Gusev, V. *MCM-41*. Available from: http://www.chm.bris.ac.uk/motm/mcm41/mcm41.htm.
33. Liu, L., et al., *Synthesis, characterization, and catalytic properties of MWW zeolite with variable Si/Al ratios.* Microporous and Mesoporous Materials, 2006. **94**(1–3): p. 304-312.
34. Hulea, V., Lallemand M. , F.Fajula, A.Finiels, *Catalytic oligomerization of ethylene over Ni-containing MCM-22, MCM-41 and USY*, in *Molecular sieves: From Basic research to industrial applications*, 2005.

Chapter 2 Procedures

The two main aspects of this work are performing an experimental study and expanding the kinetic model of the oligomerization reaction. In this chapter both the treatment of the experimental analysis and the parameter estimation will be discussed. The experiments are performed on the High Throughput Kinetic setup (HTK-1). First a description of the setup and its different sections will be given. Once experiments are performed, the results have to be evaluated. By comparing the output of the experiments at different reaction conditions, trends in the catalyst behavior can be determined. With the aid of these experiments, the model can be verified and parameters have to be estimated. The validation of the estimations is performed with several statistical tests that will be explained in this chapter.

2.1 EXPERIMENTAL SETUP

The experimental work on the oligomerization of ethylene is performed on the High-Throughput kinetic setup (HTK-1), constructed by Zeton B.V.. This reactor setup is especially designed for the experimental study of the multiphase kinetics of hydrocarbons. It consists out of 8 different plug flow reactors that are grouped per two in one furnace (see Figure 2-1). Reactor 3 is used for the experiments on the oligomerization of ethylene. Figure 2-2 shows the reactor setup with its analysis section.

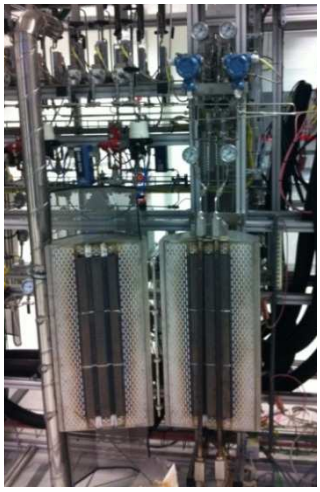

Figure 2-1: HTK-1: reactor grouped in one furnace

Figure 2-2: HTK-1: analysis section

A general flow scheme of one reactor can be found in Figure 2-3. On the overview, six different sections can be distinguished: the reactor section, the reactor overpressure safety system, the gas feed section, the liquid feed section, the back pressure system and the analysis section. The installation has both manual and pneumatic valves. The pneumatic valves are controlled with LabVIEW®. This program also controls the temperature, pressure and flow rates within the reactors. The manual valves are added to assure safe operation of the units.

The three most essential sections for controlling experiments will be discussed in detail: the feed section, the reaction section and the analysis section.

2.1.1 Feed section

The feed section can contain a liquid feed and several gas feeds which can be mixed together and sent to the reactor tube with different flow rates. For the oligomerization experiments, only a gas phase will be present and no liquid is sent to the reactor. Therefore, this liquid feed will not be discussed further.

Three different gases are sent to the oligomerization reactor, i.e. ethylene, methane as an internal standard and nitrogen. The nitrogen is necessary to make sure that the final products remain in the gas phase. A more detailed discussion of the inlet composition can be found in Chapter 3. Both the manual and the pneumatic valves have to be opened to ensure gas flow to the reactor.

The gas flows to the reactor are regulated by thermal mass flow controllers (Bronkhorst®) and are expressed in norm liters per hour (at 273K and 0.1MPa). Three different mass flow controllers are available: type 1 (max 10Nl h^{-1}), type 2 (max. 100 Nl h^{-1}) and type 3 (max. 1000 Nl h^{-1})[1]. Every controller is calibrated for a certain reference gas at a specified temperature and pressure. When

using a different gas at another pressure, a conversion factor has to be calculated in order to define the setup value for the labVIEW® interface.

$$F_2 = F_1 . CF \tag{2-1}$$

With CF: conversion factor

F_1: real flow rate through the controller

F_2: flow rate that has to be set in the LabVIEW® interface.

This conversion factor is calculated with the web application Fluidat ® that can be found on the web. A more elaborated discussion of the mass flow controllers can be found in the master thesis of W. De Wilde [1].

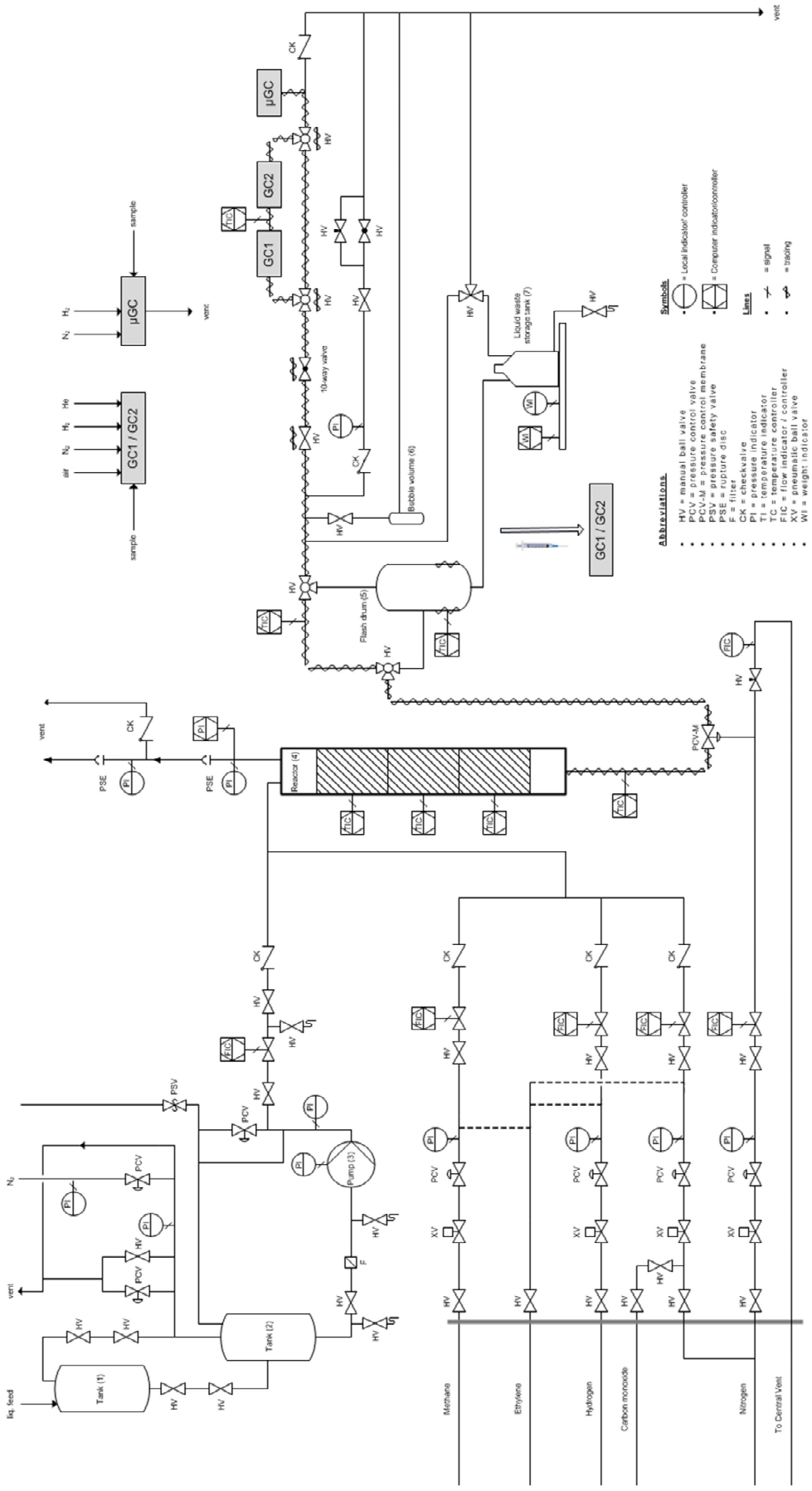

Figure 2-3: High Throughput Kinetic set up [2]

2.1.2 Reaction section

The eight reactor tubes present in the global HTK-1 setup can be regulated individually. Every reactor is put with another reactor in a single reactor block. Within one block, the temperature and the pressure can be regulated. The reactor tube consists out of steal that allows pressures up to 204barg and a temperature up to 922K. The gas and liquid flow rates can be regulated for every tube individually.

The temperature is measured with two thermocouples. One is placed within the reactor tube, and measures the temperature in the catalyst bed and the other thermocouple is placed at the outlet wall of the tube. Either thermocouple can be used to control the temperature. For measuring intrinsic kinetics, it is more interesting to use the one placed within the catalyst bed. Since this one gives the exact temperature. However, using that thermocouple has one main disadvantage: when changing the temperature, there is a longer dead time compared when measuring with the other thermocouple. This can lead to a higher overshoot or undershoot of the temperature.

Besides the temperature, a good control of the pressure is also essential, wherefore the control occurs through a back pressure system. The reactor effluent flows along one side of the membrane. Along the other side, nitrogen is sent. The nitrogen flow is controlled to assure a buildup of the pressure to the input value. The reactor effluent will only flow towards the analysis section, when the pressure at the reactor side of the membrane is slightly higher than the back pressure.

As already mentioned above, condensation of the reactor effluent should be avoided. In order to do this, tracing and an infrared furnace is available to heat the reactor outlet and the transfer lines to the analysis section.

2.1.3 Analysis section

2.1.3.1 Analysis of gas and liquid phase

The analysis section is divided into two main parts, analysis of the liquid phase and analysis of the gas phase. Both phases are separated in a flash drum at a temperature of maximum 313K and atmospheric pressure. The gas lines from the flash drum up to the analysis equipment are heated up to 373 K to avoid condensation. In this case, only the gas section was used.

2.1.3.2 Specifications of chromatogram

The analysis is performed with a gas chromatograph of the type Agilent Technologies 6850 series II network GC system. By using EZ Chrom software, the GC results can be analyzed and this information can be used to obtain conversion and selectivity values. The detector is a Flame Ionisation Detector

(FID) and is based on the detection of ions that are formed by combustion of the compounds into a hydrogen flame. The quantity of ions produced is proportional with the concentration of the compounds in the mixture. This makes it possible to detect the different compounds and their quantity. It is necessary to use a correction factor to obtain quantitative results because the FID has a different sensitivity dependent on the compound. For hydrocarbons, these correlation factors are all determined to be close to 1 [3].

2.2 CATALYST AND REACTOR LOADING

2.2.1 Catalyst type and characterization

The catalyst used for the experimental study is a Ni-β catalyst. The catalyst consists of nickel (4.89wt%) that is impregnated on a BEA-zeolite. A basic characterization of the catalyst was performed, i.e. XRD, NH_3-TPD, N_2-adsorptie and ICP/AES. A summary of the characteristics of the Ni-B-imp-4 catalyst are given in Table 2-1:

Table 2-1: Characteristics of Ni-beta catalyst

Characteristics	Ni-β catalyst
Nickel content [wt%]	4.89
Alumina content [mol%]	3.06
Silicium content [mol%]	37.87
Si/Al-ratio	12.48
BET-surface area [$m^2\ g^{-1}$]	458.32
Acid site concentration (Strong) [$mmol\ g^{-1}$]	0.634

The results of the NH_3-TPD of the Ni-B-imp-4 catalyst is given in Figure 2-4.

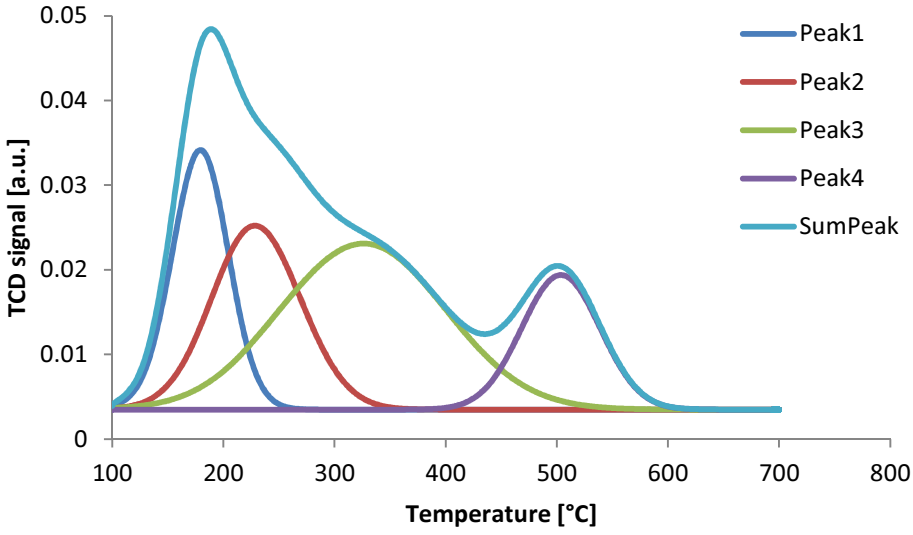

Figure 2-4: Ammonia TPD of Ni-β catalyst

When comparing the peaks with the results of the NH_3-TPD results obtained by Ramos Pinto. Et al. [4], the same results are obtained. The first peak corresponds with pure phsysisorped NH_3. The other three peaks were also detected during NH_3-TPD-experiments on a H-BEA zeolite in literature. Peak 2 corresponds with the weak acid sites, the third peak with the strong acid sites and the peak with its maximum around 500°C represents the strongest acid sites available.
The concentration of the different type of acid sites can also be calculated with the TPD-results. The peak area corresponds with the amount of NH_3 molecules chemisorped with the acid sites. XRD results, given in Appendix C, indicate the presence of a NiO phase. This shows that with such a high nickel loading, i.e., 4.89wt%, no real dispersion over the catalyst surface was obtained.

2.2.2 Reactor loading

Loading of the catalyst in the reactor tube has to be done very carefully because it can have a significant effect on the experimental results. The catalyst is a fine powder and when this would be used in the reactor tube, the catalyst would be blown out of the reactor by the gas flows to the analysis section. To avoid this, the catalyst is pelletized. The diameter of the pellets is determined by correlations to avoid transport limitations, see Chapter 3, and is in the range of 300 to 560 µm.

To make sure that the catalyst is placed in the middle of the reactor bed, first some inert material, i.e., alumina, is placed. When the catalyst would be placed at the entry of the tube, no good preheating and mixing of the gasses would be assured. The inert material has three different sizes: the smallest are from 0.5-0.8 µm, the middle-size ones from 1.5-1.8 µm and at last the biggest particles,i.e. 3 mm, that prevent any of the smaller ones for being blown out of the reactor, see Figure 2-5.

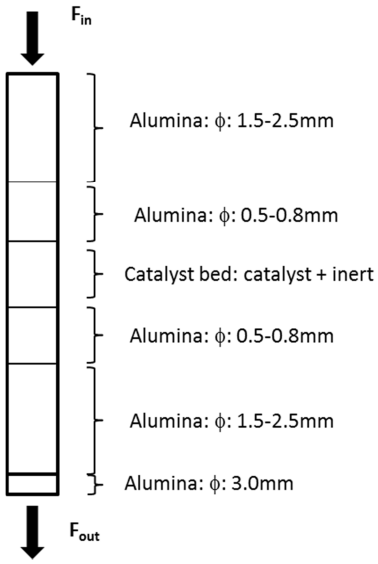

Figure 2-5: Catalyst bed loading [1]

The catalyst bed itself consists of catalyst pellets diluted with inert material of the smallest size (0.5-0.8 µm). For every experiments, 0.5g of catalyst is mixed with 10.0g of inert. This dilution was determined to minimize the temperature increment and for measering intrinsic kinetics. The determination of this dilution will be explained in Chapter 3.

Before an experiment can be performed, the catalyst has to be pretreated. The reactor is heated up to 573K under a nitrogen flow during a period of ca. 14h, i.e., a whole night. After this pretreatment at atmospheric pressure, the desired reaction conditions can be entered. Once an experiment is finished, the Ni-β catalyst has to be replaced by fresh catalyst due to relative fast and irreversible deactivation.

2.3 ANALYSIS AND CALCULATIONS

2.3.1 General definitions

When experimental data has to be processed, relevant definitions have to be used. With these definitions, comparison between different experiments can be performed. The information that is obtained with experiments is usually the outlet molar flow rate of the different compounds, whereas the inlet flow rates are given.

To compare results, two definitions are used: the conversion of reactant A and the selectivity towards product B. The conversion of reactant A defines the relative amount of moles of reactant A that is converted. The selectivity towards component B can be defined on an element molar basis, in this case of carbon.

$$X_A = \frac{F_{A,0} - F_A}{F_{A,0}} \tag{2-2}$$

$$S_{B,A} = \frac{a_{t,B}.(F_B - F_{B,0})}{a_{t,A}.(F_{A,0} - F_A)} \tag{2-3}$$

With $F_{A,0}$ the molar inlet flow rate of component A, F_B the molar outlet flow rate of component B and $a_{t,\,A}$ the number of t atoms in component A. Another variable is the yield of component B, which is the ratio of the total molar flow rate of component B that is produced to the inlet molar flow rate of reactant A.

$$Y_{B,A} = \frac{(F_B - F_{B,0})}{F_{A,0}} = S_{B,A}.X_A \tag{2-4}$$

Two other aspects concerning the loaden of the catalyst are the space time and the weight hourly space velocity (WHSV). The space time is the ratio of the catalyst mass to the inlet molar flow rate of the feed [kg_{cat} s mol^{-1}]. The WHSV defines the inlet mass flow rate of the feed divided by the catalyst mass in the reactor [kg s^{-1} kg_{cat}^{-1}] and is a more industrial used number than space-time.

$$\tau = \frac{W}{F_A} \tag{2-5}$$

$$WHSV = \frac{F_{wt,A}}{W} \tag{2-6}$$

Together with the temperature and the pressure, the space time defines the reaction conditions. The conversion, selectivity and yield are then used to describe the reactor output and the results of the experiment.

2.3.2 Interpretation and calculation of the chromatogram results

The composition of the reactor effluent is determined by a gas chromatogram. An example of a chromatogram is given in Figure 2-6. Every peak corresponds with one (or more)compound(s), i.e. the compounds can be identified by means of the retention time.

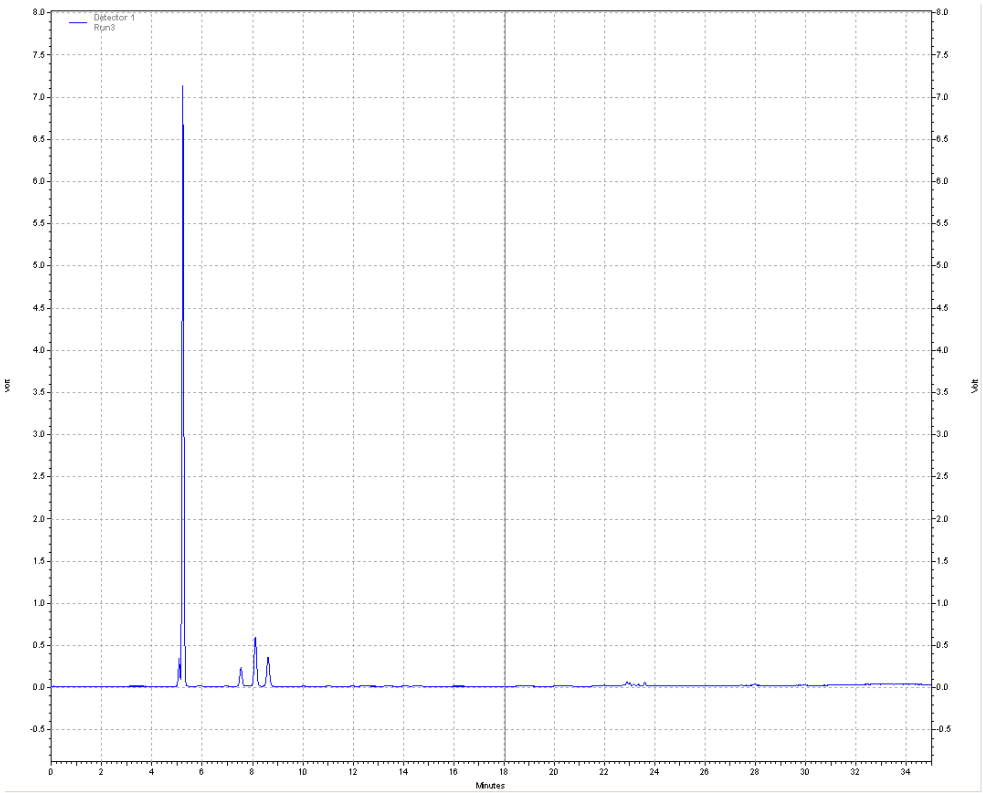

Figure 2-6: Chromatogram of ethylene oligomerization

As can be seen in the figure, a clear separation of the different peaks is necessary. This can be modified by chosing a proper GC-method. The temperature, heating rate, the inlet flow rate,… have significant influences on the retention times of the compounds. An optimized method was created and can be found in Appendix A. By adaptation of the method, a better separation of the butene isomers was found, see Figure 2-7 and Figure 2-8.

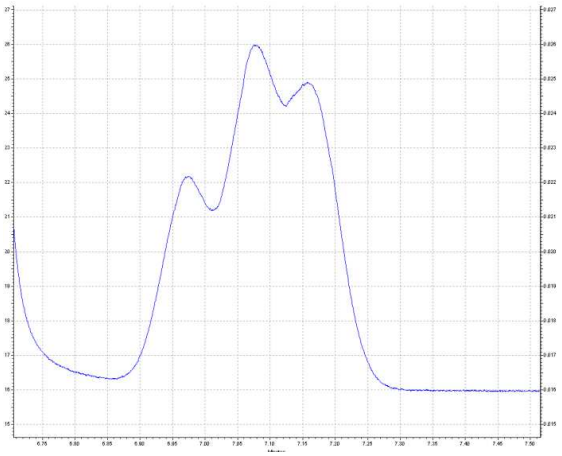

Figure 2-7: Peak corresponding with C_4 compounds with first GC-method

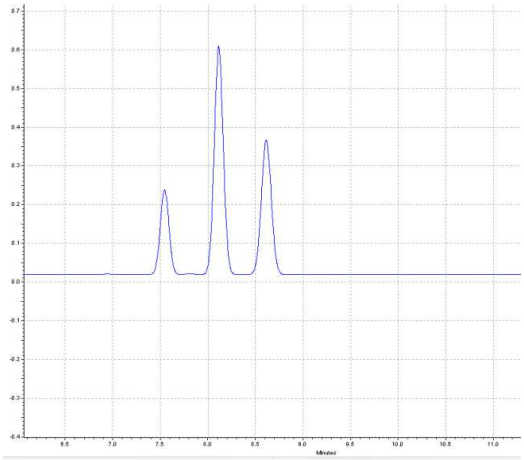

Figure 2-8: Peak corresponding with C_4 compounds after determination new GC-method

The peak surface area on the chromatogram of a certain compound is correlated with its amount. The sensitivity of the *FID* depends on the compound by means of the relative responsfactors, described by Dietz [3]. Two factors are described, i.e., the thermal respons factor (*TR*), which leads to molar fractions, and the weight factor (*WF*), leading to mass fractions. These two factors are related by the equation (2-7).

$$WF_i = \frac{MW_i}{TR_i} \tag{2-7}$$

With MW_i as the molecular weight of component *i*. By dividing the peak area by TR_i, the corrected peak surface areas are found. Once the real peak surface areas are determined, the mass fraction of the compounds can be calculated with the normalization method.

$$A_{correct,i} = \frac{A_i}{WF_i} \tag{2-8}$$

$$x_{wt,i} = \frac{A_{correct,i}}{\sum_i A_{correct,i}} \tag{2-9}$$

Once the mass fractions are determined, the molar fractions are calculated by means of equation (2-10).

$$x_{mol,i} = \frac{\frac{x_{wt,i}}{MW_i}}{\sum_i \frac{x_{wt,i}}{MW_i}} \quad (2\text{-}10)$$

Before the normalization method can be applied, first a control of the integration of the GC has to be done. By performing an error analysis, a specific procedure has been recommended [6]:

1. Define the outlet flow rates
2. Verification of the mass balance
3. Application of the normalization method to calculate the conversions and selectivities

In this case, the outlet flow rates are defined by using an internal standard. In the oligomerization experiments, methane was chosen as an internal standard, since it is not reactive and formed under the reaction conditions tested. The internal standard is only added in small amounts, circa 5 mol% of the inlet flow. The outlet molar flow rate of every component can be determined when the molar fraction of the component and the total molar outlet flow rate is known, which is calculated via the known inlet, F_{IS}^0 and thus the outlet flow rate of the internal standard:

$$F_i = \frac{F_{IS}^0}{x_{mol,IS}} . x_{mol,i} \quad (2\text{-}11)$$

Once, the molar flow rates are determined, the carbon balance can be verified. A deviation of the carbon balance can be the result of a leak or an indication that not all the compounds were integrated on the GC. The carbon balance can be calculated as the ratio of the outlet molar carbon flow rate to the inlet molar carbon flow rate.

$$Carbon\ balance = \frac{F_{C,out}}{F_{C,in}} \quad (2\text{-}12)$$

The carbon balance has been checked for experiments containing a high inlet flow rate of methane. Due to the fact of a difficult distincion between the methane peak and the ethylene peak, together with a possible instability of the methane controller at low inlet values, some deviations of the mass balance were detected. However, these were small enough to ignore, i.e., less then 5%.

Finally, the normalization method is used to determine the outlet molar flow of the different components. With the molar and mass flows, the conversion and selectivities can be calculated using the equations (2-13) and (2-14). These mass flow rates are determined with the use of the inlet mass flow rates.

$$F_{wt,i} = x_{wt,i}.F_{wt,i,0} \tag{2-13}$$

$$F_{mol,i} = \frac{F_{wt,i,0}/MW_i}{\sum_i F_{wt,i,0}/MW_i} \tag{2-14}$$

2.4 REACTOR MODEL

The experiments are performed in a(n ideal) fixed bed isothermal plug flow reactor and can be modelled by the following set of differential equations, with for every compound *i* a different equation [7]:

$$\frac{dF_i}{dW} = R_i \tag{2-15}$$

These nonlinear differential equations are a result from the mass balance over the plug flow reactor. After taken into account one boundary condition for every compound, the set of equations can be solved. The boundary conditions indicates that reaction only occurs once the flow reaches the catalyst:

$$F_i = F_{i,0} \; at \; W = 0 \tag{2-16}$$

With R_i the netto production rate of the component *i* and *W* the catalyst mass [kg].

These equations will be used in the parameter estimation model to simulate the reactor. The production rates follow from the kinetic model and are dependent of the temperature, the partial pressure of the compounds and the performance of the catalyst.

2.5 PARAMETER ESTIMATION

Once experimental data is obtained, the estimation of unknown model parameters can be executed. These parameters give an insight in the reaction mechanism and are associated with the kinetic model of the oligomerization. Both kinetic descriptors, e.g., pre-exponential factors and activation energies, and catalyst descriptors, like protonation enthalpies have to be estimated.

2.5.1 Determination optimal parameters

The estimation of the varous parameters is performed by minizing the residual sum of squares S(β), by adjusting the β-vector, containing the parameters. This function S(β) can be written as follows:

$$S(\beta) = \sum_{j=1}^{n_{exp}} \sum_{i=1}^{n_{resp}} w_i . (F_{i,j} - \widehat{F_{i,j}})^2 \quad (2\text{-}17)$$

With $F_{i,j}$ and $\widehat{F_{i,j}}$ the measured (experimental), resp. calculated molar outlet flow rate of experiment *j* and component *i*. w_i is the weight factor that allows to indicate the importance of the response variable. This weight factors are the inverse of the diagonal elements of the covariance matrix of the experimental errors:

$$w_i = \frac{1}{\sigma_{ii}^2} = \left[\frac{\sum_{j=1}^{n_{exp}} (F_{i,j} - \widehat{F_{i,j}})^2}{n_{exp} . n_{resp} - n_{par}} \right]^{-1} \quad (2\text{-}18)$$

To minimize the function S(β), different optimization methods exist. In the oligomerization model, a combination of the Rozenbrock and the Levenberg-Marquardt method is used. In the first part of the minimization, the Rosenbrock method is used, since this method has the smallest chance to diverge in case the values of the parameters are far away from the optimum. Once the function minimum is approached close enough, the Levenberg-Marquardt method further minimizes the function [8].

Due to the fact that the system is a nonlinear regression problem, next to the one global minimum, also local minima exists. This indicates the importance of the initial guess of the parameters.

2.5.2 Statistical analysis of the regression

Once the optimization has reached an optimal parameter vector, the regression has to be tested on its accuracy and significance.

2.5.2.1 Significance of the regression

The global significance of the regression is verified with the use of the F test. With this test the hypothesis of all parameters simultaneously equal to zero is tested. Therefore, a calculated *F* value, calculated as the ratio of the regression sum of squares to the residual sum of squares, both corrected for their freedom degrees, and the tabulated F value are compared. The tabulated *F* value is dependent on the degrees of freedom.

$$F_{calc,sign} = \frac{\frac{\sum_{i=1}^{n_{ob}} \sum_{j=1}^{n_{resp}} w_j \widehat{F_{i,J}}^2}{n_{par}}}{\frac{\sum_{i=1}^{n_{ob}} \sum_{j=1}^{n_{resp}} w_j (F_{i,j} - \widehat{F_{i,j}})^2}{n_{ob} n_{par} - n_{par}}} \quad (2\text{-}19)$$

The regression is significant if $F_{calc,\ sign}$ is greater than the value of $F_{tab(\alpha=0.05)}(n_{par},\ n_{ob}.n_{par}\text{-}n_{par})$.

2.5.2.2 Significance of the parameters

The confidence interval in which the individual parameter value is valid with a certainty of α is given by:

$$b_i - t_{tab,\alpha}\left(n_{obs}.n_{resp} - n_{par}\right)\frac{b_i}{\sqrt{V(b)_{ii}}} < b_i < b_i + t_{tab,\alpha}\left(n_{obs}.n_{resp} - n_{par}\right)\frac{b_i}{\sqrt{V(b)_{ii}}} \quad (2\text{-}20)$$

Where b_i is the value of the estimated parameter and $V(b)_{ii}$ is the element on position *(i,i)* of the covariance matrix *V(b)*. A commonly used value for α is 0.95.

The significance of the estimated parameters is tested with comparison of the calculated *t*-value and the tabulated *t*-value, which is dependent on the degrees of freedom. Just like in the *F* test, the calculated *t*-value has to be higher than the tabulated *t*-value to obtain a significant parameter estimation. To calculate the *t*-value, the next equation is used:

$$t_{calc} = \frac{b_i}{\sqrt{V(b)_{ii}}} \quad (2\text{-}21)$$

When the tested parameter is given to be non-significant, the zero-hypothesis can be applied for this parameter.

2.5.2.3 Binary correlation of the parameters

The binary correlation of the parameters defines the influence of the change of one parameter on the value of another parameter. The smaller the binary correlation between two parameters, the better because then it is sure that the parameters are all independant of each other. In practice, the binary correlation coefficients should be smaller than 0.95.

$$\rho_{i,j} = \frac{V(b)_{ij}}{\sqrt{V(b)_{ii}.V(b)_{jj}}} \quad (2\text{-}22)$$

2.6 CONCLUSION

In this chapter, several valuable concepts are discussed that make it possible to obtain both experimental data and significant parameters values. These concepts will be used in this work to perform the experimental study on the Ni-β catalyst. Once this data is obtained, it can be used to estimate the parameters and by using the different statistical tests explaind in this chapter, the significance of these parameters values can be verified.

2.7 REFERENCES

1. Wilde, W.D., *Oligomerisatie van Ethyleen naar Vloeibare Brandstoffen en Chemicaliën*, in *Laboratory for Chemical Technology*, 2009-2010, University of Ghent. p. 155.
2. Toch, K., *High-Throughput Kinetic Setup (HTK-1): Manual and safety guidelines*, 2012.
3. Dietz, W.A., *Response Factors for Gas Chromatographic Analyses.* 1966.
4. Pinto, R.R., et al., *Correlating NH3-TPD and 1H MAS NMR measurements of zeolite acidity: proposal of an acidity scale.* Applied Catalysis A: General, 2005. **284**(1–2): p. 39-46.
5. Louis, B., S. Walspurger, and J. Sommer, *Quantitative Determination of Brönsted Acid Sites on Zeolites: A New Approach Towards the Chemical Composition of Zeolites.* Catalysis Letters, 2004. **93**(1-2): p. 81-84.
6. Toch, K. and G.B. Marin, *Calculation of outlet composition, flow rates, conversions and selectivities in continuous flow (multiphase) reactors.* 2011.
7. Marin, G.B., *Chemische reactoren: principes en toepassingen.* Universiteit Gent, 2008.
8. Thybaut, J.W., *Kinetische modelbouw en simulatie* 2011.

Chapter 3 Experimental study of ethylene oligomerization

One main part of this thesis is the experimental study of bifunctional catalyzed ethylene oligomerization. For this purpose, a Ni-β catalyst was chosen. This catalyst is known to have acid sites, which favor the carbenium involved reactions. A broad range of reaction conditions is tested. This gives information about the selectivity and the behavior of the catalyst. It is however necessary to obtain intrinsic information, otherwise not only the effect of the catalyst and reaction conditions will be measured, but also diffusion limitations, etc. would influence the experimental results.

This chapter contains the methods and the criteria that were used to verify if intrinsic kinetics is measured. Secondly, the influences of the reaction conditions, like temperature and pressure, and the catalyst properties, e.g., selectivity, product distribution, deactivation, etc. on the experimental results will be discussed. The Ni-β activity will be compared with the behavior of the reference catalyst, i.e., 1.8wt%Ni-SiO_2-Al_2O_3. Finally, based on the experimental data, a possible reaction network will be proposed.

3.1 REACTION CONDITIONS FOR WORKING IN GAS PHASE

Before any experiment can be performed, the reaction conditions at which valuable information is obtained have to be determined. For the HTK-1 setup, a good analysis is assured when the compounds are in gas phase in both reactor and analysis section. Therefore, the reaction conditions for working in gas phase are determined first.

During experiments, several compounds are produced. Only a small amount of liquid production at normal conditions is expected, due to the low ethylene molar flow rate and the rather limited

conversion to higher hydrocarbons. However, even a small amount of liquid phase present in the reactor setup, leads to flow problems in the analysis section.

To ensure the gas phase condition of the compounds in the reactor, the transfer lines and the analysis section are heated. There is however a limit on this temperature, so also other measures have to be taken. Another simple way to avoid condensation is by dilution of the ethylene inlet flow. A mixture of ethylene and nitrogen is send into the reactor. This assures that only a small amount of larger hydrocarbons are produced and these compounds will not condensate at the given reaction conditions. These larger hydrocarbons have a higher boiling point which favors condensation.

With Aspen©, the nitrogen dilution necessary to work in gas phase was determined. The oligomerization of ethylene was represented by a reactor working at 423K and 3MPa. Selectivity values were obtained from an experimental study on a Ni-AlMCM-41 catalyst. An ethylene conversion of 60% was chosen to simulate the ethylene oligomerization. In practice, these kind of high conversion values were never reached, which ensures a kind of safety barrier.

It could be concluded that with a minimum of 88mol% nitrogen condensation was avoided throughout the entire reactor setup, even at high conversion. The final inlet composition of the mixture is given in Table 3-1.

Table 3-1: Composition of inlet mixture

Compound	Fraction [mol%]
Ethylene (C_2H_4)	11.4
Nitrogen (N_2)	88.0
Methane (CH_4)	0.6

3.2 REACTION CONDITIONS TO OBTAIN INTRINSIC KINETICS

There can be drastic deviations between the catalytic system performance compared to the intrinsic kinetic regime due to the intrusion of temperature and/or concentration gradients. Therefore, experimental data has to be obtained in which transport resistances are negligible. A number of criteria and experimental methods have been collected, to detect this non-ideal reactor behavior. These criteria are referred to as [3]:

1. Ideality of flow patterns: plug flow or continuously stirred
2. Isobaricity: pressure drop in the catalyst bed
3. Interfase gradients: thermal and concentration (Not applicable in this case)
4. Intraparticle gradients: thermal and concentration
5. Interparticle (intrareactor) gradients : thermal and concentration

The information that affect the criteria can be classified in the following domains:

1. The operating conditions of the experimental study, i.e. the temperature, the operating pressure, the total inlet molar flow and the reactant composition
2. The reactor setup, i.e., the dimensions of the reactor, the type of reactor (CSTR vs. PFR), the total catalyst bed volume, etc.
3. The catalyst properties and its dilution, like the BET-surface, the bed porosity, etc.
4. The kinetic and thermodynamic data, i.e., reaction rates, enthalpy of formation, conversion of the reactant
5. Some physical properties of the products in the reactor, i.e., heat capacities, thermal conductivities, etc.

All this information can have an influence on the measured reaction rate, which makes it difficult to obtain perfect reaction conditions where intrinsic kinetics occur. In what follows the criteria, applicable for the experimental setup will be discussed.

To determine kinetics, transport should be taken into account both on reactor scale as on catalyst particle scale, see Figure 3-1. There has to be a uniform transport of the reactant through the reactor and this reactant also has to “enter” the catalyst particles. Both scales will be discussed separately.

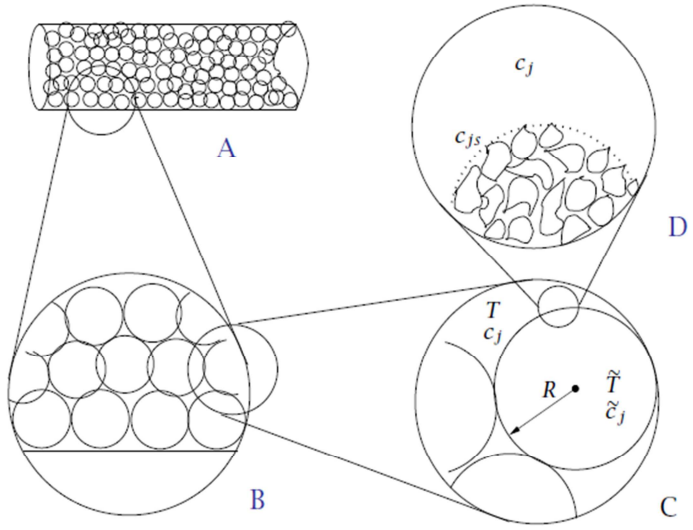

Figure 3-1: Intrinsic kinetics on reactor and catalyst particle scale [4]

3.2.1 Intrinsic kinetics on reactor scale

The most significant influences on the intrinsic kinetics are the plug flow regime and the heat transport limitations. It has to be verified if the conditions together with the reactor setup form a

uniform plug flow regime. The heat transport limitations have to make sure that temperature is uniform throughout the entire reactor tube both in axial as radial direction.

3.2.1.1 Plug flow regime

The reactor model, discussed in Chapter 2, assumed a plug flow regime, see Figure 3-2. This reactor consists of a long tube in which the following assumptions are made [5]:

- Only flow in the axial-direction is possible, which is parallel with the reactor axis.
- The flow is uniform in the radial direction, which is perpendicular to the reactor axis.
- Only forced convection takes place.

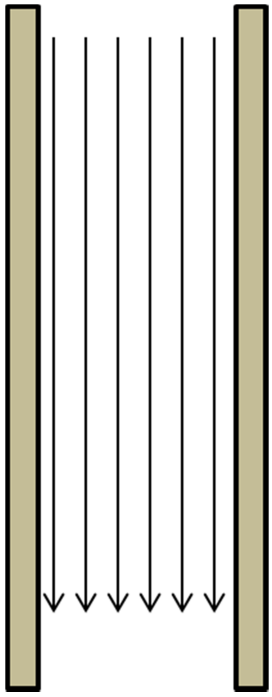

Figure 3-2: Plug flow regime within reactor tube

To assure this plug flow regime, the following correlations for radial and axial dispersion have to be satisfied:

$$\frac{d_t}{d_p} > 8 \tag{3-1}$$

$$\frac{L}{d_p} > \frac{8}{Bo}.n.\ln(\frac{1}{1-X_A}) \tag{3-2}$$

With d_p: Diameter catalyst particle [m]

d_t: Diameter reactor tube [m]

L: Length of the reactor tube [m]

Bo: Bodenstein number [$Bo = Pe_p = \frac{u_0 . d_p}{D_{A,ax}}$]

n: Reaction order

X_A: Conversion of reactant *A*, which is ethylene in this case.

If this first equation is not satisfied, the reaction rate at the wall will be higher than in the center of the reactor. This is due to a thinner stacking of catalyst particles at the reactor wall and will cause deviation of the plug flow regime. A measure of this deviation is the effective radial diffusion coefficient. De Kimpe B. has performed a study in previous master thesis to determine the maximum pellet diameter of the catalyst [6]. It could be concluded that the catalyst pellets should be smaller than ca. 500µm to satisfy the plug flow regime. For the experiments, the catalyst is pelletized to pellets with a diameter between 300 and 560µm, as this was the available sieve that was closest to the desired value. A lower diameter will also satisfy this correlation, however, it can be blown out of the reactor, get stuck in the analysis section and will lead to an increased pressure drop [6].

One major difficulty concerning the plug flow regime, is the realization of isothermicity throughout the reactor. And even more, due to the low flow rate through the reactor, a temperature- and concentration profile can arise around the catalyst particle, together with a radial temperature profile. The latter will be discussed separately.

3.2.1.2 Inert bed dilution

Since heat is produced during reaction, an axial temperature profile can arise, i.e., a higher temperature is obtained at the end of the reactor than at the beginning. To overcome this problem, the catalyst bed is diluted with inert material, i.e., alumina particles. Hence, the ratio of the surface area, that enhances heat exchange, to the reaction volume will increase, which eliminates the existence of a temperature gradient. However, a maximum of dilution is considered, since this can have a negative influence on the conversion, see Figure 3-3.

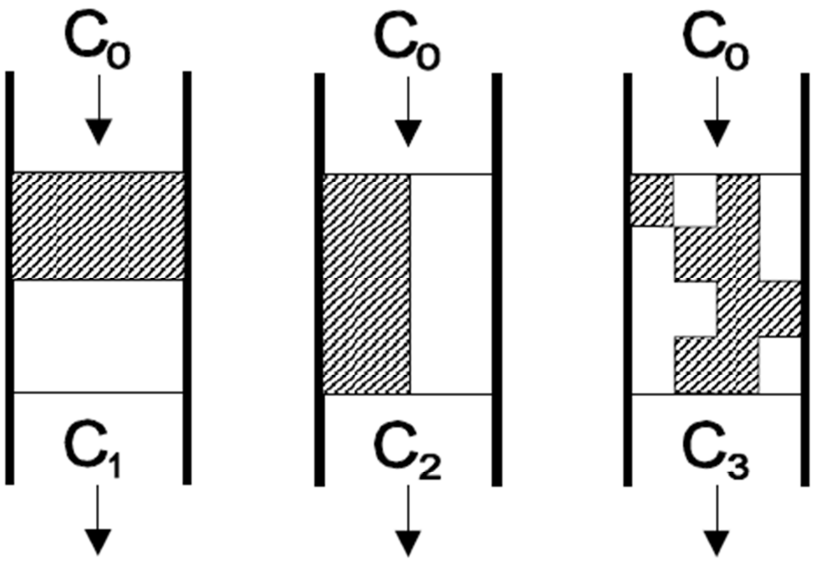

Figure 3-3: Influence of dilution on conversion

When increasing the amount of inert material, the probability that a part of the gas feed will pass through the catalyst bed via a zone containing little catalyst and more dilution, will increase. This will have its influence on the conversion, because some feed doesn't have the opportunity to convert due to lack of contact with the catalyst. Figure 3-3 indicates the importance of the distribution of the inert material. Van den Bleeck et al. have determined a criteria indicating if there is a significant effect on the conversion [7]:

$$b < \frac{0{,}4.\,L.\,\delta/d_p}{1 + 0{,}4.\,L.\,\delta/d_p} \tag{3-3}$$

Where b: Volume of inert material as a fraction of total solids [$m^3_{inert}/m^3_{inert+cat}$]

δ: The maximum allowed error caused by the dilution relative to the error in the experimental results. δ is mostly chosen as 0,1.

L: Length of the catalyst bed [m]

d_p: Diameter of the catalyst pellet [m]

In equation (3-3) only the ratio of the length of the bed to the particle diameter influences the dilution. The particle diameter was already defined in section 3.2.1.1, and by using this value, the maximum allowable dilution is 99.0vol% [vol_{dil}/vol_{tot}]. In the experiments a dilution of 83.0vol% [vol_{dil}/vol_{tot}], i.e. 10g inert for 0.5 g catalyst, is used.

3.2.1.3 Radial heat transport limitations

Radial heat transport can be responsible for a temperature difference in the center and at the wall of the reactor. This will lead to a temperature gradient, as can be seen in Figure 3-4. The temperature profile inside the bulk of the packed bed can be described by a parabolic shaped curve. Near the wall,

a steep decrease of the temperature takes place, due to the generally lower packing density. The heat transfer through this layer is described by means of a heat transfer coefficient at reactor wall (α_w). Since the reactor wall consists of a solid material, the heat transfer through this wall is much faster in comparison with the heat transfer in the bed. Therefore, for an exothermic reaction, the temperature will be the highest in the middle of the reactor.

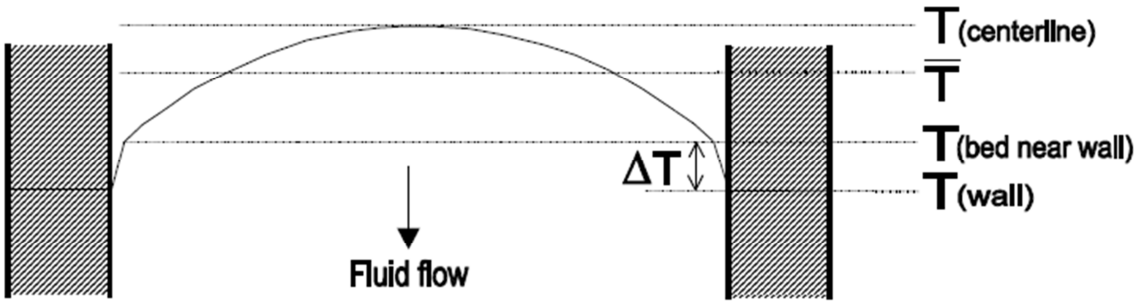

Figure 3-4: Radial temperature profile in the reactor for an exothermic reaction

The criteria to minimize this radial temperature profile, can be obtained by setting up a heat balance over the reactor bed. The temperature difference is assumed to be low enough when the reaction rate deviation, caused by this temperature difference, is lower than 5% [5]:

$$0{,}95 < \frac{R_A(T)}{R_A(T + \Delta T)} < 1{,}05 \tag{3-4}$$

In practice, the maximum allowable temperature difference is given by equation (3-5), in the assumption that the temperature in the bed can be measured. If the temperature of the reactor wall is measured, equation (3-6) should be applied. This last equation contains also the heat transfer through the reactor wall.

$$\Delta T = \frac{R_{v,A}^{obs}.|\Delta H_r|.(1-\varepsilon_b).(1-b).d_t^2}{32.\lambda_{er}} < \frac{0{,}05.R.T_w^2}{E_a} \tag{3-5}$$

$$\Delta T = \left(1 + \frac{8}{Bi_w}\right).\frac{R_{v,A}^{obs}.|\Delta H_r|.(1-\varepsilon_b).(1-b).d_t^2}{32.\lambda_{er}} < \frac{0{,}05.R.T_w^2}{E_a} \tag{3-6}$$

Where: $R_{v,A}^{obs}$: Observed volumetric production rate of reactant *A* [mol m_{cat}^{-3} s^{-1}]

ΔH_r: Enthalpy of reaction [J mol^{-1}]

ε_b: Bed porosity [m^3_{space} m^{-3}_{bed}]

b: Volume fraction of inert material in the catalyst bed [m^3_{dil} (m^3_{dil} + m^3_{cat})$^{-1}$

d_t: Diameter of the reactor [m]

λ_{er}: Effective radial bed thermal conductivity [W m^{-1} K^{-1}]

R: Gas constant [J mol^{-1} K^{-1}]

T_w: Temperature of the wall [K]

E_a: Activation energy [J mol^{-1}]

$Bi_w = \frac{\alpha_w . d_t}{\lambda_{er}}$: Biot's number at the reactor wall

α_w: Heat transfer coefficient at the reactor wall [W m^{-2} K^{-1}]

The parameter that is used to satisfy equation (3-6) and (3-5) is the catalyst bed dilution. A dilution of 79.0 vol% is necessary, since the reaction heat is considerable, i.e., maximum value of 55kJ mol^{-1}. This value stays under the maximum value that was obtained in section 3.2.1.2.

3.2.1.4 Maximum allowable pressure drop

Due to friction, a pressure increase takes place. However, this pressure increase should be limited because it will influence the kinetics of the reactions. To avoid the existence of a pressure drop, the following equation has to be satisfied:

$$\Delta P < \frac{0{,}2 . P_{tot}}{n} \tag{3-7}$$

Several empirical correlations are available to determine the pressure drop. In this case the Ergun equation was used to determine the modified Fanning friction factor [8]:

$$f_m = \frac{(1-\varepsilon_b)}{{\varepsilon_b}^3} . \left(1.75 + 150 . \frac{(1-\varepsilon_b)}{Re}\right) \tag{3-8}$$

$$f_m = 2 . f_f \tag{3-9}$$

$$\frac{\Delta P}{L} = \frac{f_m . \rho . \langle u \rangle^2}{d_{pe}} \tag{3-10}$$

With f_f: Fanning friction factor [-]

f_m: Modified Fanning friction factor [-]

d_{pe}: Diameter of a sphere with the same volume as the particle of the catalyst [m]

ε_b: Bed porosity [m^3_{space} m^{-3}_{bed}]

n: Reaction order ethylene

By implementing this correlation, no problem concerning pressure drop has to be accounted for.

3.2.2 Intrinsic kinetics on the catalyst particle scale

When intrinsic kinetics have to be measured, not only temperature and concentration profiles on reactor scale have to be avoided, but on the catalyst particle scale these profiles should be avoided as well, as can be seen in Figure 3-5.

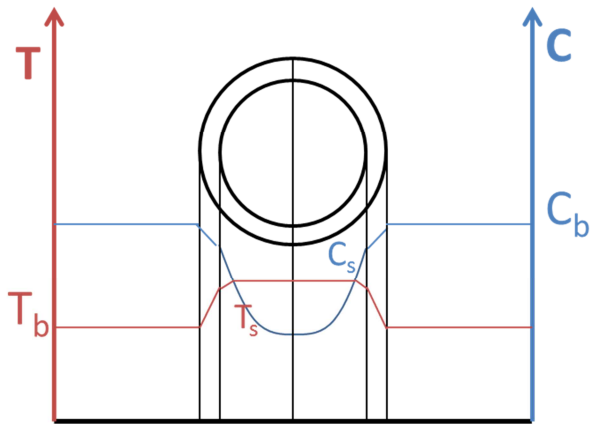

Figure 3-5: Temperature and concentration particle outside and inside of catalyst particle

Only the values of C_{bulk} and T_{bulk} can be measured, so one has to verify if the obtained reaction rate R(T,C) is really a consequence of the reaction at C_{bulk} and T_{bulk} or if other aspects influence the measured reaction rate.

Both the temperature and the concentration can have an external and internal profile which should be avoided. The criteria to make sure that these profiles do not exist will be discussed. The following sequence of importance is present in a small plug flow reactor:

1. External temperature gradients
2. External concentration gradients
3. Internal concentration gradients
4. Internal temperature gradients

3.2.2.1 External heat transport limitation

Due to reaction, the temperature at the catalyst surface will differ from the temperature in the bulk phase. Oligomerization is an exothermic reaction, which means that the temperature on the catalyst surface will be higher than the bulk temperature. This temperature profile can be seen in Figure 3-6 and is assumed to be linear.

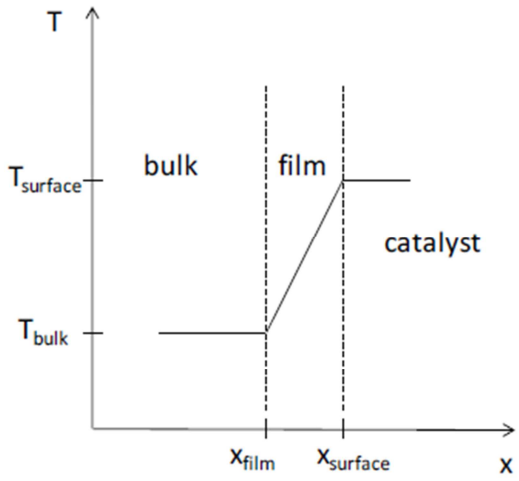

Figure 3-6: External temperature profile

The criteria is obtained by assuming that the reaction rate difference should not be higher than 5%:

$$0{,}95 < \frac{R_A(T)}{R_A(T+\Delta T)} < 1{,}05 \tag{3-11}$$

Using this condition, together with the heat balance over the gas film surrounding the catalyst particles, the criteria of external temperature limitations is obtained:

$$\Delta T(film) = \frac{R_{v,A}^{obs}.|\Delta H_r|.d_p}{6.\alpha_p} < \frac{0{,}05.R.T_f^2}{E_a} \tag{3-12}$$

Where:

$R_{v,A}^{obs}$: Observed volumetric production rate of reactant *A* [mol m_{cat}^{-3} s^{-1}]

d_p: Diameter of the catalyst pellet [m]

α_p: Heat transfer coefficient between pellet and gas [W m^{-2} K^{-1}]

ΔH_r: Enthalpy of reaction [J mol^{-1}]

R: Gas constant [J mol^{-1} K^{-1}]

T_f: Temperature of the fluidum [K]

E_a: Activation energy [J mol^{-1}]

In equation (3-12), there are only two parameters that can be modified, i.e., the temperature of the reactor and the pellet diameter. In section 3.2.1.1, the pellet diameter was determined to be between 560µm and 300µm. To determine the maximum temperature difference, the maximum value of the pellet diameter was chosen. The maximum allowable temperature difference ΔT should be smaller than 0.14K. Even with the minimum temperature used for experiments, i.e., 443K, the criteria for external temperature limitations is satisfied.

3.2.2.2 Internal temperature limitation

Within the catalyst particle, also heat transfer can occur. This indicates that also within the particle, a temperature gradient can be present, see Figure 3-7. For exothermic reactions, the temperature in the center of the catalyst particle will be higher than at the surface. To obtain a criterion, the same allowable deviation of the reaction rate due to a temperature difference of 5% is used, like in the other cases. When considering a heat balance over one catalyst particle, the maximum temperature difference is obtained:

$$\Delta T = \frac{R_{v,A}^{obs}.|\Delta H_r|.{d_p}^2}{6.\lambda_p} < \frac{0{,}05.R.T_f^2}{E_a} \quad (3\text{-}13)$$

Where:

$R_{v,A}^{obs}$: Observed volumetric production rate of reactant *A* [mol m_{cat}^{-3} s^{-1}]

d_p: Diameter of the catalyst pellet [m]

λ_p: Heat conductivity of the catalyst pellet [W m^{-1} K^{-1}]

ΔH_r: Enthalpy of reaction [J mol^{-1}]

R: Gas constant [J mol^{-1} K^{-1}]

T_f: Temperature of the fluidum [K]

E_a: Activation energy [J mol^{-1}]

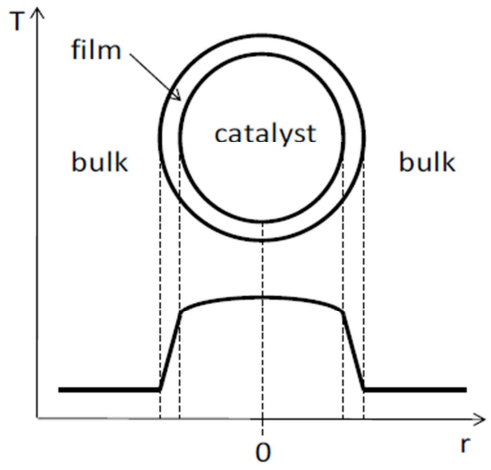

Figure 3-7: Temperature profile within catalyst

For this criterion, the modified parameters are the pellet diameter and the temperature. Increasing the pellet diameter, will make it harder to satisfy the criterion. Therefore, the maximum pellet diameter will be used, i.e., 560µm, see discussion 3.2.1.1. When implementing this value, a minimum temperature of 321K is necessary. In this experimental study, the minimum temperature that will be used is 443K, indicating that this criterion is always satisfied.

3.2.2.3 External mass transport limitations

Due to conversion, the concentration of the reactant in variable. On the surface of the catalyst, reaction occurs, meaning that reactant is converted into products which will induce a concentration gradient between the surface and the bulk phase. Again, a linear profile is assumed in this film around the catalyst particle, see Figure 3-8, with a higher concentration of reactant in the bulk phase than on the catalyst surface. Again a criterion can be defined, by stating that the reaction rate difference, due to the concentration gradient, should not exceed 5%:

$$\frac{R_{v,A}^{obs}}{k_f . a_v . C_{A,b}} = \frac{C_{A,b} - C_{A,s}}{C_{A,b}} < \frac{0{,}05}{n} \; (n > 0) \qquad (3\text{-}14)$$

Where:

$R_{v,A}^{obs}$: Observed volumetric production rate of reactant *A* [mol m_{cat}^{-3} s^{-1}]

k_f: Mass transfer coefficient between pellet and fluidum [m s^{-1}]

a_v: Heat specific external surface area of one pellet [m^2 m^{-3}]

$C_{A,b}$: Bulk concentration of reactant *A* [mol m^{-3}]

$C_{A,s}$: Surface concentration of reactant *A* [mol m^{-3}]

n: reaction order (For oligomerization n=1)

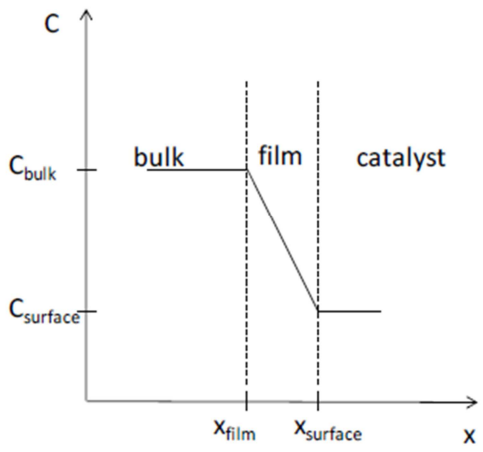

Figure 3-8: Concentration profile

The most essential parameter in this criterion, is the concentration of the bulk phase. To fulfill this criterion, the total molar inlet flow rate of ethylene should be higher than 10^{-10} mol s^{-1}. It is obvious that this criterion is always satisfied, because it is not practical to work with these kind of small flow rates. In this case, an inlet molar flow rate of 4.10^{-4} mol s^{-1} is used.

3.2.2.4 Internal mass transport limitations

Within the catalyst particle, a concentration profile is present due to diffusion limitations. The concentration in the center of the particle will be lower than the surface concentration. Two parameters for internal diffusion are the Thiele-modulus (ϕ) and the efficiency (η):

$$\phi = \frac{d_p}{6} \cdot \sqrt{\left(\frac{n+1}{2}\right) \cdot \frac{R_{v,A}}{D_{A,eff} \cdot C_{A,s}}} \tag{3-15}$$

$$\eta = \frac{1}{\phi} \cdot \left(\frac{1}{\tanh(3.\phi)} - \frac{1}{3.\phi}\right) \tag{3-16}$$

Where: $R_{v,A}$: Volumetric production rate of reactant *A* [mol m_{cat}^{-3} s^{-1}]

d_p: Diameter of the catalyst particle [m]

n: Reaction order

$D_{A,eff}$: Effective diffusion coefficient of reactant *A* [m^2 s^{-1}]

$C_{A,s}$: Surface concentration of reactant *A* [mol m^{-3}]

Pore diffusion limitation is negligible when the efficiency is high enough [5]:

$$\eta > 0{,}95 \tag{3-17}$$

Or when the Thiele-modulus has low enough values:

$$\phi \ll 1 \tag{3-18}$$

If this modulus approaches the value of zero, the concentration is uniform throughout the catalyst particle, and equal to the bulk concentration. This indicates that the diffusion is fast in comparison with the reaction rate. For example, a value of one for the Thiele-modulus, indicates that the reaction rate is much faster and the molecules don't have time to diffuse to obtain a uniform concentration. The efficiency expresses the ratio of the production rate with diffusion to the production rate at surface concentrations, i.e., maximum concentration. A high efficiency corresponds with a low Thiele-modulus and a uniform concentration profile.

Calculating the Thiele-modulus is rather difficult, since the intrinsic reaction rate has to be known. Therefore the Weisz-modulus Φ is introduced. To calculate this Weisz-modulus, only the observed reaction rate has to be known and expresses the ratio between the observed rate and the diffusion rate:

$$\Phi = \eta . \phi^2 \tag{3-19}$$

$$\Phi = \left(\frac{n+1}{2}\right).\frac{R_{v,A}^{obs}.\left(\frac{d_p}{6}\right)^2}{D_{A,eff}.C_{A,s}} < 0{,}08 \quad (3\text{-}20)$$

Where: $R_{v,A}^{obs}$: Observed volumetric production rate of reactant *A* [mol m_{cat}^{-3} s^{-1}]

d_p: Diameter of the catalyst pellet [m]

n: Reaction order

$D_{A,eff}$: Effective diffusion coefficient of reactant *A* [m^2 s^{-1}]

$C_{A,s}$: Surface concentration of reactant *A* [mol m^{-3}]

Calculating the Weisz-modulus, taking into account all the limitations on the variables as derived in the previous sections, shows that this value is lower than 0.08. This indicates that no further adjustments have to be made. The efficiency that is obtained in this case, is 99.8%, which is very close to a value of one so no internal mass transport will occur.

3.3 SUMMARY OF CONDITIONS

The conditions that will be tested on the Ni-β catalysts are summarized in Table 3-2. These conditions were chosen in such way that both the conditions for intrinsic kinetics and gas phase are satisfied.

Table 3-2: Reaction conditions for experimental study

Reaction conditions	Experimental range
Temperature [K]	443-503
Partial pressure of ethylene [MPa]	0.17-0.40
Space time [kg_{cat} s mol^{-1}]	4.0-12.0
Nitrogen dilution [mol%]	88.0

3.4 EXPERIMENTAL STUDY OF CATALYST BEHAVIOR

Experiments were performed on the HTK-1 setup as described in Chapter 2. The influence of several parameters such as temperature, pressure and space time on conversion and selectivity values is experimentally tested and will be discussed in this paragraph.

Different olefins are produced during reaction. No olefins with more than 8 carbon atoms were observed, which is due to the low ethylene conversion. For most compounds, different isomers are detected. However, since it is difficult to separate and identify every single peak, the different isomers of one olefin are grouped. Except for the butene isomers, i.e., 1-butene, 2-trans-butene, 2-cis-butene and iso-butene can be separated easily.

Propylene and pentene are produced through cracking of the octene molecules. Although the production of odd-numbered hydrocarbons is very limited, it is essential to detect these compounds. This is because the β-scission reaction, responsible for this cracking, will be implemented in the kinetic model. Detection of these compounds, makes it possible to estimate the kinetic parameters related with these scission reactions.

3.4.1 Influence reaction conditions

A broad range of reaction conditions was tested for ethylene oligomerization, see Table 3-2. By varying the reaction conditions, insight is obtained in the effect of the partial pressure of ethylene, temperature and space time on the selectivity and activity of the catalyst.

3.4.1.1 Influence of the partial pressure of ethylene

During experiments, the ethylene partial pressure was varied between 0.17MPa and 0.40MPa. When the pressure was increased, also an increase in conversion of ethylene was detected, as can be seen in Figure 3-9. With increasing pressure, the reaction rate will increase due to an increased physisorption of the reactant. It can be stated that at a certain total pressure, no free active sites will be available on the surface and the conversion will no longer increase, since maximum saturation is obtained.

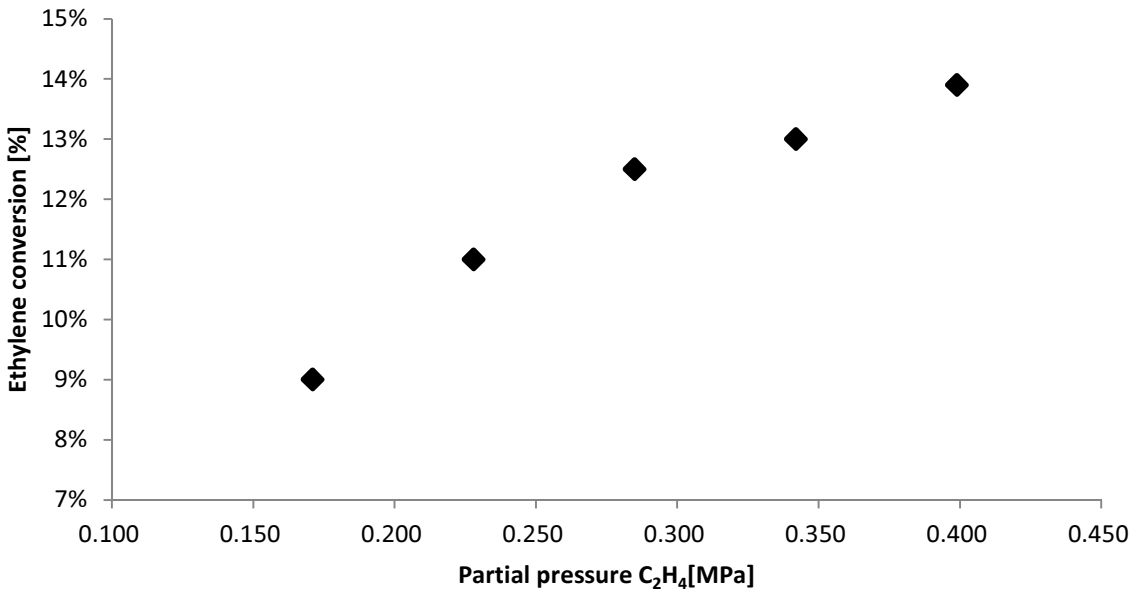

Figure 3-9: Ethylene conversion as function of partial pressure of C_2H_4, a temperature at T=523K and a space time of 10 $kg_{cat}s\ mol^{-1}$. The composition of the inlet mixture is given in Table 3-1.

The increase of physisorption at higher pressure increases the production of butene, see Figure 3-10. Ethylene molecules are able to physisorb more easily at higher partial pressure on the catalyst where the insertion of ethylene produces butene. This increase is, however, very limited. Hexene, indicated on Figure 3-10, shows no clear behavior.

The *cracking* behavior of the Ni-β catalyst is given in Figure 3-11. By cracking of octene, propylene and pentene are produced. It is observed that with increasing pressure, cracking is becoming less pronounced. Combining the observations of increasing C_4 selectivity and decreasing cracking selectivity, it can be concluded that the reaction rate of metal ion catalyzed reactions increases more rapidly with increasing pressure than the cracking rate.

Moreover, it can be seen on Figure 3-11 that the selectivity towards propylene is about one third of the selectivity towards pentene. Probably this is due the acid catalyzed dimerization of propylene towards hexene. This increased quantity produced of hexene, however, is insufficient to observe an increase in the selectivity towards hexene, see Figure 3-10. The fact that no clear increase of hexene is detected can indicate the importance of the metal catalyzed insertion mechanism for the production of hexene, since the rate of the metal ion catalyzed reactions also increases with pressure. This shows that for all the compounds there is always an metal catalyzed and an acid catalyzed route, increasing the complexity of the reaction mechanism.

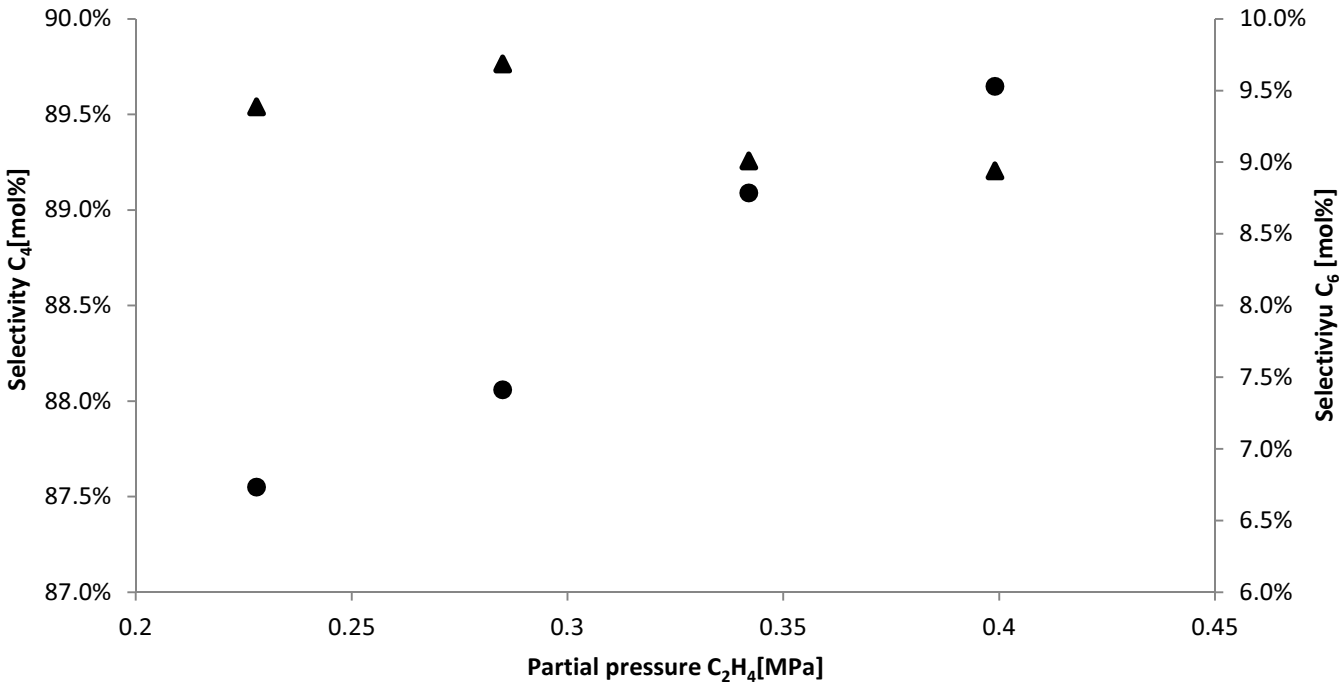

Figure 3-10: Selectivity to lumped butene (●) and lumped hexene (▲) as function of ethylene partial pressure, a temperature of 523K and a space time of 10 $kg_{cat}s\ mol^{-1}$.

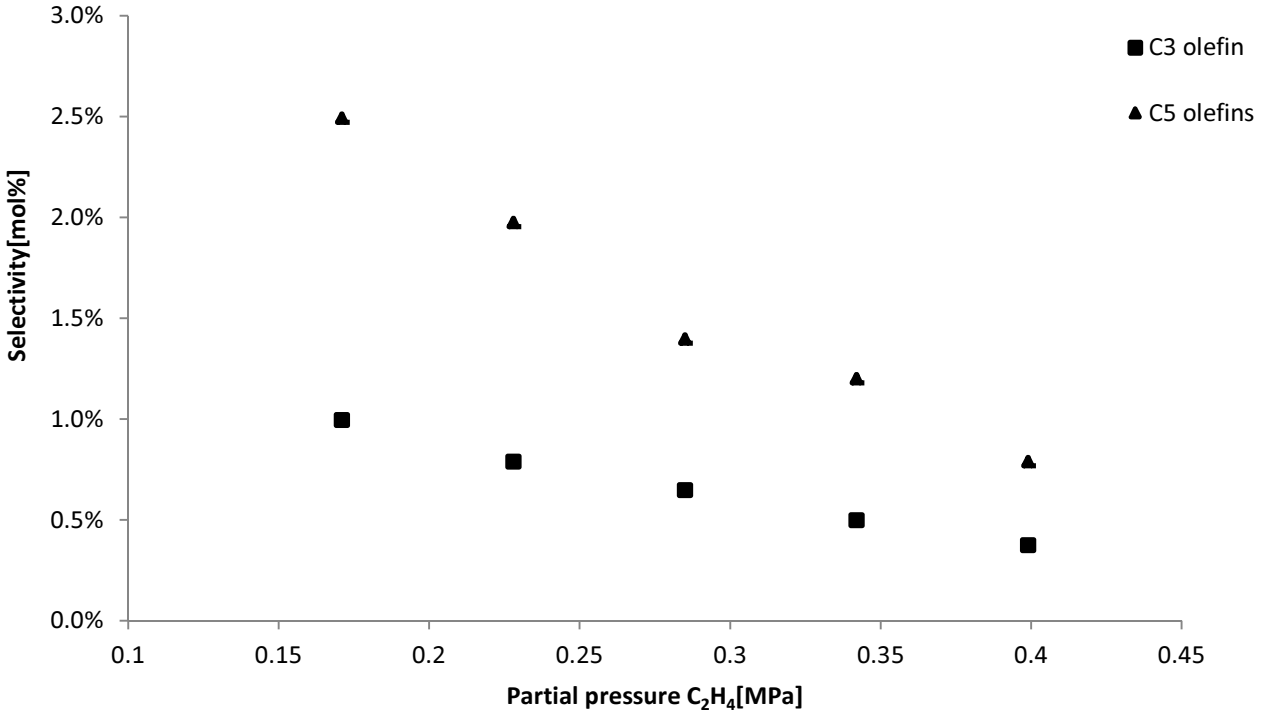

Figure 3-11: Selectivity to propylene (■) and lumped pentene (▲) as function of ethylene partial pressures and a temperature of 523K and a space time of 10 $kg_{cat}s\ mol^{-1}$.

3.4.1.2 Influence of the reaction temperature

With increasing temperature, the conversion of ethylene is increasing, see Figure 3-12. At higher temperatures, the reaction rate of all reactions are increasing. Most importantly, the acid catalyzed reactions are becoming more favored with increasing temperature [2].

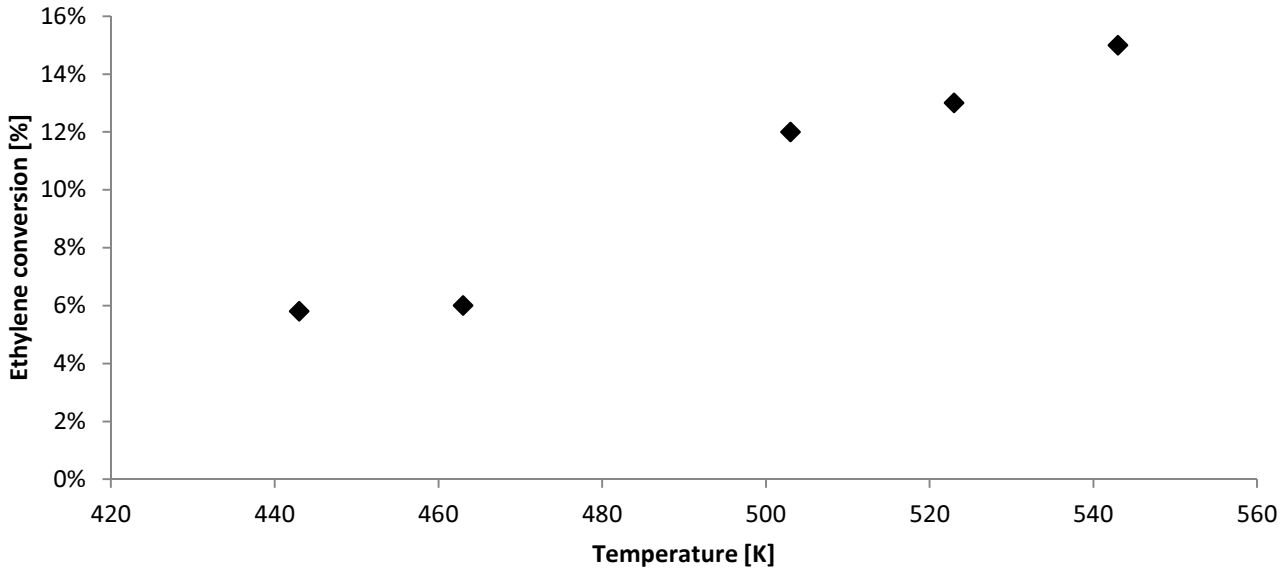

Figure 3-12: Conversion of ethylene as function of temperature, for experiments with an inlet partial pressure of ethylene of 0.342MPa and a space time of 10 $kg_{cat}s\ mol^{-1}$.

This increase of acid catalyzed reactions is represented in Figure 3-13 and Figure 3-14. With increasing temperature, more cracking occurs and the C_3 and C_5 olefins are increasing. The activation energy for these cracking reactions are determined by B.D. Vandegehuchte et al, circa 120kJ mol^{-1} [9]. Comparing these values with the activation energies for the metal ion catalyzed reactions, determined by K. Toch et al. [10], i.e., about 75kJ mol^{-1}, shows that the cracking reactions have a much higher activation energy. Thus, increasing temperature favors the ease of the cracking more than oligomerization on the metal ion sites. At low temperature, i.e., 443K, the production of odd numbered olefins was not observed, indicating that acid catalyzed cracking does not take place at this relative mild reaction temperature.

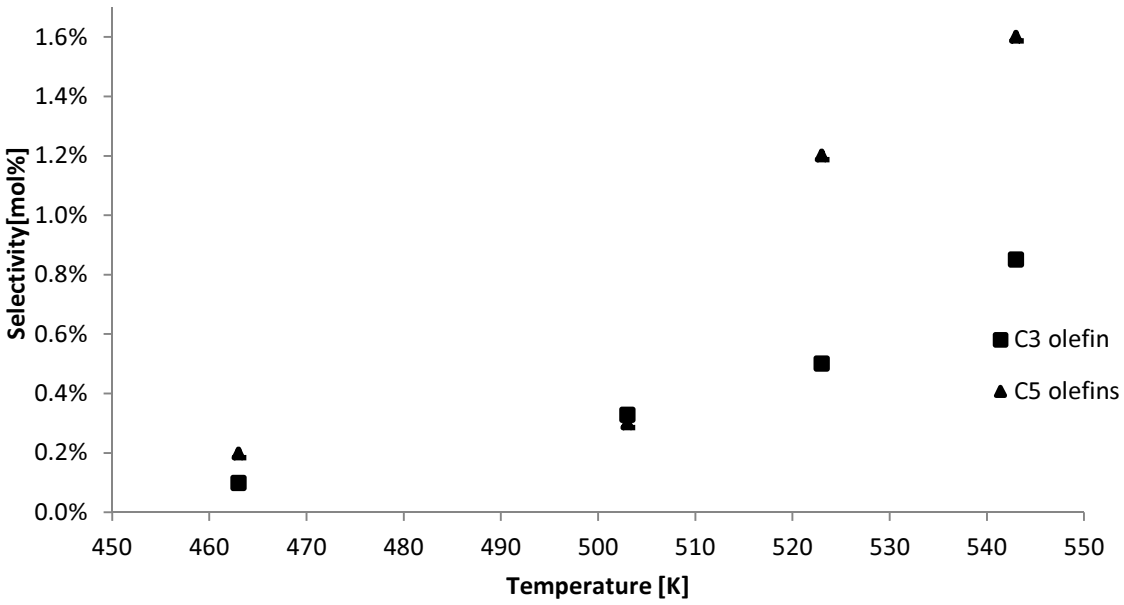

Figure 3-13: Selectivity to propylene (■) and lumped pentene (▲) as a function of temperature with an inlet ethylene partial pressure of 0.342MPa and a space time of 10 $kg_{cat}s\ mol^{-1}$.

Additionally, the butene selectivity was decreasing with higher temperature, see Figure 3-14. This decrease of C_4 selectivity and an increase of selectivity towards C_6, see Figure 3-15, and cracking products, see Figure 3-13, indicates that at higher temperatures further oligomerization of C_4 is favored, both catalyzed by metal-ions as acid sites. The latter results in the production of C_8 olefins which are subsequently cracked to propylene and pentene. This decline of butene production also is in correspondence with observations from literature [2].

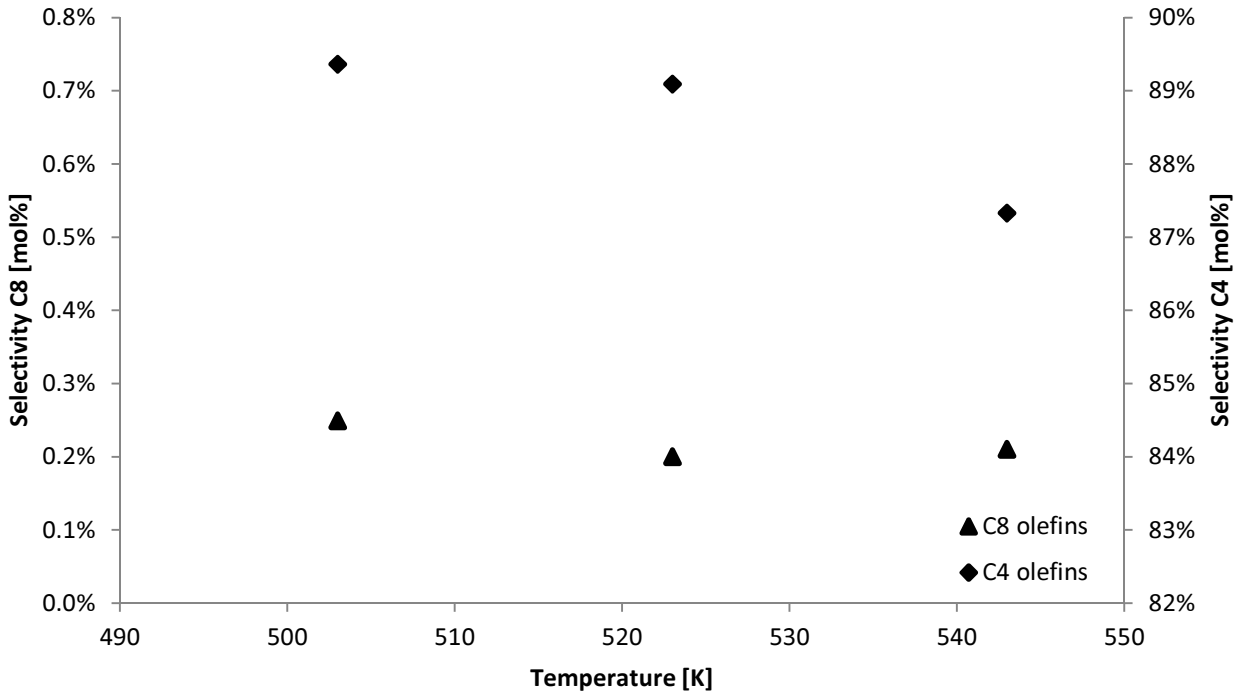

Figure 3-14: Selectivity to lumped octene (▲) and lumped butene (◆) as a function of temperature with an inlet ethylene partial pressure of 0.342MPa and a space time of 10 $kg_{cat}s\ mol^{-1}$.

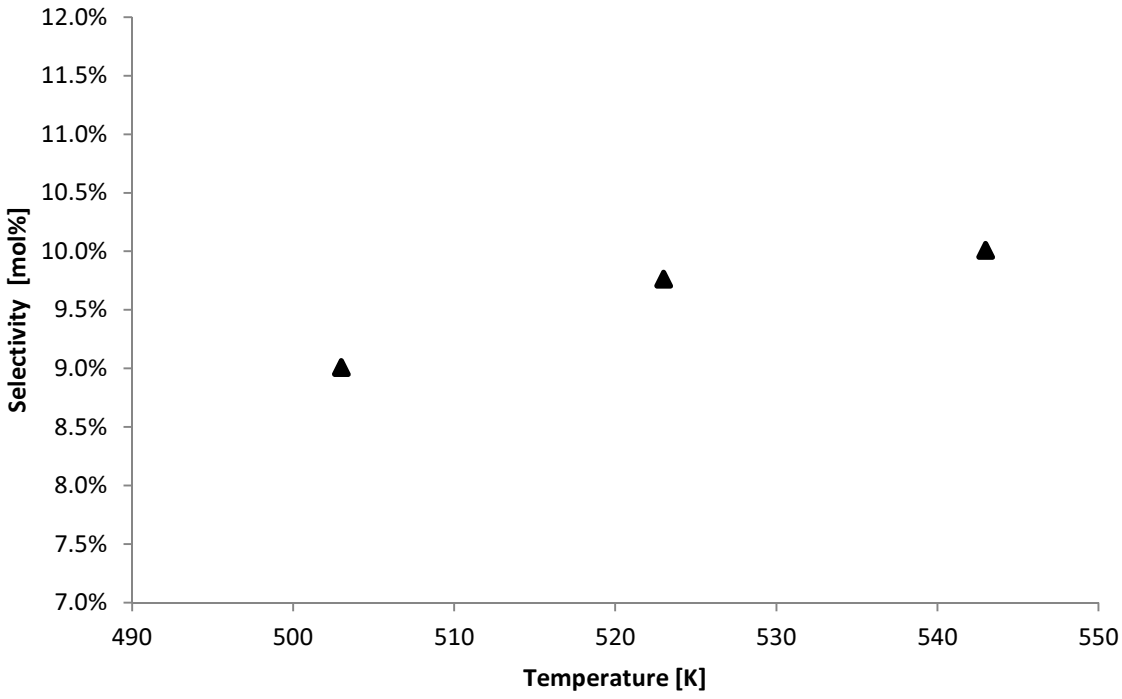

Figure 3-15: Selectivity to lumped hexene (▲) as function of temperature with an inlet ethylene partial pressure of 0.342MPa and a space time of 10 $kg_{cat}s\ mol^{-1}$.

As an additional remark, it can be stated that within the temperature range tested, , no volcano-curve was measured as discussed in paragraph 1.4.2. The determination of the low and high temperature range would be a valuable asset since it highly defines the properties of the products,

i.e., resp. linear alpha olefins and fuel. However, most probably, the temperature range applied is too small to detect these two regions of activity.

3.4.1.3 Influence of the space time

An increasing space time results in a higher conversion of ethylene, see Figure 3-16. With a low molar flow rate of ethylene, i.e., a high space time, the bulk concentration of ethylene throughout the catalyst bed will decrease. This can result in a deviation of the linear relation between space time and conversion, as can be slightly seen from a space time equal to 10-12 $kg_{cat}s\ mol^{-1}$.

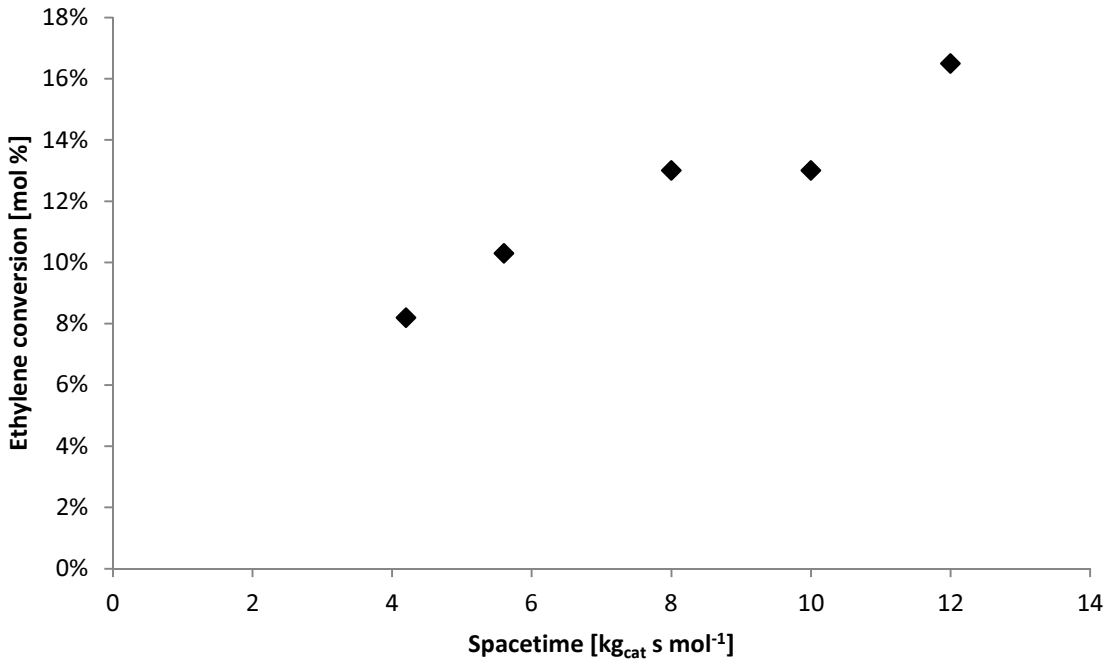

Figure 3-16: Conversion of ethylene as function of space time, an inlet partial pressure of ethylene of 0.342MPa and a temperature of 523K.

Figure 3-17 indicates that there is a small increase in selectivity towards butene. On the other hand, it shows that with increasing space time, also the cracking is favored.

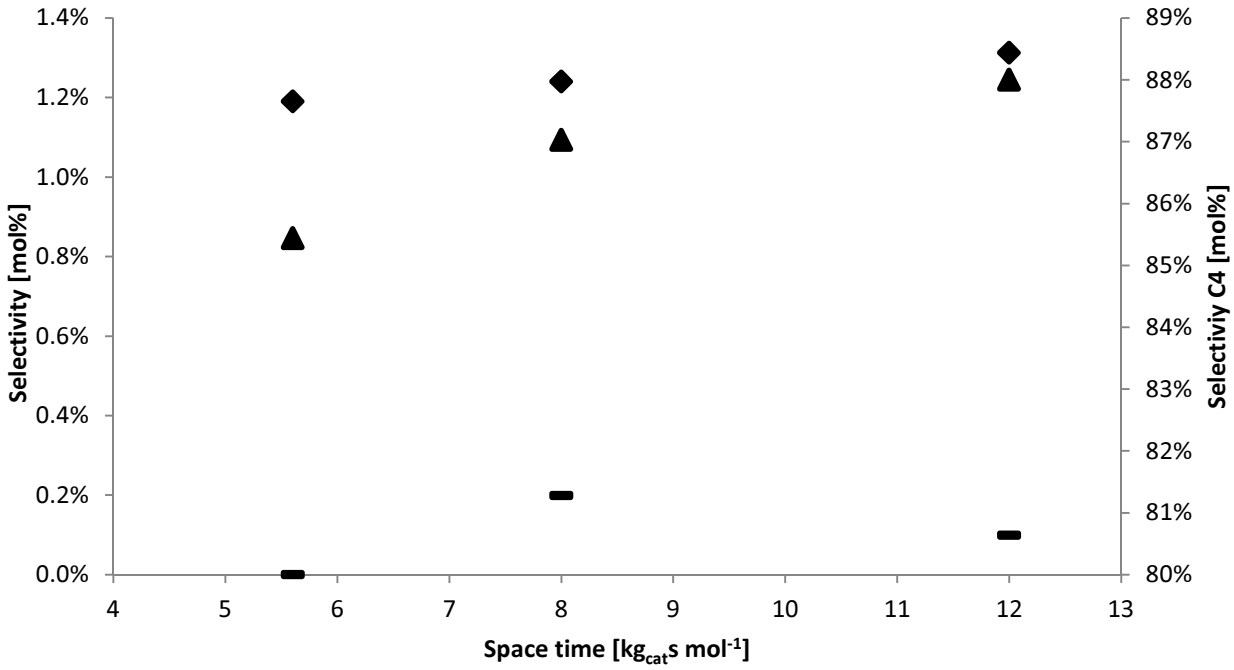

Figure 3-17: Selectivity to lumped butene (◆), lumped pentene(▲) and lumped octene(▬) as a function of space time with an inlet ethylene partial pressure of 0.342MPa and a temperature of 523K.

3.4.2 Catalyst behavior

3.4.2.1 Catalyst properties

The properties of the catalyst were already discussed in Chapter 2. Here, these values are used to interpret the catalyst behavior. The nickel content and the concentration of acid sites were determined, see Table 3-3.

Table 3-3: Active site content on the catalyst

Nickel	4.89wt%
Concentration acid sites	0.634 mmol g^{-1}

A relative high weight percentage of nickel is present on the catalyst. In Chapter 1, section 1.4.2.1, it was stated that the amount of nickel that was impregnated on the catalyst has an effect on the ethylene conversion. An optimal value of 1.5wt% was found. With increasing nickel weight percentage, a decrease of the ethylene conversion took place. The high Ni-loading on the tested catalyst could give an explanation for the low conversion values. Additionally, in appendix C, the XRD of the Ni-β catalyst clearly indicate the presence of a NiO phase. This indicates that the impregnation of nickel during synthesis does not led to a fine dispersion of nickel on the whole catalyst surface. An amount of nickel molecules blocks the acid sites present on the pure β-zeolite. Fan et al. consider the Ni-H as the active site for ethylene oligomerization [11]. So the higher the nickel loading, the more

acid sites are blocked and less *Ni-H*-complexes are available on the surface, due to NiO clustering, to initiate the oligomerization.

Additionally, investigation concerning the effect of the acid site concentration has shown that the amount of oligomers ($g_{oligomers}$ mol_{Ni}^{-1} h^{-1}) strongly increases when the acid site concentration decreases [2]. A comparison study was performed concerning the activity for catalysts with different acid site concentrations, see Figure 3-18 [2].The NiMSA80 represents the catalyst with the lowest concentration of acid sites, i.e., 0.27mmol g^{-1}, whereas the NiMSA10 contains 0.72mmol g^{-1}. Synthesizing a catalyst with a lower concentration of acid sites would increase the activity of the catalyst and could lead to a higher ethylene conversion. However, this lower acidity may then eliminate the production of odd-numbered hydrocarbons. The highly acidic catalyst suffers the highest deactivation, leading to a very low olefin production.

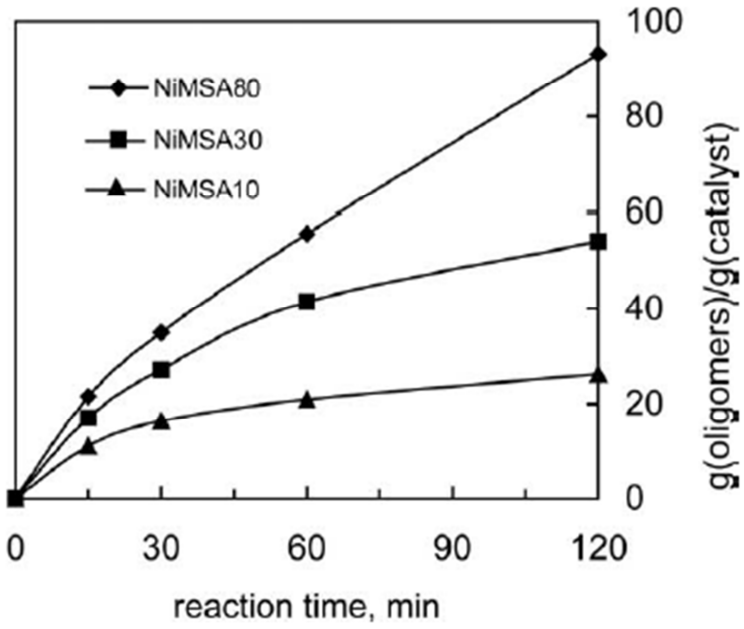

Figure 3-18: Evolution of catalytic activity along reaction time during C_2H_4 oligomerization in n-heptane, at 423K and 3.5MPa[2]

3.4.2.2 Deactivation of Ni-β catalyst

When initiating the experimental work, the catalyst stability was tested for a longer period. It became clear that quick deactivation of the catalyst took place. Also no catalyst regeneration method was applicable in this case. Therefore, it was chosen to reload the reactor with fresh catalyst after every experiment, hence the rather limited experimental data.

In Figure 3-19, the deactivation of the catalyst can be seen as function of time-on-stream. It is clear that during time-on-stream, the conversion of ethylene is exponentially decreasing. During one single

experiment, the deactivating behavior was already seen. Therefore, to obtain one experimental point, five analyses were performed over a time-on-stream of 5hrs. By extrapolating these data to time zero, the initial catalyst behavior at the reaction conditions was determined.

As explained in section 3.4.2.1, the acid site concentration can be considered relatively high which leads to fast deactivation. In literature, it is supposed that this is due to the acid catalyzed reactions which are responsible for the formation of strong adsorbed long-chain olefins. In this case the deactivation due to pore blockage of these compounds is very unlikely, since the very low production of larger hydrocarbons. However, after every experiment, it was observed that the catalyst changed color, i.e., from white to black, indicating that cokes could be present after reaction.

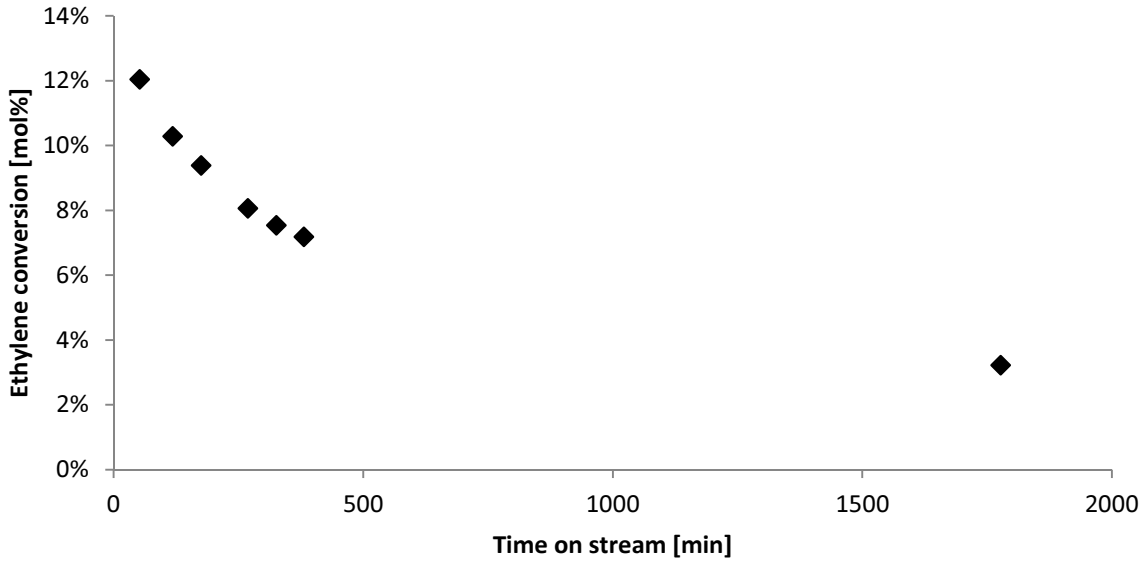

Figure 3-19: Experimentally obtained ethylene conversion as function of time-on-stream at 523K, with a partial pressure of ethylene of 0.342MPa and a space time of 10kg_{cat}s mol^{-1}.

Comparing Figure 3-20 and Figure 3-21 shows that the activity of the acid catalyzed reactions decreases, whereas the activity of the metal ion catalyzed reactions increases. This confirms that mainly the acid sites deactivate during time. Moreover, due to this lower conversion by the acid sites, the metal ion sites are able to convert relatively more ethylene towards butene, see Figure 3-21.

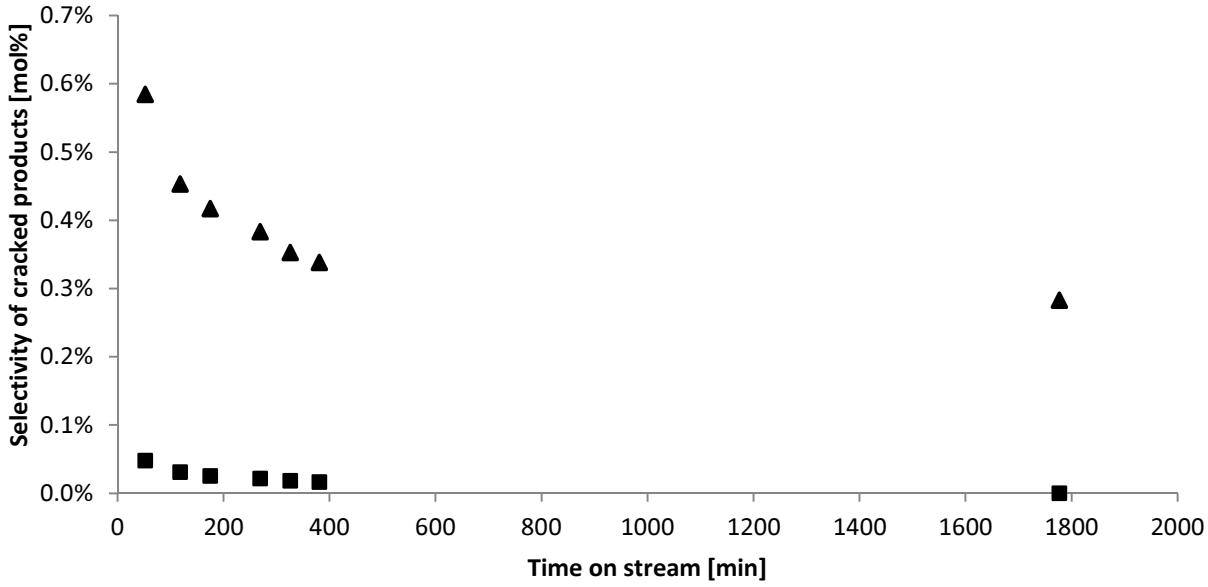

Figure 3-20: Experimentally obtained selectivity to cracking products; (■): propylene; (▲):lumped-pentene, as function of time-on-stream at 523K, , with a partial pressure of ethylene of 0.342MPa and a space time of 10kg$_{cat}$s mol^{-1}.

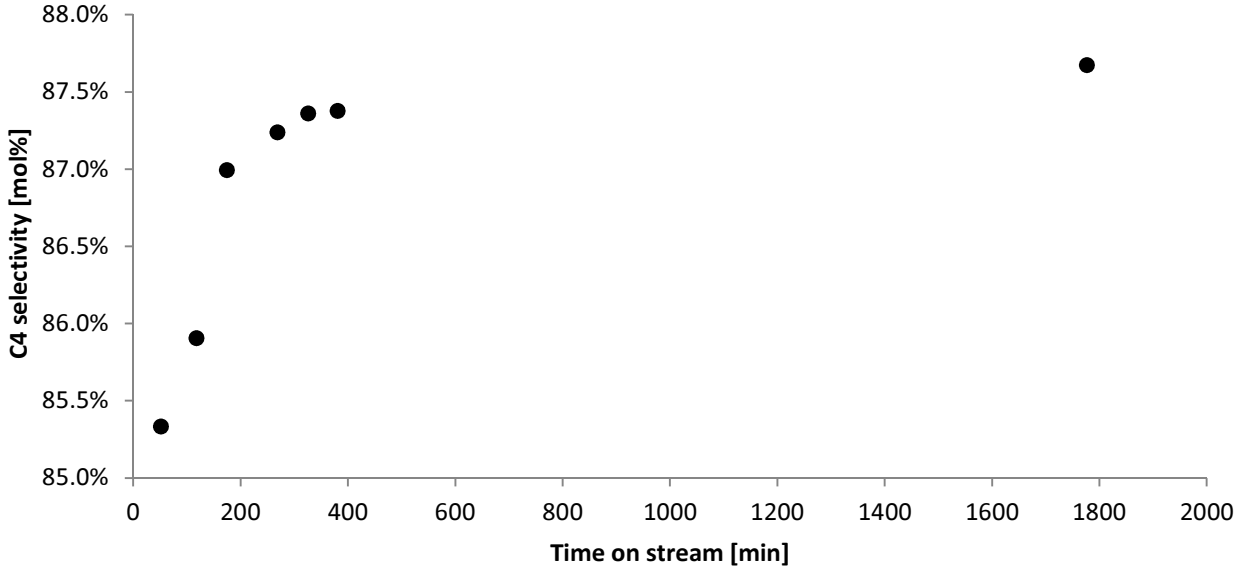

Figure 3-21: Experimentally obtained selectivity of lumped butylene as function of time-on-stream at 523K, with a partial pressure of ethylene of 0.342MPa and a space time of 10kg$_{cat}$s mol^{-1}.

3.5 PRODUCT DISTRIBUTION OBTAINED ON NI-β- CATALYST

3.5.1 *Anderson Schultz Flory* distribution

In Figure 3-22 it can be seen that mainly *"true"* oligomerization occurs, i.e., production of C_4 and C_6 olefins. At higher temperatures, the octene fraction is increasing, since more acid catalyzed

dimerization of butene takes place. However, also more cracking occurs at these higher temperatures. But this amount is relatively small in comparison with the increased production by dimerization.

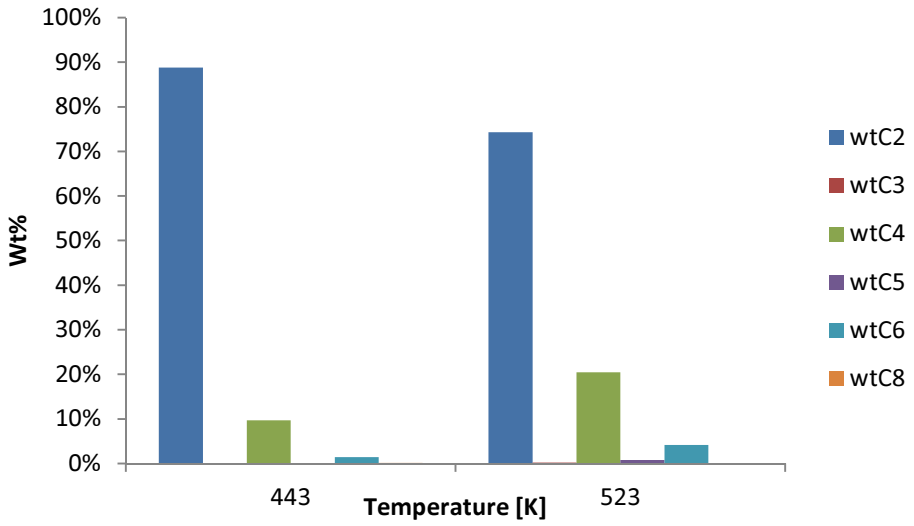

Figure 3-22: Experimentally obtained *Anderson Schultz Flory* distribution for the even carbon numbered components at two temperatures, i.e. 443K and 523K, and a partial pressure of ethylene of 0.342MPa and a space time of 10 $kg_{cat}s\ mol^{-1}$.

The near *Anderson Schultz Flory* distribution for the even-numbered hydrocarbons is in line with a homogeneous catalysis inspired mechanism of oligomerization involving insertion of ethylene in a metal-carbon bond and termination. This indicates that the influence of the acid catalyzed reactions is of secondary importance for the linear olefins, especially at mild reaction conditions.

When investigating the product yields, i.e., of butene and hexene, as function of the ethylene conversion, a linear relationship exists, see Figure 3-23. This indicate that mainly dimerization of ethylene occurs and strengthen the idea that the importance of the acid catalyzed reactions on this Ni-β catalyst is small [10]. A deviation of the C_4 yield from this linear behavior would indicate an increased importance of acid catalyzed dimerization towards octene [10].

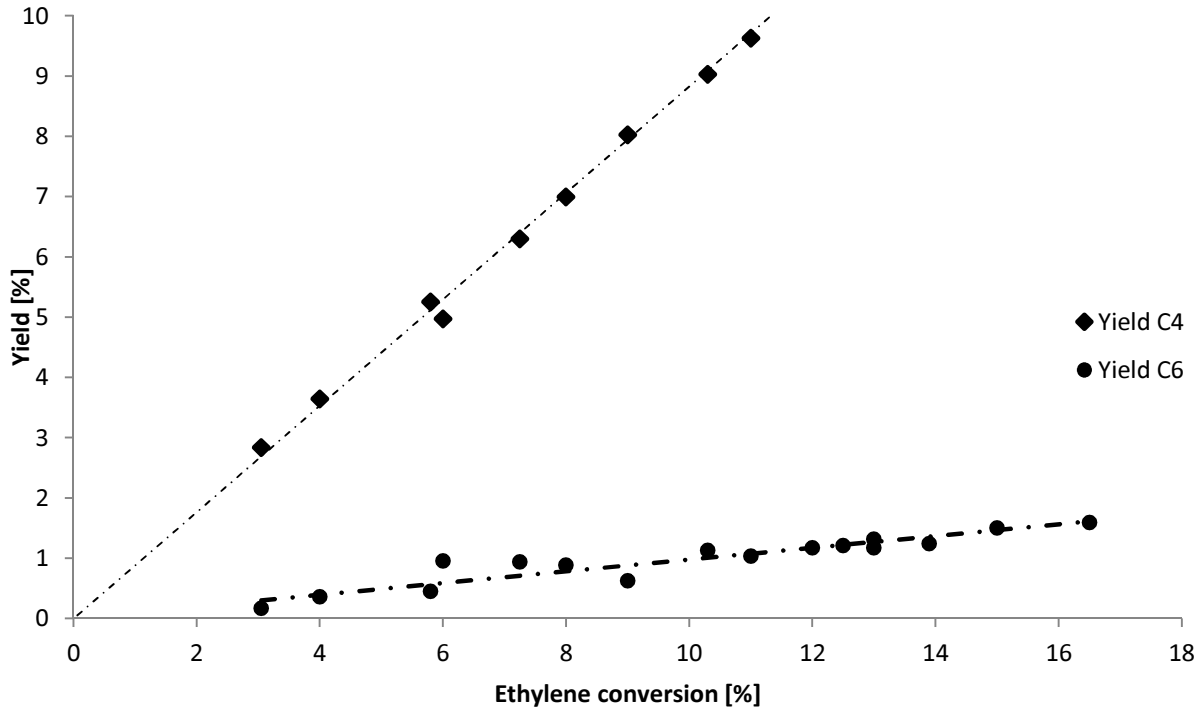

Figure 3-23: Experimentally obtained product yields, i.e., C_4(◆) and C_6(●), as function of ethylene conversion

3.5.2 Distribution of double bond isomers

It is interesting to analyze the distribution of the double bond isomers within one C_n-olefin. During the experimental study, a good separation of the different double bond isomers of butene was necessary, i.e., 1-butene, 2-trans-butene and 2-cis-butene to determine if thermodynamic equilibrium was obtained for these isomers. Also trace amounts of iso-butene were detected among the C_4-isomers, but these were rather limited and will not be discussed further.

In literature it is stated that the double bond isomer distribution within C_4 or C_6 hydrocarbons is dependent on the acidic properties of the catalyst [12]. Lower acid site density results in a higher selectivity towards 1-butene and 1-hexene. This suggests that 1-butene is the initial product formed from ethylene oligomerization and that with acid catalyzed isomerization this 1-butene can be converted into 2-butene [2]. Since double bond isomerization is a shift reaction, that goes through a carbenium ion, i.e., acid catalyzed reaction. Equation (3-21) shows the double bond isomerization of 1-butene to 2-trans-butene.

(3-21)

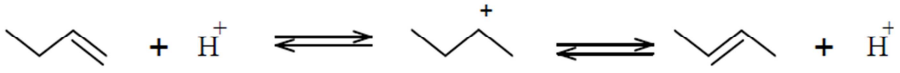

At higher temperatures, the influence of the acid catalyzed reactions should be more pronounced. This would mean that the relative mol% of 2-trans-butene and 2-cis-butene would increase and deviate more from the equilibrium percentage. However, for the experiments on the Ni-β catalyst, this is not the case. Figure 3-24 represent the relative mol% of the isomers of butene. No systematical difference appears between the experimental and the equilibrium concentrations, which indicates that the double bond isomerization is at quasi-equilibrium under the conditions tested. It can be concluded that the low amount of acid sites on the catalyst is enough for the double bond isomers to be in thermodynamic equilibrium or that double bond isomerization can be catalyzed by the nickel-ion sites.

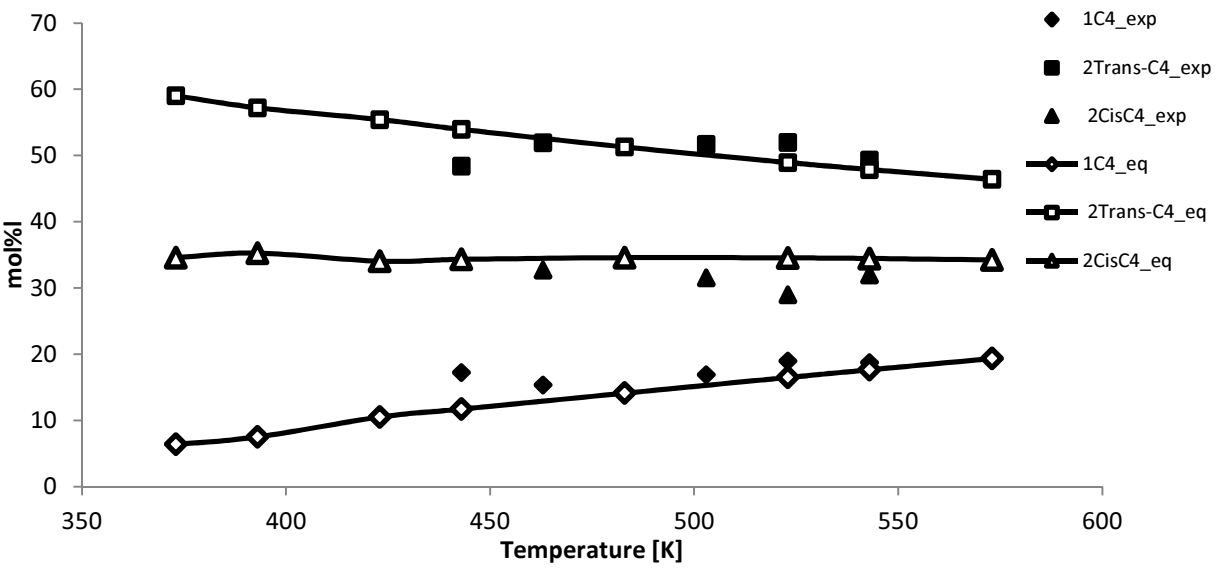

Figure 3-24: Comparison between equilibrium [eq] and experimental [exp] produced butene isomers at different temperatures and a partial pressure of ethylene of 0.342MPa. The equilibrium distribution was determined by means of simulation in Aspen©.

3.5.3 Conclusion concerning product distribution

Different measurements were used to obtain information about the significance of the acid catalyzed reactions for ethylene oligomerization on this Ni-β catalyst. They all indicate the importance of the metal catalyzed reactions towards linear olefins and the limited influence of the acid sites. Although, small fractions of propylene and pentene are detected, the main production route is still the insertion of ethylene. At higher temperatures, more acid catalyzed reactions occur, resulting in an increase of propylene and pentene production.

3.6 COMPARISON WITH REFERENCE CATALYST

Finally, the activity of the Ni-β catalyst is compared with the activity of the reference catalyst tested before this master thesis. The reference catalyst is an amorphous 1.8wt% Ni-SiO_2-Al_2O_3 [10]. Figure

3-25 indicates that this catalyst has a higher activity, since for the same temperatures, a higher conversion of ethylene is obtained. However, for this catalyst, no production of odd-numbered hydrocarbons were detected.

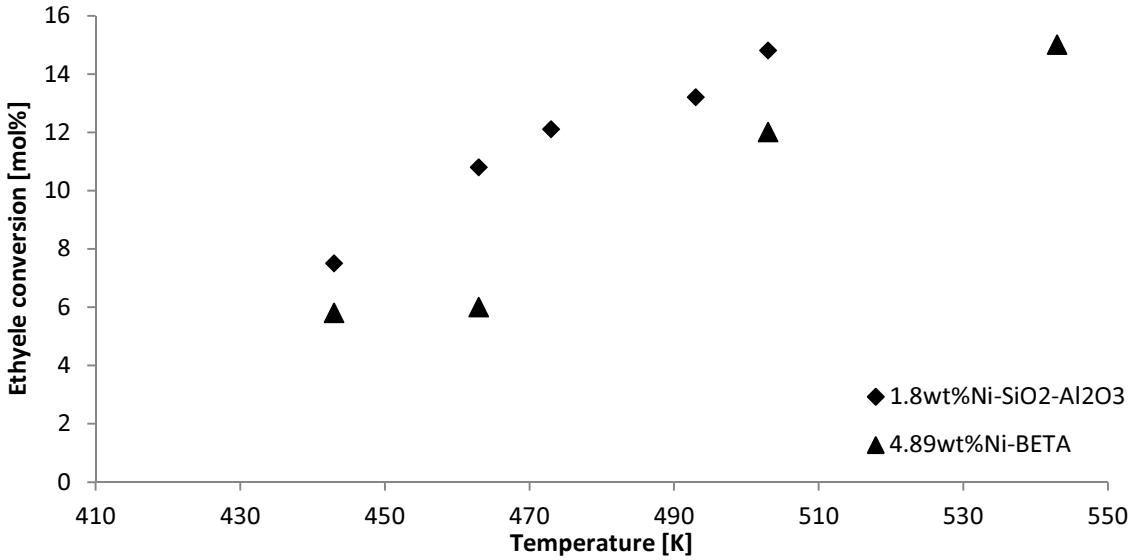

Figure 3-25: Experimentally obtained ethylene conversion on the HTK-1 setup as function of temperature for two catalysts; (◆) 1.8wt%Ni-SiO_2-Al_2O_3 and (▲) 4.89wt%Ni-β.

Table 3-4 summarizes the most significant characteristics of the two catalysts. Both the nickel content and the BET surface area are the highest for the 4.89wt% Ni-β catalyst, the concentration of acid sites is however smaller. As reported before in section 3.4.2.1, this should lead to a higher conversion of ethylene. But in this case, besides the concentration, the acid strength should be considered too. On the reference catalyst, the acid sites can be considered very weak, which corresponds with the absence of odd-numbered hydrocarbons. The 4.89wt% Ni-β has less acid sites but they are very strong, which then leads to a high deactivation, see section 3.4.2.1. Additionally, the high nickel content on the Ni-β catalyst leads to the presence of NiO on the surface, which is not found on the XRD results of the reference catalyst, see Appendix C. The NiO-phase blocks the active sites and consequently, leads to a lower ethylene conversion.

Table 3-4: Characteristics of reference catalyst and Ni-β catalyst

Property	1.8wt%Ni-SiO_2-Al_2O_3	4.89wt%Ni-BEA
Nickel content [wt%]	1.8	4.89
BET area [m^2 g^{-1}]	199.11	458.32
Concentration acid sites [mmol g^{-1}]	0.79 (WEAK)	0.634 (VERY STRONG)

3.7 REACTION NETWORK

Several parallel and consecutive reactions occur on the bifunctional Ni-β catalyst under the reaction conditions considered in this thesis. This makes it difficult to describe one main reaction path for the different compounds. The network is governed by both the metal ion and acidic properties of the catalyst and the reaction conditions. In Chapter 6, a reaction path analysis will be performed.

A possible reaction network on the Ni-β catalyst for oligomerization of ethylene is given in Figure 3-26. Several *oligomerization* (o) reactions lead to even numbered end of chain olefins, which occur on the metal ion sites. Once large enough hydrocarbons are produced, isomerization can occur. In this case, mainly double bond isomerization occurs. However also other *isomerization* (i) reactions, i.e., 1,2-alkyl shift and PCP-branching can take place, but were not all represented for the simplicity of the figure. Out of one molecule of octene, two *cracked* (c) products can be produced, i.e., propylene and pentene. This propylene can then again *dimerize* (d) into one hexene molecule. Octene can also crack into two butene molecules. One last remark can be said about the production of heptene. No heptene production was detected. Therefore, it can be concluded that the alkylation of C_3 and C_4, which is the only possible production route for heptene, does not occur. The highest olefin that is produced on the Ni-β catalyst is octene.

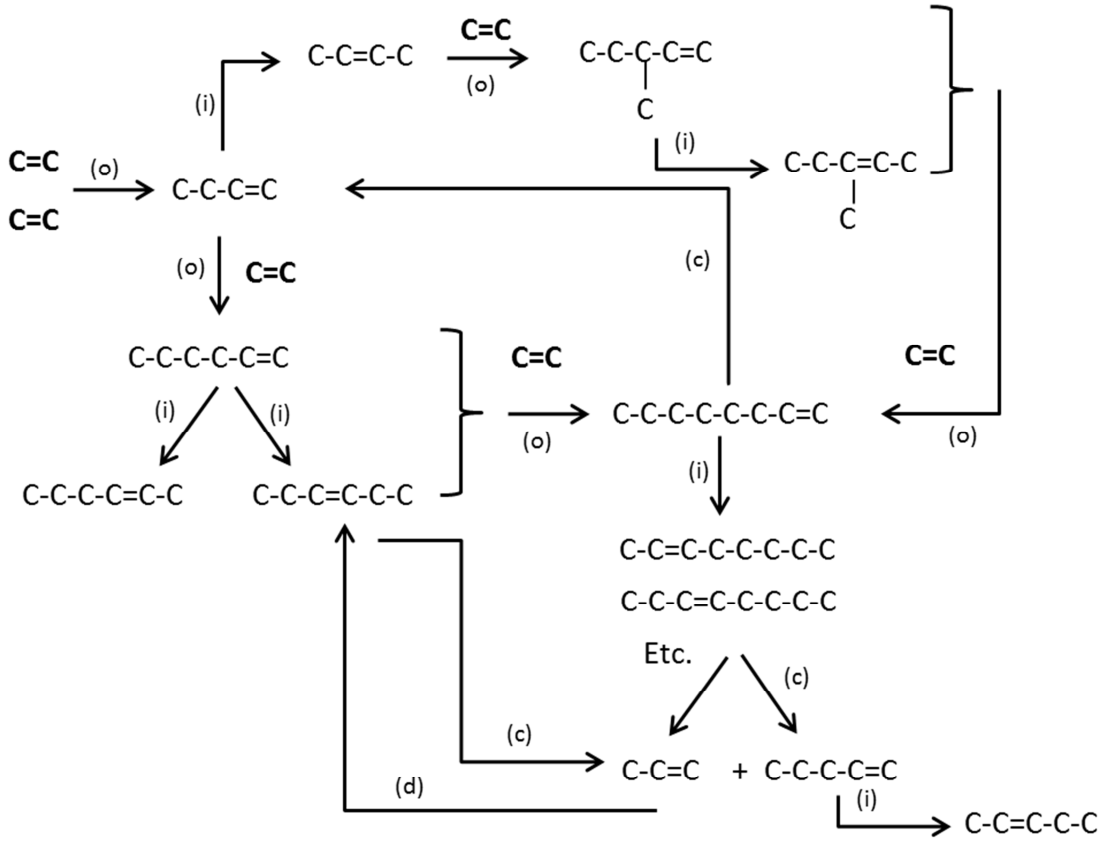

Figure 3-26: Reaction scheme for oligomerization of ethylene

3.8 CONCLUSION

In this chapter, the experimental work concerning the oligomerization of ethylene on a 4.89wt%Ni-β catalyst is discussed. First, the reaction conditions for which intrinsic kinetics is measured, were determined. Furthermore, the mixture had to remain in the gas phase in the setup to facilitate kinetic measurement. This is assured by means of dilution of the ethylene stream with nitrogen together with heated transfer lines and an infrared furnace.

During experiments, the influence of the pressure, temperature and space time was investigated. An increase in ethylene conversion with increasing pressure, temperature and space time was detected, in correspondence with literature. The main attention was put on the acidic behavior of the Ni-β catalyst. Additional to the linear alpha olefins, small amounts of odd-numbered olefins, i.e., propylene and pentene, were produced. This was favored with a low partial pressure of ethylene and a high temperature. By inspecting the composition of the Ni-β catalyst, its catalytic behavior was explained. The high weight percentage of nickel and the relative “high” acid sites concentration leads to pore blocking, hence the quick deactivation and low ethylene conversion.

The performance of the catalyst was compared with the reference catalyst, i.e., 1.8wt%Ni-SiO_2-Al_2O_3. A lower activity was detected, but the Ni-β catalyst was able to produce odd-numbered hydrocarbons. Although Ni-β has much more nickel and less acid sites, the acid sites are stronger and favor propylene production. On the other hand a quicker deactivation occurs, since the huge amount of nickel led to the clustering of NiO which blocks the active sites. This was not the case for the reference catalyst.

By using the insight obtained during experiments, a reaction network was proposed. The main reactions were metal ion oligomerization, isomerization, cracking and dimerization. Octene was the highest detected hydrocarbon and no C_7 was detected during the experiments. Through cracking of octene, propylene and pentene were produced.

3.9 REFERENCES

1. Reid, R.C., J.M. Prausnitz, and B.E. Poling, *The properties of gases and liquids*, ed. M.-H.I. editions. 1988.
2. Hulea, V. and F. Fajula, *Ni-exchanged AlMCM-41—An efficient bifunctional catalyst for ethylene oligomerization.* Journal of Catalysis, 2004. **225**(1): p. 213-222.
3. Quintana-Solórzano, R., *Single-Event Microkinetics for Coking in Catalytic Cracking: Development and Application.* 2007.
4. *Fluid bed catalytic Reactor*. 2011; Available from: http://jbrwww.che.wisc.edu/home/jbraw/chemreacfun/ch7/slides-masswrxn-2up.pdf.
5. Marin, G.B., *Chemische reactoren: principes en toepassingen.* Universiteit Gent, 2008.
6. Kimpe, B.D., *Ethylene oligomerization towards liquid fuels and chemicals* 2011.
7. Van Den Bleek, C.M., K. Van Der Wiele, and P.J. Van Den Berg, *The effect of dilution on the degree of conversion in fixed bed catalytic reactors.* Chemical Engineering Science, 1969. **24**(4): p. 681-694.
8. S., E., *Flow through Packed Columns.* Chemical Engineering Progress, 1952. **48**.
9. Vandegehuchte, B.D., et al., *n-Hexadecane hydrocracking Single-Event MicroKinetics on Pt/H-beta.* Applied Catalysis A: General, 2012. **441–442**(0): p. 10-20.
10. Toch, K., J.W. Thybaut, and G.B. Marin, *Ethylene oligomerization on amorphous Ni-SiO2-Al2O3: Experimental Investigation and Single-Event Kinetic Modeling*, 2012: Ghent University.
11. Fan, L., et al., *A theoretical study of ethylene oligomerization by organometallic nickel catalysts*, in *Studies in Surface Science and Catalysis*, J.B. M. Absi-Halabi and A. Stanislaus, Editors. 1996, Elsevier. p. 507-514.
12. Heveling, J., C.P. Nicolaides, and M.S. Scurrell, *Catalysts and conditions for the highly efficient, selective and stable heterogeneous oligomerisation of ethylene.* Applied Catalysis A: General, 1998. **173**(1): p. 1-9.

Chapter 4 Kinetic modeling

In this master thesis, the single-event microkinetic methodology is used to simulate the oligomerization of ethylene. To obtain a kinetic model that can be represented in a simulation program, a reaction network has to be generated. The network should consist of all the reactions that occur in the gas mixture, together with all the compounds present in this mixture. Once this reaction network is constructed, the reaction kinetics can be defined.

The kinetic of oligomerization will be described with several parameters that have to be estimated. These parameters consist of both catalyst descriptors, describing the effect of the catalyst properties on the kinetic, e.g., protonation enthalpies, and kinetic descriptors, describing the intrinsic properties of the reaction, e.g., activation energies. The outcome of the parameter values will then be evaluated by use of statistical tests as discussed in Chapter 2. Once a set of parameter values is defined, simulations can be performed with the kinetic model. Comparison between the experimental data and the simulations can then indicate the good practice of the model.

4.1 REACTION NETWORK GENERATION

When setting up a kinetic model, the compounds and reactions involved in that model have to be known. This is done by generating a reaction network which is a reflection of all the possible reactions that can occur. In this reaction network, kinetics are not accounted for. The construction of a reaction network can become easily a gargantuan effort. Therefore, a computer algorithm, ReNGeP, generated at the Laboratorium of Chemical Technology, LCT was used. ReNGeP was initially developed by Clymans and Froment for thermal cracking of (iso)alkanes [1] and further extended to acid catalyzed reactions by Baltanas and Froment [2].

4.1.1 Representation of molecules

ReNGeP uses a structural approach and takes into account some specified conditions, i.e., the maximum number of carbon atoms in the hydrocarbons, the amount of branches on the molecules, etc. The compounds are represented mathematically which makes it practical to implement into the

program. Boolean matrices and labels are chosen as the best way to represent every molecule in the network. As an example, the representation of 4-methyl-1-pentene will be given:

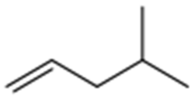

Figure 4-1: Representation of 4-methyl-1-pentene

	C_1	C_2	C_3	C_4	C_5	C_6
C_1	0	1	0	0	0	0
C_2	1	0	1	0	0	0
C_3	0	1	0	1	0	0
C_4	0	0	1	0	1	1
C_5	0	0	0	1	0	0
C_6	0	0	0	1	0	0
C_{sat}	1	1	0	0	0	0
C^+	0	0	0	0	0	0

When representing a hydrocarbon containing *n* carbon atoms, a 20x20 Boolean matrix is used. To indicate the connection between two carbon atoms *i* and *j*, the matrix element A_{ij} equals one. Otherwise when carbon *i* and carbon *j* are not connected, the corresponding matrix element equals zero. Not only the connection between the different carbon atoms is of importance, but also the degree of saturation of the carbon atom or its charge. Therefore a saturation vector, i.e., 'C_{sat}', and a carbenium ion vector, i.e., 'C^+', are added. When '$\mathrm{C_{sat_i}}$' equals one, the carbon atom *i* is unsaturated. The same representation is used for the carbenium ion vector. Hetero atoms are indicated with an extra column and every atom has a unique index, mostly corresponding with its atom number.

Since these matrices would consume an abundant amount of the memory, a 'smaller' label notation is used for every compound. This label summarizes all the necessary information of the matrix into 41 characters. To make sure that with every hydrocarbon only one label corresponds, a set of rules is introduced:

1. The first carbon is always a primary carbon.
2. The choice of the first carbon is made to obtain a chain length that has the maximum possible value.
3. For adsorbed species on a nickel ion, the numbering starts at the metal ion
4. Branched carbon atoms are numbered so that the carbon atom that is connected with the main branch has the lowest number.

5. For atoms with a double bond, the numbering starts closest to the double bound. Which means that the carbon atoms of the double bond have the lowest possible number.

An example of the label notation of 4-methyl-1-pentene is given:

0																		
1	2	2	3	1	1	0	0	0	0	0	0	0	0	0	0	0	0	0
28	28	29	29	29	29	0	0	0	0	0	0	0	0	0	0	0	0	0

The first value corresponds with the presence of a carbenium ion, i.e., the number of the carbon atom bearing the carbenium ion, is placed there. When no carbenium ion is present in the molecule, for example for an olefin, this value is zero. In the second row, the construction of the chain length is given. In the last row, the corresponding atoms are given. For a saturated carbon atom, this value is 29 and for an unsaturated carbon atom 28.

4.1.2 Representation of reactions

A reaction can be considered as a mathematical operation on the molecules and is also implemented in this way in the network. An example of an alkylation reaction is given in Figure 4-2.

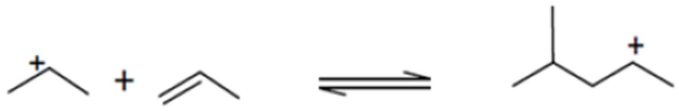

Figure 4-2: Alkylation reaction for production of pentene carbenium ion

This reaction is implemented in the model as a mathematical operation on the labels of the compounds, like is represented here:

```
Carb.Ion Olefin  Carb.Ion  type R  type P   ne
38       37      29        2       2        2.000000
```

The meaning of each column is described below [3]:

1st: Rank number of the reactant specie

2nd: Rank number of the second reactant

3rd: Rank number of the product

4th: Type of carbenium ion reactant, i.e., 1,2 or 3 corresponding respectively with primary, secondary or tertiary carbenium ions or zero for uncharged species

5th: Type of carbenium ion product, i.e., 1,2 or 3 corresponding respectively with primary, secondary or tertiary carbenium ions or zero for uncharged species

6th: Number of single-events of the elementary step

4.1.3 The ethylene oligomerization network

When generating the reaction network, some conditions have to be implemented to make sure it corresponds with the observations. In this thesis, only olefins containing up to 8 carbon atoms are produced experimentally and only one molecule is given as a start molecule, i.e., ethylene. Concerning the reactions, only the β-scission is added when comparing the network of the master thesis of B. De Kimpe [4].

To describe catalytic behavior only the most stable carbenium ion intermediates are considered, i.e. secondary and tertiary. Primary carbenium ions are considered to be not stable enough at the experimentally tested reaction conditions [5].

A summary of the reaction network that is used in the simulation is given in Table 4-1 and Table 4-2.

Table 4-1: Compounds involved in reaction network

Type of Compound	Number
Olefins	116
Carbenium ions	88

Table 4-2: Reactions involved in reaction network

Type of reaction	Number
Protonation	165
1,2 Alkyl shift	58
PCP branching	158
Beta-scission	23
Alkylation	23
Metal oligomerization	3
Desorption of metal site	4
Deprotonation	165

4.2 PARAMETER ESTIMATION PROGRAM

The aim of this thesis is to have a set of optimal parameter values for both kinetic and catalytic descriptors. To obtain the optimal set, an estimation program is used. In this paragraph, the global idea behind the program will be explained, see Figure 4-3.

The basis of the program is the kinetic model for the ethylene oligomerization. Here, the single-event methodology (SEMK) is chosen to represent the kinetics. This method uses the single-event concept

which reduces the number of reaction rate coefficients to one per reaction family. A more elaborate description of this SEMK model will be given in Chapter 5.

Besides a kinetic model, a reactor model is necessary. The reactor model describes the plug flow regime, as discussed in section 2.4. This model consists of a set of differential equations, where the right hand side corresponds with the net production rate R_i, see equation (2-15). Additionally thermodynamic data is necessary to assure the thermodynamic consistency of the model, i.e., the enthalpies and entropies of formation, etc. This data is calculated with the Benson's group contribution method [6].

Once all this information is combined, the differential equations can be solved with the aid of the DDASPK-routine, which is available in the NETLIB software library [7]. The output of these equations gives molar flow rates at the catalyst weight inputted that can be compared with the experimental data. As can be seen in Figure 4-3, all this information is coupled with two parameter estimation methods, i.e., the Rosenbrock and Levenberg-Marquardt methods [8]. These optimization algorithms minimize the difference between the simulated and the experimental data. Finally, a number of statistical tests, see section 2.5.2, are performed to control the accuracy and significance of the parameter estimation.

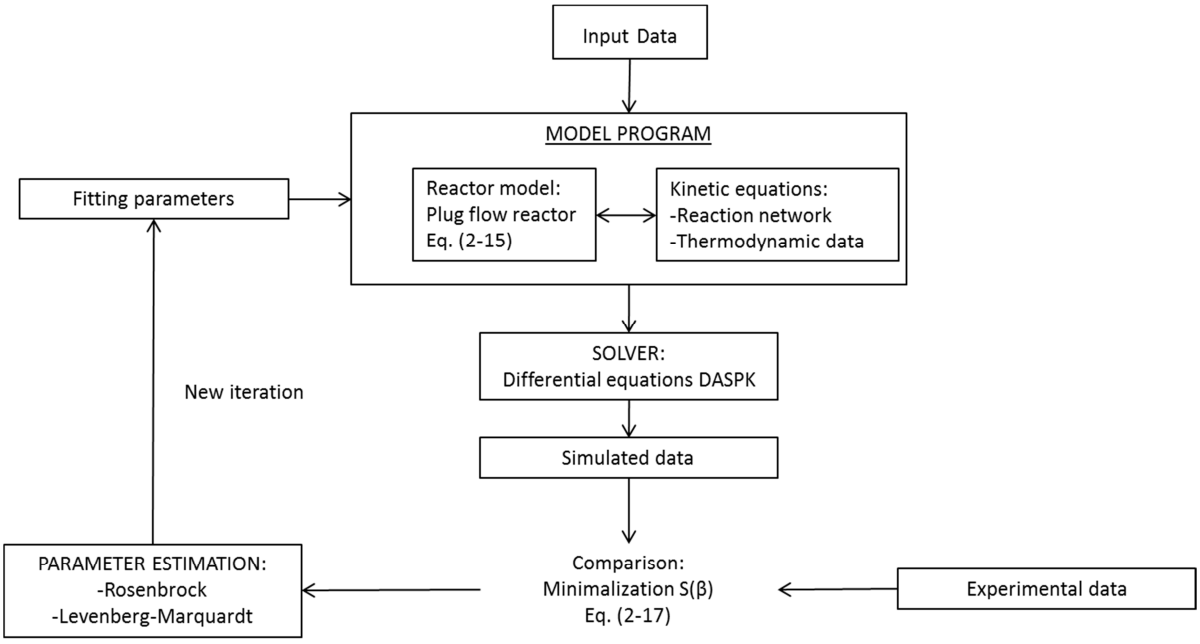

Figure 4-3: Flow sheet of the parameter estimation program

4.3 REFERENCES

1. Clymans, P.J. and G.F. Froment, *Computer-generation of reaction paths and rate equations in the thermal cracking of normal and branched paraffins.* Computers & Chemical Engineering, 1984. 8(2): p. 137-142.
2. Baltanas, M.A. and G.F. Froment, *Computer generation of reaction networks and calculation of product distributions in the hydroisomerization and hydrocracking of paraffins on Pt-containing bifunctional catalysts.* Computers & Chemical Engineering, 1985. 9(1): p. 71-81.
3. Quintana-Solórzano, R., *Single-Event Microkinetics for Coking in Catalytic Cracking: Development and Application.* 2007.
4. Kimpe, B.D., *Ethylene oligomerization towards liquid fuels and chemicals* 2011.
5. Van Borm, R., M.-F. Reyniers, and G.B. Marin, *Catalytic cracking of alkanes on FAU: Single-event microkinetic modeling including acidity descriptors.* AIChE Journal, 2012. 58(7): p. 2202-2215.
6. Benson, S.W., *THE PREDICTION OF THERMOCHEMICAL AND KINETIC DATA FOR GAS-PHASE REACTIONS - CURRENT STATUS.* Pure and Applied Chemistry, 1980. 52(7): p. 1767-1771.
7. Netlib. *DDASPK Routine*. 1/05/2013]; Available from: http://www.netlib.org/.
8. Thybaut, J.W., *Kinetische modelbouw en simulatie* 2011.

Chapter 5 Single-event microkinetic modeling (SEMK)

Kinetic modeling is an important technique that is often used to get an insight into the reaction mechanism of industrially relevant processes. By using the single-event microkinetic modeling (SEMK) methodology, the number of estimated parameters can be reduced significantly. This method is based on the single-event concept, that will be explained in this chapter. By grouping the elementary reaction steps in different reaction families, only one particular single-event reaction rate coefficient should be determined per family. To differentiate between different reactions in one reaction family, an individual number of single-events is introduced.

It is clear that this SEMK methodology is an excellent way to describe the kinetics for extensive reaction mechanisms. This approach describes the conversion of the hydrocarbons based on the chemistry that occurs on the catalyst surface with the aid of elementary reactions [1]. The purpose is to make the kinetic parameters independent on the feedstock and the length of the reactants.

Not only the reaction itself can have an influence on the reaction rate, but also the involved molecules. When taking about carbenium ions, different stabilization effects will occur between primary, secondary and tertiary ions. So this is an aspect that the model has to take into account. In order to reduce the set of estimated parameters, some thermodynamic constraints will be imposed to the model.

In this chapter the theory of the SEMK methodology will be discussed, together with an introduction of the assumptions and thermodynamic constraints that are applicable for oligomerization of ethylene.

5.1 SINGLE-EVENT MICROKINETIC MODELING (SEMK)

In the SEMK methodology, reactions families are defined rather than product based lumping. In addition, in this work, due to the bifunctional character of the catalyst, the reaction families can be categorized based on the type of catalytic center participating in the reaction, i.e., metal ionic or acidic. For the first, the reaction families are initiation, insertion and termination reactions while for the latter protonation, deprotonation, isomerization, i.e., 1,2 alkyl shift and PCP-branching, alkylation and beta-scission, see Figure 5-1.

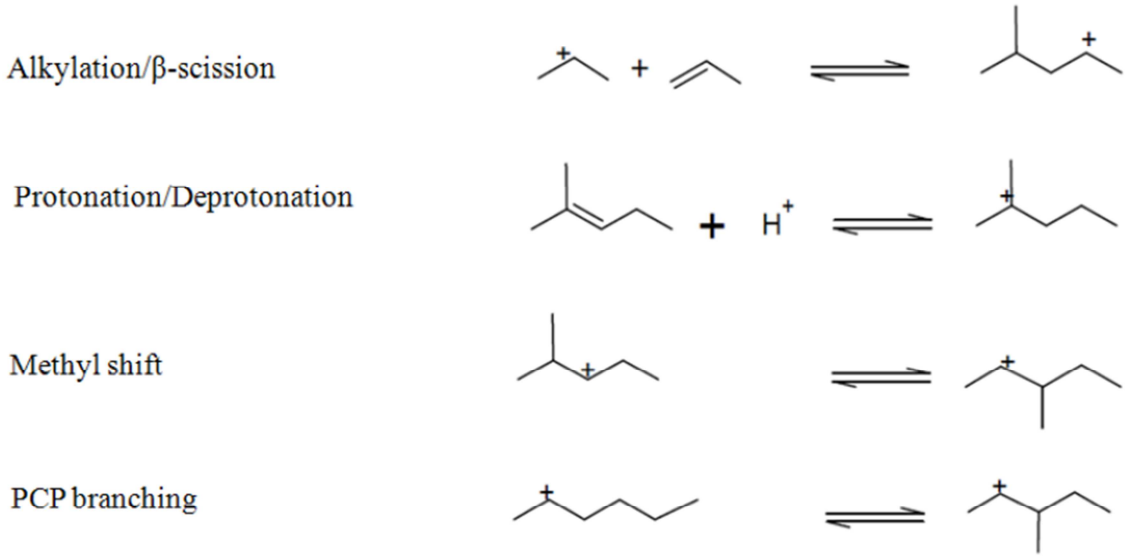

Figure 5-1: Elementary steps in the reaction mechanism

However, this first classification by reaction family still has to be extended, since the reaction rate coefficient within one family is still dependent on the structure of the molecules involved. In addition, for every reaction family involving carbenium ions, a distinction is made based upon the stability of the carbenium ions, i.e., secondary or tertiary.

The base equations of this single-event microkinetic modeling will be derived in the following paragraph. There, the influence of the structure of the compounds on the reaction rate coefficient will be taken into account with the use of statistical thermodynamics and the transition state theory.

5.1.1 The single-event concept

The single-event concept is based on the transition state theory. The rate coefficient of an elementary reaction that describes the reaction from reactants to products, passing through a transition state, consists out of an enthalpic and entropic term. To determine these terms, the energy

level of the transition state is required. The expression for the reaction rate coefficient for an elementary step is given by the Eyring equation [2]:

$$\tilde{k} = \frac{k_B.T}{h}.e^{\frac{\Delta G^{0,\neq}}{R.T}} = \frac{k_B.T}{h}.e^{\frac{\Delta S^{0,\neq}}{R.T}}.e^{-\frac{\Delta H^{0,\neq}}{R.T}} \quad (5\text{-}1)$$

with the k_b the Boltzmann constant, *T* the temperature, *h* the Planck-constant and *R* the universal gas constant. $\Delta S^{0\neq}$ and $\Delta H^{0\neq}$ correspond with the standard entropy and respectively standard enthalpy difference between the transition state and the reactants, see Figure 5-2.

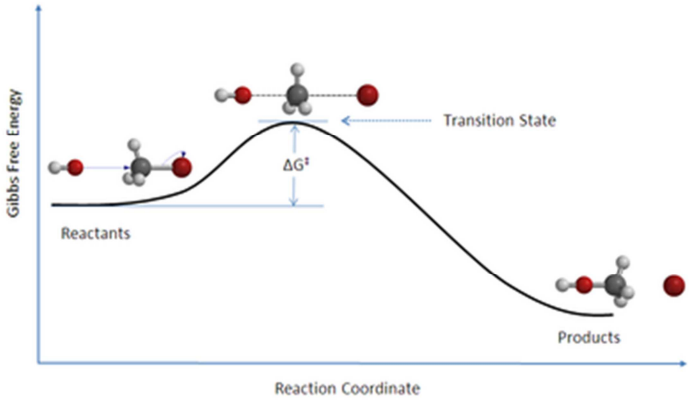

Figure 5-2: Transition state theory

In the transition state theory, the entropy change from the reactants to the transition state has four contributions, i.e., an internal and external rotational entropy term, a translational entropy term and a vibrational entropy term [3].

$$S = S_{trans} + S_{rot,int} + S_{rot,ext} + S_{vib} \quad (5\text{-}2)$$

The rotational entropy term will indicate the influence of the molecular structure of the reactants and the transition state into the reaction rate. It makes sure that, for every elementary reaction, the molecular structure is taken into account when calculating the rate coefficient.

Assuming that both the internal and external rotational entropy changes the symmetry of the molecule, these terms can be described by two contributions: the intrinsic standard entropy and a contribution coming from the symmetry:

$$S_{rot,int} = \widehat{S_{rot,int}} - R.\ln\sigma_{int} \quad (5\text{-}3)$$

$$S_{rot,ext} = \widehat{S_{rot,ext}} - R.\ln\sigma_{ext} \quad (5\text{-}4)$$

Where σ_{int} and σ_{ext} are the internal, respectively external symmetry number of the corresponding molecule.

Another aspect of the structure of the molecules is the presence of a chiral center. This center will increase the symmetry aspect of the entropy with a factor S_{chir} due to the fact that the mixture can contain different enantiomers. This contribution can be written as:

$$S_{chir} = R.\ln 2^n \tag{5-5}$$

in which *n* represent the number of chiral atoms in the molecule and 2^n corresponds with the number of enantiomers that are possible.

Combining equations (5-3), (5-4) and (5-5) leads to:

$$S_{rot} = \widehat{S_{rot}} - R.\ln\frac{\sigma_{int}.\sigma_{ext}}{2^n} \tag{5-6}$$

Introducing a global symmetry number:

$$\sigma_{gl} = \frac{\sigma_{int}.\sigma_{ext}}{2^n} \tag{5-7}$$

With σ_{int} the internal symmetry number and σ_{ext} the external symmetry number.

When the entropy difference between the transition state and the reactants is taken into account, it can be written as:

$$\Delta S^{0,\neq} = \Delta S^{0,\neq}_{trans} + \Delta S^{0,\neq}_{vib} + \widehat{\Delta S^{0,\neq}_{rot}} + R.ln\left(\frac{\sigma^r_{gl}}{\sigma^{\neq}_{gl}}\right) \tag{5-8}$$

Finally, this equation can be implemented into the Eyring equation:

$$\tilde{k} = \frac{\sigma^r_{gl}}{\sigma^{\neq}_{gl}}.\frac{k_B.T}{h}.e^{\frac{\widehat{\Delta S^{0,\neq}}}{R.T}}.e^{-\frac{\Delta H^{0,\neq}}{R.T}} \tag{5-9}$$

With:

$$\widehat{\Delta S^{0,\neq}} = \Delta S^{0,\neq}_{trans} + \Delta S^{0,\neq}_{vib} + \widehat{\Delta S^{0,\neq}_{rot}} \tag{5-10}$$

Equation (5-11) shows that the rate coefficient of an elementary step is given in terms of the single-event rate coefficient, $\tilde{k}$, and the number of single-events, n_e.

$$k = n_e.\tilde{k} \tag{5-11}$$

The influence of the molecular structure of reactants and the transition state is taken into account by implementing the number of single-events corresponding with the respective elementary reaction. The single-event rate coefficient is equal for every elementary step within one reaction family.

However, the carbenium ions involved in this case are not free, but linked in a zeolite structure. Kazansky et al. have investigated that its effect would be identical on the energy level of the reactant and the transition state, so that n_e the ratio of global symmetry numbers would be the same as that for free carbenium ions [4].

5.1.2 Single-event rate coefficients

As already stated, the single-event rate coefficients are influenced by their reaction family as well as by the carbenium ions involved. In the reaction network only the two most stable carbenium ions are considered, i.e., secondary and tertiary. It is assumed that the energy level of a carbenium ion is completely defined by its type, i.e., secondary or tertiary [4].

In Figure 5-3 the stability effects of the different carbenium ions are represented: a tertiary carbenium ion is the most stable one due to the increasing number of substituents capable of hyper conjugation.

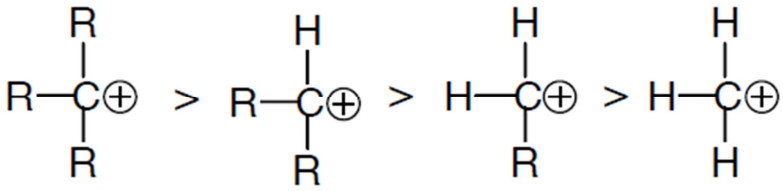

Figure 5-3: Stability of the different carbenium ions

Practically this means, that for one reaction family, e.g., alkylation, only four different reaction rate coefficients have to be considered, i.e. $k_{alk(s,s)}$, $k_{alk(s,t)}$, $k_{alk(t,s)}$ and $k_{alk(t,t)}$, where *s* stands for secondary, *t* for tertiary and the '*alk*' for alkylation reaction. With these four reaction rate coefficients only, the alkylation kinetics can be described.

Only for deprotonation, also the formed olefin is of importance. Which means that for every olefin, two deprotonation reaction rate coefficients are necessary, i.e. $k_{depr(s,O_i)}$ and $k_{depr(t,O_i)}$. By using thermodynamic consistency, this number can be reduced.

As a justification for the fact that for alkylation and protonation the rate coefficient is not dependent on the olefin, it can be stated that the structure of the activated complex is very close to the reacting olefin [5].

5.2 THERMODYNAMIC CONSTRAINTS

All the parameters have to be thermodynamically independent of each other. For the deprotonation and isomerization, this leads to a reduction of the estimated parameters. Also a thermodynamic constraint between alkylation, i.e. acid oligomerization, and β-scission is present. In this chapter, these thermodynamic constraints will be demonstrated.

5.2.1 Deprotonation rate coefficients

Considering the protonation and deprotonation reaction that can isomerize a double bond from olefin O_1 and olefin O_2:

$$O_1 + H^+ \leftrightarrow C_1^+ \leftrightarrow O_2 + H^+ \tag{5-12}$$

Thermodynamically this can be represented as:

$$K_{iso}(O_1 \leftrightarrow O_2) = \frac{k_{pr(m)}}{k_{depr(m,O_1)}} . \frac{k_{depr(m,O_2)}}{k_{pr(m)}} = \frac{k_{depr(m,O_2)}}{k_{depr(m,O_1)}} \tag{5-13}$$

Where *m* defines the type of carbenium ion, which can be secondary *'s'* or tertiary *'t'*. This equation indicates that for every deprotonation leading to another olefin a different single-event reaction rate coefficient is needed. Additionally, a distinction should be made between deprotonation starting from a secondary or a tertiary carbenium ion.

For a large reaction mechanism, this can lead to an extensive number of rate coefficients. Therefore it would be interesting to link every olefin with a reference olefin, from where the reaction rate coefficient can be considered. Choosing a proper reference olefin, containing all the necessary information, e.g., type carbenium ion, number of carbon atoms, etc., and by taking equation (5-13) into account, the number of deprotonation coefficients can be reduced:

$$k_{depr(m,O_i)} = K_{iso(O_i \leftrightarrow O_r)} . k_{depr(m,O_r)} \tag{5-14}$$

With O_r the corresponding reference olefin of O_i. This equation indicates that now, only one rate coefficient for deprotonation for every olefin has to be taken into account[6].

5.2.2 Isomerization rate coefficients

For the isomerization reactions, the single-event rate coefficients were, up to now, only depending on the type of carbenium ions of the reactants and products, which led to 4 rate coefficients per

isomerization: $k_{iso(s,s)}$, $k_{iso(s,t)}$, $k_{iso(t,s)}$ and $k_{iso(t,t)}$. When considering the next reaction, starting from a secondary to a tertiary carbenium ion:

$$O_1 + H^+ \leftrightarrow R_1^+ \leftrightarrow R_2^+ \leftrightarrow O_2 + H^+ \tag{5-15}$$

Assuming that R_1^+ corresponds with a secondary carbenium ion and R_2^+ with a tertiary carbenium ion.

The isomerization equilibrium coefficient can be written as:

$$K_{iso} = \frac{k_{pr(s)}}{k_{depr(s,O_1)}} \cdot \frac{k_{iso(s,t)}}{k_{iso(t,s)}} \cdot \frac{k_{depr(t,O_2)}}{k_{pr(t)}} \tag{5-16}$$

By substituting the relation between the k_{depr} and K_{iso} of equation (5-14), a relation between $k_{iso(s,t)}$ and $k_{iso(t,s)}$ is found:

$$k_{iso(t,s)} = k_{iso(s,t)} \cdot \frac{k_{pr(s)}}{k_{pr(t)}} \cdot \frac{k_{depr(t,O_r)}}{k_{depr(s,O_r)}} \tag{5-17}$$

Which means that for every isomerization reaction, the number of single-event rate coefficients is reduced to three instead of four.

5.2.3 Thermodynamic consistency between alkylation and β-scission reaction

Finally, the relationship between alkylation and β-scission reactions is investigated. Because the alkylation reaction is the reverse reaction of the β-scission reaction, the reaction rate coefficients are dependent of each other.

Consider the following β-scission reaction:

$$O_3 + H^+ \leftrightarrow R_3^+ \leftrightarrow R_2^+ + O_1 \leftrightarrow O_1 + O_2 + H^+ \tag{5-18}$$

With a corresponding equilibrium coefficient:

$$K\ (O_3 \leftrightarrow O_2 + O_1) = \frac{k_{pr(m)}}{k_{depr(m;O_3)}} \cdot \frac{\widetilde{k_{cr(m;n)}}}{\widetilde{k_{alk(n;O3,m)}}} \cdot \frac{k_{depr(n;O2)}}{k_{pr(n)}} \tag{5-19}$$

From equation (5-19), $k_{cr(m,n)}$ is correlated with $k_{alk(n,m)}$. By using a Born Haber cycle, see Figure 5-4, the activation energy of the β-scission reaction can be written in terms of the activation energy of the alkylation reaction.

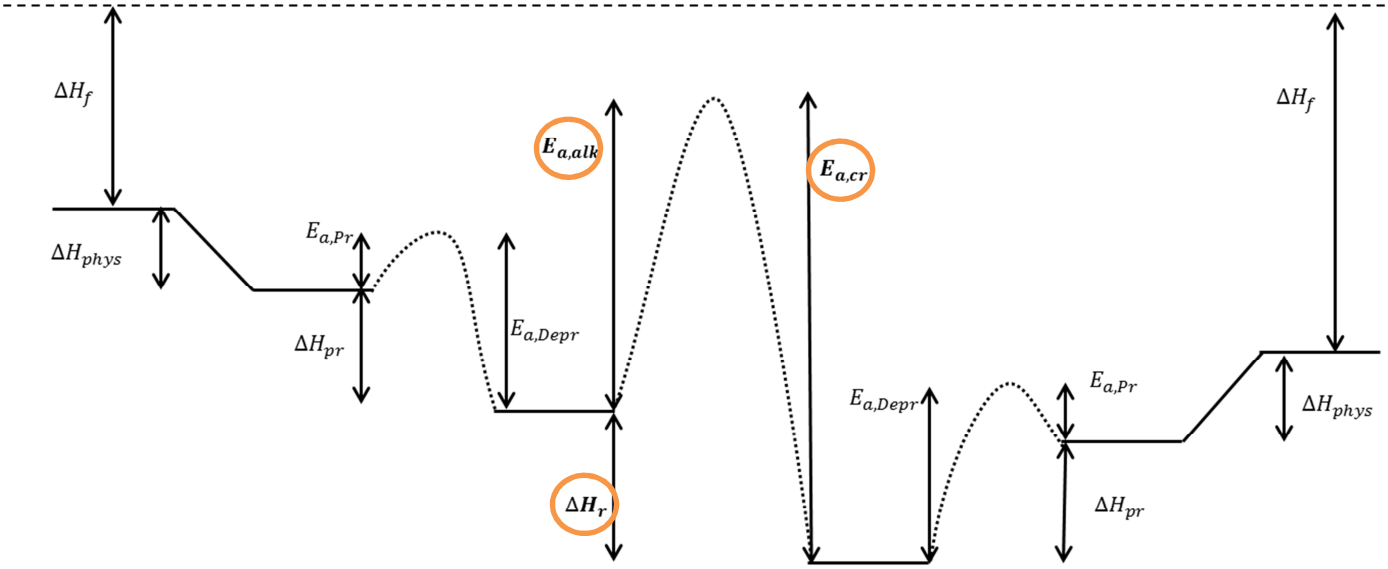

Figure 5-4: Born haber cycle of alkylation/β-scission reaction

From Figure 5-4 the following equations can be obtained:

$$E_{a,cr} = E_{a,alk} - \Delta H_r \tag{5-20}$$

Where ΔH_r is the reaction enthalpy of the alkylation reactions and this can be written as follows:

$$\Delta H_r = [\Delta H_{f,O_2} + \Delta H_{f,O_1} - \Delta H_{f,O_3}] - \Delta H_{phys,O_1} - \Delta H_{phys,O_2} - \Delta H_{pr,O_2} + \Delta H_{phys,O_3} + \Delta H_{pr,O_3} \tag{5-21}$$

These assumptions make it possible to describe all the alkylation and beta-scission reactions with only four activation energies that have to be estimated. However, next to the activation energy, also an entropy factor is present in the reaction rate coefficient. This entropy factor is different for alkylation and beta-scission reaction, since the reactant molecules are different. For the alkylation reaction, no definition of the entropy change is found. However, the entropy change of β-scission reaction can be described by means of the translational entropy [7]:

$$\Delta S_{cr}^{\circ\neq} = \frac{1}{3} S_{trans}^{\circ}(R_3^+) \tag{5-22}$$

Translation entropy is completely related with the molecular weight of carbenium R_3^+. In the transition state the C-C bond in the β-position of the positive charge is being broken. This enlarges the distance between the ionic part at the acid site and the olefin being physisorbed on the zeolite surface. Since this requires translational motion of the leaving olefin, the transition state is assumed to possess one degree of translational freedom [8].

Both entropy changes are correlated with the global reaction entropy:

$$\Delta S_r = \Delta S_{cr}^{\circ\neq} - \Delta S_{alk}^{\circ\neq} \quad (5\text{-}23)$$

From which the $\Delta S_{alk}^{\circ\neq}$ can be determined. The ΔS_r is determined in a similar way as the ΔH_r.

5.3 DETERMINATION OF REFERENCE OLEFINS

In Paragraph 5.2, the importance of well-chosen reference olefins was already emphasized. Every carbenium ion should be connected to one specific reference olefin. The main aspect to define the reference olefins, is that they contain the right information, i.e. the number of carbon olefins and the possibility to produce a carbenium ion. In this case, 2-methyl-2-olefins were chosen as reference olefins. This olefin is able to form both a secondary carbenium ion and a tertiary carbenium ion, as can be seen in see Figure 5-5.

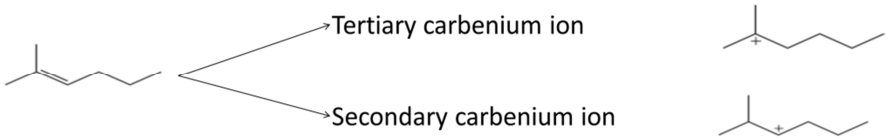

Figure 5-5: Choice of reference olefin

5.4 COLLECTION OF SINGLE-EVENT RATE COEFFICIENTS

The methods that were discussed in the paragraphs above were used to minimize the number of rate coefficients. Here, a brief description will be given of all the rate coefficients that will be implemented and estimated by the model. In Table 5-1 a summary of all the single-event rate coefficients are given for the elementary reactions with carbenium ions.

Table 5-1: Conclusion of single-event rate coefficients for the elementary reactions where carbenium ions are involved

Reaction	Single-event rate coefficients			
Isomerization: Alkyl shift, PCP-branching	$k_{iso(s,s)}$	$k_{iso(s,t)} = f(k_{iso(t,s)})$		$k_{iso(t,t)}$
alkylation	$k_{alk(s,s)}$	$k_{alk(s,t)}$	$k_{alk(t,s)}$	$k_{alk(t,t)}$

5.5 THE NUMBER OF SINGLE-EVENTS (n_e)

In paragraph 5.1.1 the concept of single-event was introduced and the importance of the number of single-events was indicated. The number of single-events is the ratio of the global symmetry number from the reactants to the global symmetry number of the transition state:

$$n_e = \frac{\sigma_{gl}^{r}}{\sigma_{gl}^{\neq}} \tag{5-24}$$

with:

$$\sigma_{gl} = \frac{\sigma_{int} \cdot \sigma_{ext}}{2^n} \tag{5-25}$$

Introducing the number of single-events for every elementary step makes it possible to differentiate the reaction rate within one reaction family, characterized with only one single-event rate coefficient $\tilde{k}$. Physically, the number of single-events describes the symmetry of the reactant molecules and of the transition state. It is a measure of the number of geometrically independent ways in which the transition state can be formed out of the reactant [9]. This indicates that for this single-event concept, a lot of insight in the symmetrical properties of the reactant molecules and especially in the structure of the transition state has to be known.

For example, an ethylene molecule does not have any chiral atom, thus, *n* equals zero. Due to the presence of π-electrons, even no internal symmetry axis is present. In gas phase, ethylene has three external symmetry axis, i.e., the x, y and z axis. However, a physisorbed ethylene molecule, is not able to rotate along axis perpendicular to the catalyst surface. Hence, only one symmetry axis will remain after physisorption [10].

As an example, the determination of the number of single-events for a β-scission reaction will be explained in detail. For this type of reactions, the empty p-orbital of the charged C-atom with the σ C-C bond in β-position of the charge location, causes a cleavage of this bond. This results in a smaller carbenium ion and formation of a double bond using the electron pair of the cleaving C-C bond. During this β-cleavage, two of the sp^3-orbitals of the α-carbon change in two sp^2-orbitals. The third sp^3-orbital, that is connected with the leaving group, changes into a completely filled p-orbital. This filled orbital will combine with the vacant p-orbital of the electron-deficient carbon, forming the original carbenium ion, to the double bond [8].

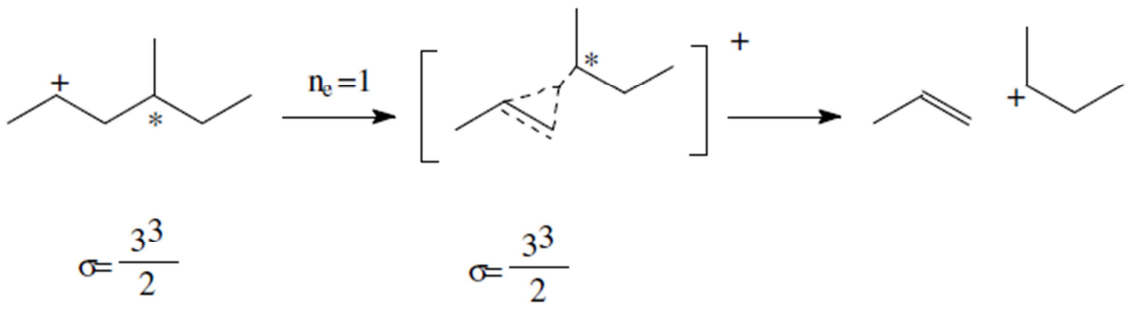

Figure 5-6: Determination number of single-events for beta-scission [8]

During the formation of the transition state an energy-lowering overlap occurs between the vacant p-orbital and the electrons of the sp^3-orbital forming the breaking C-C bond. This interaction will be maximal when the two orbitals are coplanar. Figure 5-6 indicates the determination of the number of single-events. For β-scission, only one way exists between the reactant and its transition state, i.e. n_e equals one. The asterisks(*) indicates the presence of a chiral center.

5.6 REFERENCES

1. Borm, R.V., *Single-Event Microkinetics of Hydrocarbon Cracking on Zeotype Catalysts: Effect of Acidity and Shape Selectivity*, 2011.
2. Wilde, W.D., *Oligomerisatie van Ethyleen naar Vloeibare Brandstoffen en Chemicaliën*, in *Laboratory for Chemical Technology*, 2009-2010, University of Ghent. p. 155.
3. Baltanas, M.A., et al., *Fundamental kinetic modeling of hydroisomerization and hydrocracking on noble metal-loaded faujasites. 1. Rate parameters for hydroisomerization.* Industrial & Engineering Chemistry Research, 1989. **28**(7): p. 899-910.
4. Dewachtere, N.V., F. Santaella, and G.F. Froment, *Application of a single-event kinetic model in the simulation of an industrial riser reactor for the catalytic cracking of vacuum gas oil.* Chemical Engineering Science, 1999. **54**(15–16): p. 3653-3660.
5. Froment, G.F., *Kinetic modeling of acid catalyzed oil refining processes.* Catalysis Today, 1999. **52**(2–3): p. 153-163.
6. Quintana-Solórzano, R., *Single-Event Microkinetics for Coking in Catalytic Cracking: Development and Application.* 2007.
7. Vynckier, E., *Kinetische modellering van de katalytische hydrokraking.* Universiteit Gent, 1997.
8. Gert, M., *Hydrocracking on Pt/US-Y zeolites fundamental kinetic modelling and industrial reactor simulation.* 2000.
9. Toch, K., et al., *A Single-Event Micro Kinetic model for "ethylbenzene dealkylation/xylene isomerization" on Pt/H-ZSM-5 zeolite catalyst.* Applied Catalysis a-General, 2012. **425**: p. 130-144.
10. Toch, K., J.W. Thybaut, and G.B. Marin, *Ethylene oligomerization on amorphous Ni-SiO2-Al2O3: Experimental Investigation and Single-Event Kinetic Modeling*, 2012: Ghent University.

Chapter 6 SEMK model for oligomerization of ethylene

A second part of this master thesis is the design of a kinetic model for oligomerization of ethylene that is capable to describe the acid catalyzed reactions. From a previous thesis, a SEMK model describing the metal catalyzed reactions was available. To expand this model, first the elementary reaction steps have to be determined and a series of hypothesis have to be made. By considering the thermodynamic constraints, as introduced in Chapter 5, the acid catalyzed reactions are introduced with a minimum number of parameters.

The experimental dataset, obtained on the Ni-β catalyst, shows signs of acid reactions, so it can be used in the adapted kinetic model. With this dataset, parameter values for kinetic descriptors, i.e., activation energy for cracking, and catalytic descriptors, e.g., protonation enthalpies are determined. By performing a statistical study on the set of parameters, the significance of the regression and the individual values is tested.

Once values for these descriptors are obtained, simulations are performed. By comparing the simulated behavior with the experimental behavior, the performance of the model and the parameter values is verified.

Finally, to obtain an insight into the reaction network, a reaction path analysis is executed. There, the most significant production route for every compound is determined, giving an idea about the relative importance of the different reactions.

6.1 ETHYLENE OLIGOMERIZATION MECHANISM

For the determination of a SEMK model, first, the elementary steps based on the reaction mechanism have to be known. A description of the mechanism is given in section 1.4.2 and the reaction network,

with the different reaction families, in section 4.1.3. Figure 6-1 gives a schematic overview of the reactions on the bifunctional catalyst.

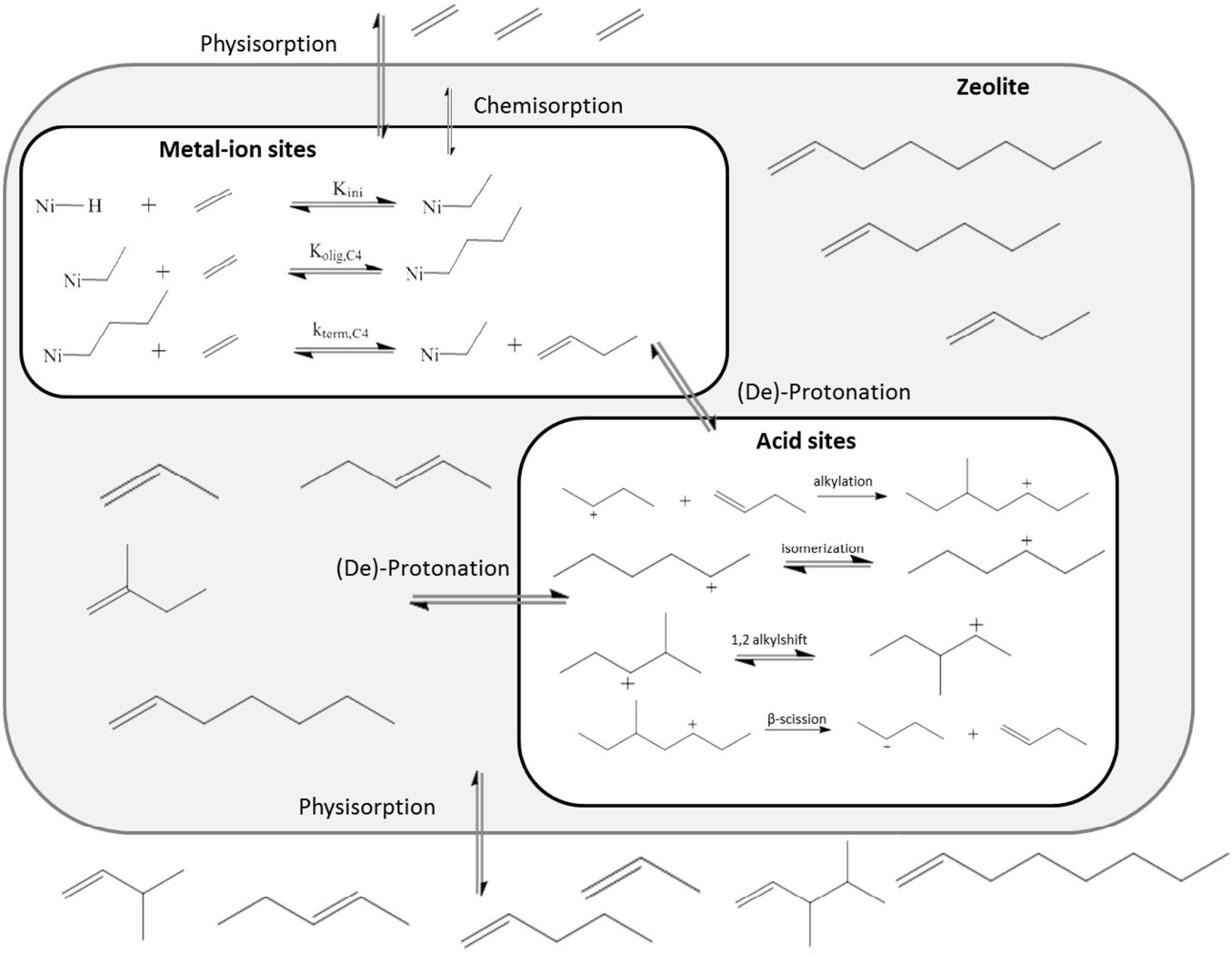

Figure 6-1: Reaction mechanism on zeolite structure

The implementation of the different reactions will now be discussed in more detail.

6.2 KINETIC MODEL FOR ETHYLENE OLIGOMERIZATION

In this part, the kinetic model for the oligomerization of ethylene on a heterogeneous catalyst will be elaborated. The kinetic model consists out of equations determining the production rate of each olefin in the reaction mixture. The model makes a distinction between the reactions that occur on the metal ion sites and the acid sites. Besides the elementary reaction steps, also the physisorption is implemented. This step is determined by using the Langmuir assumptions.

6.2.1 Langmuir physisorption of olefins

Every olefin has the possibility to physisorb on the catalyst surface as a consequence of physical interactions. It is clear that the partial pressure of that olefin will have a significant influence on the degree of physisorption. Increasing the partial pressure will lead to a higher physisorbed concentration of that olefin, as long as the surface is not completely saturated:

$$O_i + phys^* \overset{K_{phys}}{\longleftrightarrow} O_{i,phys} \tag{6-1}$$

The site balance over the catalyst can be represented as follows:

$$C_{phys,tot} = C_{phys^*} + \sum_{i=1}^{n_{ole}} C_{O_{i,phys}} \tag{6-2}$$

Where C_{phys^*} corresponds with the concentration of free sites for physisorption on the surface [mol g_{cat}^{-1}] and $C_{O_{i,phys}}$ the concentration of the physisorbed species of olefin i [mol g_{cat}^{-1}].

For every olefin, the equilibrium between the olefin in the gas phase and the physisorbed molecules is calculated by means of the Langmuir assumptions [2]:

1. The adsorption takes place at specific centers of the catalyst.
2. The adsorption is limited to a monolayer.
3. All the adsorption sites are equivalent.
4. The ability of a molecule to adsorb is independent of the total occupation at that moment. So no interaction occurs between different adsorbed molecules.

Equation (6-1) indicates the first assumption considered in this kinetic model:

Hypothesis 1: The physisorbed species are in quasi equilibrium.

6.2.2 Reactions on the metal ion sites

For the modeling of the reactions occurring on the metal ion sites, one has to understand the reaction mechanism on these sites. A good insight in this mechanism, makes it possible to determine the elementary reaction steps. These steps form the basis of the single-event kinetic model, as explained in Chapter 5.

In literature, the knowledge of the mechanism on a heterogeneous catalyst is quite limited and not detailed enough. Therefore the reaction mechanism describing the metal ion catalyzed reactions is based on the homogeneous catalyzed mechanism. This mechanism consists out of three main steps,

i.e. an initiation step, an oligomerization step and a termination step. A detailed description of this reaction mechanism can be found in previous work [3], [4],[9].

The most important elementary reactions steps will be discussed very briefly. The nickel ion in equation (6-3) indicates the active metal ion site that is present in the matrix of the heterogeneous catalyst. About the oxidation state of this nickel ion still a lot of debating is going on, so a detailed discussion will not be given.

1. Initiation of a nickel ion, i.e., formation of the actual active species, by ethylene chemisorption

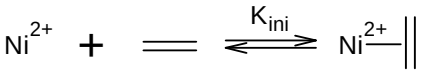

(6-3)

1. Chemisorption of an ethylene molecule on a nickel-ethyl species.

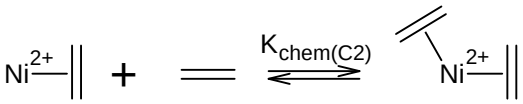

(6-4)

2. 1,2 insertion of a nickel-di-ethyl species

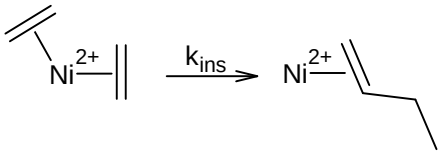

(6-5)

3. Chemisorption of an ethylene molecule on a nickel-butyl specie

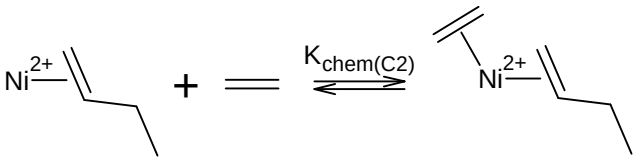

(6-6)

4. Termination of a nickel-ethyl-butyl species by β-hydride transfer leading to a butene molecule

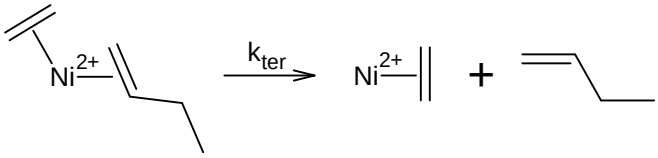

(6-7)

5. 1,2 insertion of a nickel-ethyl-butyl species for further oligomerization towards hexene

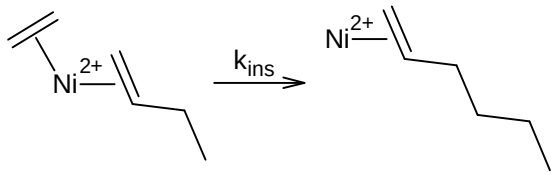

(6-8)

The production rate can be derived by assuming a steady state for the nickel complexes, i.e., the net rate of formation of the ethyl-nickel complexes is zero.

Hypothesis 2: The initiation is always in equilibrium, in other words, oligomerization and termination are rate determined.

Hypothesis 3: The chemisorbed olefins on the Ni^{2+} centers are in pseudo steady state.

Hypothesis 4 : Insertion of ethylene in the nickel-alkyl complex is irreversible.

6.2.3 Reactions on the acid sites

The first acid catalyzed reactions are protonation and deprotonation. Once a carbenium ion is produced, several secondary acid catalyzed reactions can occur: alkylation/acid catalyzed oligomerization, PCP-branching, 1,2-alkyl shifts and β-scission/ cracking. These last reactions are responsible for the formation of isomers and the product distribution of the mechanism.

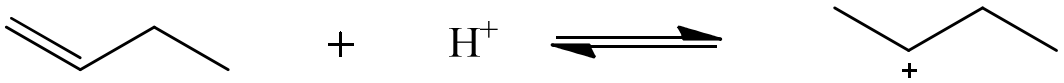

(6-9)

Hypothesis 5: Protonation and deprotonation are in quasi equilibrium.

The protonation of ethylene is not considered, due to the very low stability of a primary carbenium ion. This means that in the kinetic model, only secondary and tertiary carbenium ions will be available. Equation (6-10), (6-11) and (6-12) represents several acid catalyzed reactions, respectively 1,2-alkyl shift, alkylation vs. β-scission and PCP-branching.

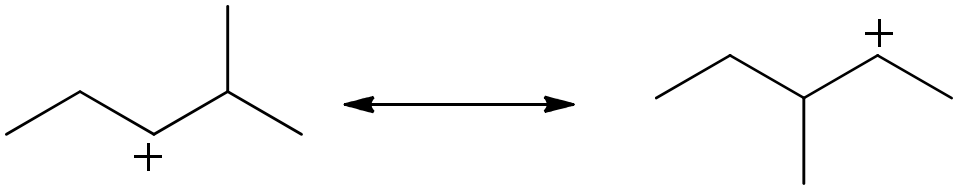

(6-10)

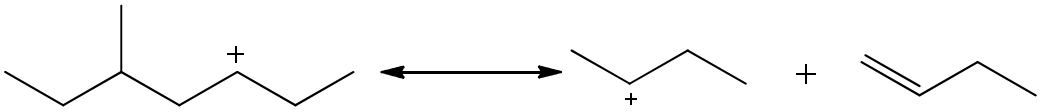

(6-11)

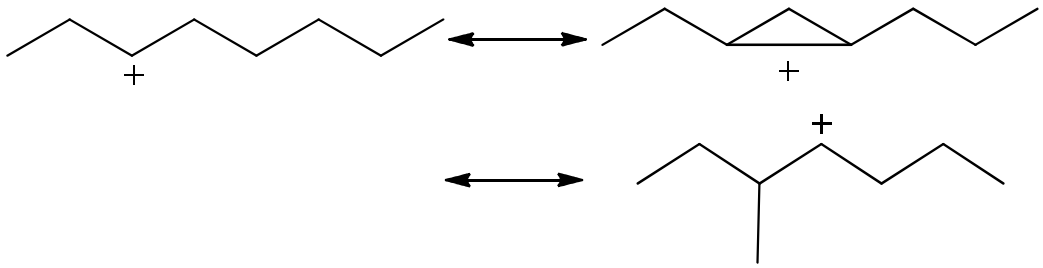

(6-12)

The presence of these reactions can be detected by means of the presence of hydrocarbons with an odd carbon number, i.e. propylene and pentene. Concerning the carbenium ions, one additional hypothesis will be introduced.

Hypothesis 6: The carbenium ions are in quasi steady state.

This assumption indicates that the net production rate of every carbenium ion is equal to the production rate of the olefin as a consequence of the acid activity of the catalyst [3]. Practically, all the olefins with the same carbon skeleton are lumped. This means that within the kinetic model all the reaction rates for the carbenium ions within the same lump are count together.

6.3 PARAMETERS IN THE KINETIC MODEL

In this paragraph, the adjustments to the model and the new parameters will be discussed. A number of kinetic parameters will be kept constant as they were determined by K. Toch, i.e., the activation energies for the metal catalyzed oligomerization [4]. This is valid within the SEMK concept since these are kinetic descriptors and are equal for these nickel-ion catalyzed reactions, which is not the case for catalyst descriptors.

6.3.1 Determination model parameters

In total, 4 single-event rate coefficients, 1 physisorption coefficient and 1 (de)-protonation equilibrium coefficient need to be determined. The (de)-protonation equilibrium coefficient can be calculated as in equation (6-13). The protonation enthalpy will be determined by regression, see section 6.3.4.1.

$$K_{pr} = e^{\frac{\Delta S_{pr}}{R}} . e^{-\frac{\Delta H_{pr}}{R.T}} = e^{-\frac{(\Delta S_{trans} + \Delta S_{phys})}{R}} . e^{-\frac{\Delta H_{pr}}{R.T}} \quad (6\text{-}13)$$

The Langmuir physisorption coefficient is calculated as the ratio of the Henry coefficient H and the saturation concentration C_{sat} of the considered component [7]:

$$K_{phys}(C_i) = \frac{H}{C_{sat}} \tag{6-14}$$

With the Henry coefficient defined as follows:

$$H = e^{\frac{\Delta S_{phys}}{R}}.e^{-\frac{\Delta H_{phys}}{R.T}}.\frac{C_{sat}}{2.p^0} = A_{phys}.e^{-\frac{\Delta H_{phys}}{R.T}} \tag{6-15}$$

One physisorption coefficient has to be introduced per carbon length. In this case, eight different coefficients will be determined. A more detailed discussion of this physisorption enthalpy, and its estimation is given in section 6.3.4.1.

Finally, the reaction rate coefficients have to be determined for 1,2-alkyl shift, PCP-branching, alkylation and β-scission.

$$\tilde{k} = \frac{k_B.T}{h}.e^{\frac{\Delta S^{\neq}}{R}}.e^{-\frac{E_a}{R.T}} = A.e^{-\frac{E_a}{R.T}} \tag{6-16}$$

Where the pre-exponential factors are calculated based on the transition state theory, see section 6.3.2. The values for the activation energies can be estimated, as for cracking, or took from literature, since they are kinetic descriptors [7].

In this chapter, only the acid catalyzed reactions are discussed, since the metal catalyzed reactions were already available in the model.

6.3.2 Calculation of the pre-exponential factors

By determining the entropy change between the reacting species and the transition state, the values for the pre-exponential factors are determined. As discussed in section 5.2.3, the entropy change for β-scission is determined as one third of the translational entropy. There, it was also discussed how to determine the entropy change, and so the pre-exponential factor, for alkylation.

For the PCP-branching and the 1,2-alkyl shift, no entropy change is considered, since no loss of translational entropy occurs during the reaction.

6.3.3 Calculation of the physisorption entropies

For the determination of the entropy change due to physisorption, the loss of one degree of freedom is assumed during physisorption, i.e., translational movement on the surface is still allowed. Thus, the entropy change during physisorption is approximated by one third of the translation entropy [7].

6.3.4 Activation energy, protonation and physisorption enthalpy

6.3.4.1 Physisorption enthalpy

As explained in section 6.2.1, the Langmuir assumptions are considered for physisorption. However, still a physisorption enthalpy has to be applied in the model. In the model, the physisorption will be described by two parameters, i.e., ΔH_{phys} and $\Delta\Delta H_{phys}$. The first describing the physisorption of ethylene, the second parameter is then added to take into account the carbon number of the molecule. Since physisorption enthalpy is considered to be linearly dependent on the hydrocarbon length, as determined by B. De Moor et al [5]. The two physisorption parameters are considered to be catalytic descriptors and will be estimated.

6.3.4.2 Protonation enthalpy

As explained in Chapter 5, the stability of the carbenium ions is dependent on its type. For the oligomerization of ethylene, it is considered that no primary carbenium ions are present in the model. Therefore, only secondary and tertiary carbenium ions are involved. To indicate the stability effect between the different ion types, the factor $\Delta\Delta H_{pr}$ was estimated. With equation (6-17) the protonation enthalpy of the tertiary carbenium ion can be calculated:

$$\Delta H_{pr}(t) = \Delta H_{pr}(s) - \Delta\Delta H_{pr} \tag{6-17}$$

B.D.Vandegehuchte et al. have shown that this stability value should be around 30kJ mol^{-1} [6].

Subsidiary for short molecules, the stability of the carbenium ions depends on the possibility to distribute the charge through hyper conjugation, i.e. the longer the substituents, the more stable [5]. This indicates that also the length of the substituents has a stabilization effect. In this kinetic model, this influence will not be taken into account, to reduce complexity.

6.3.4.3 Alkylation and cracking reaction

Four parameters are implemented to subscribe the kinetics of the alkylation reactions, taking into account the type of carbenium ions involved. By using the thermodynamic consistency between alkylation and β-scission, see section 5.2.3, only the activation energies of alkylation are estimated.

6.3.4.4 Isomerization

Two reaction families are responsible for isomerization, i.e., 1,2-alkyl shift and PCP-branching. By using the thermodynamic consistency introduced in section 5.2.2, each family is described by three activation energies, e.g., $E_{a,12AS}$(s,s), $E_{a,12AS}$(s,t) and $E_{a,12AS}$(t,t).

6.4 REGRESSION OF EXPERIMENTAL DATA

The aim is to obtain values for the catalytic and kinetic descriptors by performing regression. Due to the limited number of experimental points, together with the fact that the acid behavior on this Ni-β catalyst is not very pronounced, see Chapter 3, it was difficult to obtain a set of significant parameter values. Therefore, the following procedure was used:

- Regression of data with only metal ion catalyzed reactions. In this way, initial values for ΔH_{phys}, $\Delta\Delta H_{phys}$ and ΔH_{chem} could be defined. Since the selectivity towards butene is very high, i.e., circa 90mol%, in comparison with the selectivity towards the cracking products, i.e., circa 0.1mol%, this is a valid assumption.
- Further regression and estimation of the acidic parameters, i.e., protonation enthalpy and the activation energies for alkylation, keeping the parameter values as obtained in the previous step fixed.
- Estimation of all the parameters together with the previous estimated values as initial guesses.

Still the difference in the stabilization effect of protonation was difficult to find. As such, it was very challenging to estimate all four activation energies for alkylation independently. In literature, a set of initial parameter values was found for the activation energies of β-scission, which is directly related to the activation energies for alkylation. However, since these reported values for β-scission were found for hydrocracking in which the reverse reaction, i.e., alkylation was not considered, it is assumable that the absolute values for the activation energies for β-scission, and, thus, alkylation, are not fully applicable in this case. On the other hand, it can be assumed that the absolute difference between the activation energies reported will remain identical. This difference between the activation energies for alkylation has been taken constant while the absolute value of $E_{a(s,s)}$ is estimated. By doing so, values for all the activation energies could be determined.

6.4.1 Summary of the parameters

A summary of the kinetic and catalytic descriptors, i.e., parameters for the model, is given in Table 6-1. Within the SEMK methodology, a distinction is made between kinetic and catalytic descriptors. A kinetic descriptor is used for describing the intrinsic properties of an elementary reaction, e.g., activation energy, pre-exponential factor, etc. which is supposed to be independent from external factors such as the catalyst used. In contrast, a catalyst descriptor is used for describing the effect of the catalyst properties on the kinetics, e.g. protonation and physisorption coefficients or total active site concentration [7]. Not all these descriptors will be estimated. For some values, e.g., E_a for

insertion and termination, the value was already defined, for others, values from literature were used.

Table 6-1: Summary of kinetic and catalytic descriptors

Kinetic descriptor		Catalytic descriptor	
E_a 1,2Alkyl shift for (s,s) *	$E_{a,12AS}(s,s)$	Protonation enthalpy secondary C^+	$\Delta H_{pr}(s)$
E_a 1,2 alkyl shift for (s,t)*	$E_{a,12AS}(s,t)$	Delta protonation enthalpy	$\Delta\Delta H_{pr}$
E_a 1,2 alkyl shift for (t,t) *	$E_{a,12AS}(t,t)$	Physisorption enthalpy	ΔH_{phys}
E_a PCP branching for (s,s) *	$E_{a,PCP}(s,s)$	Delta physisorption enthalpy	$\Delta\Delta H_{phys}$
E_a PCP branching for (s,t) *	$E_{a,PCP}(s,t)$	Chemisorption enthalpy	ΔH_{chem}
E_a PCP branching for (t,t) *	$E_{a,PCP}(t,t)$		
E_a alkylation for (s,s)	$E_{a,alk}(s,s)$		
E_a alkylation for (s,t) **	$E_{a,alk}(s,t)$		
E_a alkylation for (t,s) **	$E_{a,alk}(t,s)$		
E_a alkylation for (t,t) **	$E_{a,alk}(t,t)$		
E_a insertion***	$E_{a,ins}$		
E_a termination***	$E_{a,ter}$		

*: Values from literature were used: B.D.Vandegehuchte et al.[6] ;

**: Values were determined out of the estimated value for $E_{a,alk}(s,s)$ with the additional term, see Table 6-2;

***: Values were determined on reference catalyst, i.e., 1.8wt%Ni-SiO_2-Al_2O_3 [4],

6.4.2 Regression results

A regression is obtained with the experimental data set on the Ni-β catalyst. The importance of a set of valuable initial guesses was already indicated above. The initial parameter values were obtained from a SEMK model for hydrocracking, see Table 6-2 [6].

Table 6-2: Summary of initial parameter values

Parameter	Value [kJ mol^{-1}]	Parameter	Value[kJ mol^{-1}]
$E_{a,12AS}$ (s,s)	81.4	$E_{a,alk}$ (s,s)	21.4
$E_{a,12AS}$ (s,t)	76.8	$\Delta E_{a,alk}$ (s,t)	-1.0
$E_{a,12AS}$ (t,t)	105.0	$\Delta E_{a,alk}$ (t,s)	19.6
$E_{a,PCP}$ (s,s)	109.0	$\Delta E_{a,alk}$ (t,t)	10.0
$E_{a,PCP}$ (s,t)	92.6		
$E_{a,PCP}$ (t,t)	125.0		

Secondly, the kinetic descriptors concerning the metal ion kinetics were already determined in previous work [4],see Table 6-3.

Table 6-3: Parameter values for metal catalyzed reactions [4]

Parameter	Value [kJ mol^{-1}]
$E_{a,ins}$	76.3
$E_{a,ter}$	67.8

The results of the regression are found in Table 6-4, together with the standard deviation and calculated t values.

Table 6-4: Summary of the results of the regression analysis

Parameter	Estimated value [kJ mol^{-1}]
ΔH_{chem}	-107.10 ±0.13
$\Delta H_{pr}(s)$	-32.20 ± 6.20
$\Delta\Delta H_{pr}$	0.99 ± 0.01
ΔH_{phys}	-9.99 ± 1.6
$\Delta\Delta H_{phys}$	-31.03 ± 0.38
ΔE_a	21.35 ± 1.26
$F_{calc,\ sign}$	$F_{tab,sign}(\alpha=0.95)$
234.0	3.1

The best results were obtained with a very small difference between the protonation enthalpy of a secondary and a tertiary carbenium ion, i.e., 0.99kJ mol^{-1}. A possible explanation for this, is the low acid activity of the catalyst. Since the molar flows of the cracked products, i.e., propylene and pentene are relatively small, i.e., 10^{-2}-10^{-3}µmol s^{-1}, it is difficult for the simulation program to determine the effect of the stability of the ion. However, literature suggests that this amounts to 30 kJ mol^{-1} [6].

Physically, the high chemisorption enthalpy for the Ni-β indicates the high interaction between ethylene and the metal ion sites. Compared to the reference catalyst with a chemisorption enthalpy of-49.9kJ mol^{-1}, the ethylene molecules have a higher tendency to interact with the metal ion sites on the Ni-β catalyst. This can be explained by the formation process of these metal-ions as suggested by Fan et al. [8].The nickel ion sites interact with acid site to become active. It could be that the interaction of nickel-ions with the more acidic sites of Ni-β compared to the reference catalyst, leads to much stronger nickel-ion sites. The occupancy of, preferentially, the strong acid sites by a large

amount of nickel, i.e., about 5wt%, can lead to a decrease of the overall acid site strength, and hence the relative low protonation enthalpy, i.e., -32kJ mol^{-1}, compared to literature, i.e., -70kJ mol^{-1}.

The physisorption enthalpy is only slightly lower than the value obtained on the 1.8wt%Ni-SiO_2-Al_2O_3, i.e., -12.3kJ mol^{-1}. Moreover, a higher $\Delta\Delta H_{phys}$ is found on the Ni-β catalyst. Indicating that the hydrocarbon length has a higher influence on the Ni-β catalyst.

Concerning the activation energies obtained for acid catalyzed oligomerization and cracking, the value for $E_{a,alk}(s,s)$ was estimated as 42.7 kJ mol^{-1}. The other activation energies for alkylation can then be determined starting from this value, and the additional differences given in Table 6-2. With the application of the thermodynamic constraints, given in section 5.2.3, the activation energies for β-scission were determined. A value of 150-160kJ mol^{-1} is found, which is in comparison with was found in literature [6].

6.4.3 Statistical analysis

6.4.3.1 Significance of the regression

From Table 6-4, it is clear that the obtained regression is significant, as the calculated F_{sign} value is much higher than the tabulated F_{tab} value. If the regression would not be significant, the zero-hypothesis should be considered.

6.4.3.2 Binary correlation between the parameters

The correlation matrix can be found in Table 6-5. Two parameters can be considered independent if the absolute value of their corresponding correlation coefficient is smaller than 0.95. For this simulation, all the coefficients are much smaller than this value, indicating that the parameters are independent.

Table 6-5: Correlation matrix

	ΔH_{chem}	$\Delta H_{pr}(s)$	ΔH_{phys}	$\Delta\Delta H_{phys}$	$\Delta\Delta H_{pr}$	ΔE_a
ΔH_{chem}	1.00	-0.00	-0.15	0.00	0.00	-0.15
$\Delta H_{pr}(s)$	-0.00	1.00	-0.02	-1.00	-0.00	0.02
ΔH_{phys}	-0.15	-0.02	1.00	0.02	-0.14	0.86
$\Delta\Delta H_{phys}$	0.00	-1.00	0.02	1.00	0.00	-0.02
$\Delta\Delta H_{pr}$	0.00	-0.00	-0.10	0.00	1.00	-0.12
ΔE_a	-0.15	0.02	0.86	-0.02	-0.12	1.00

6.4.4 Model simulations

Once the parameters were estimated, simulations with these values could be done. The simulated values are then compared with the results obtained by experimental study. Figure 6-2 represents all the parity plots of the compounds produced during reaction. A parity plot of heptene, i.e., C_7, is not given since this was not detected both during experiments as during simulation.

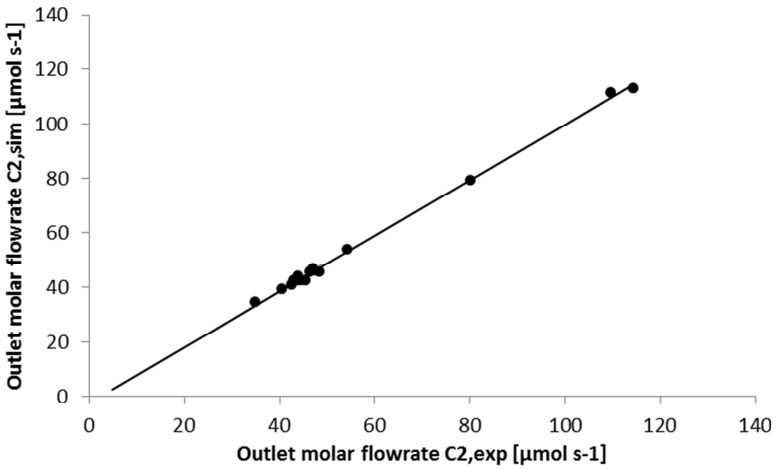

(A)

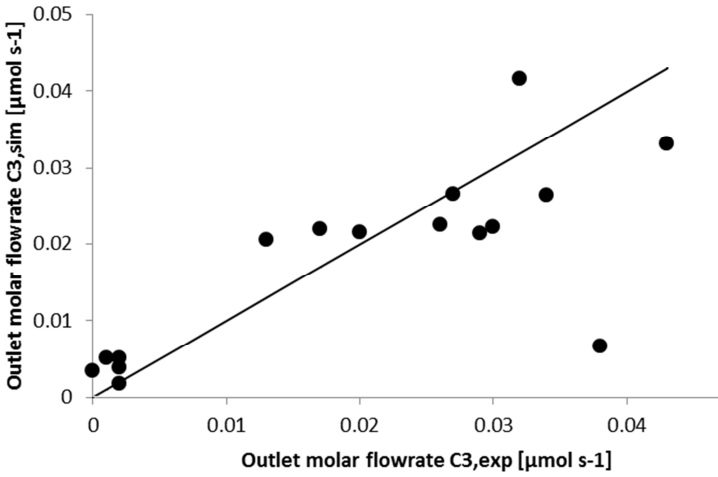

(B)

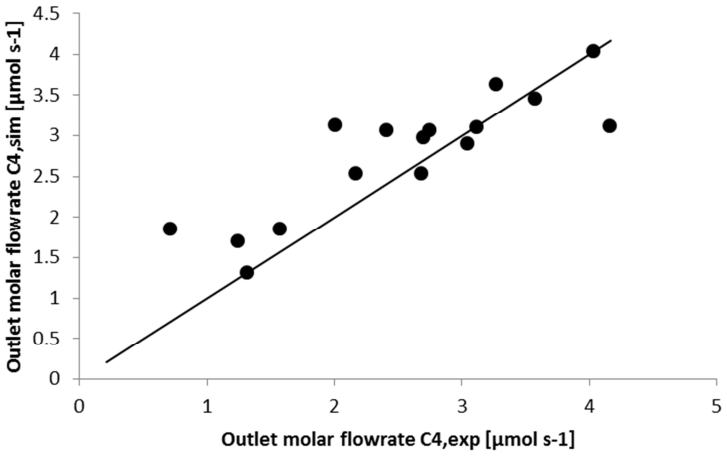

(C)

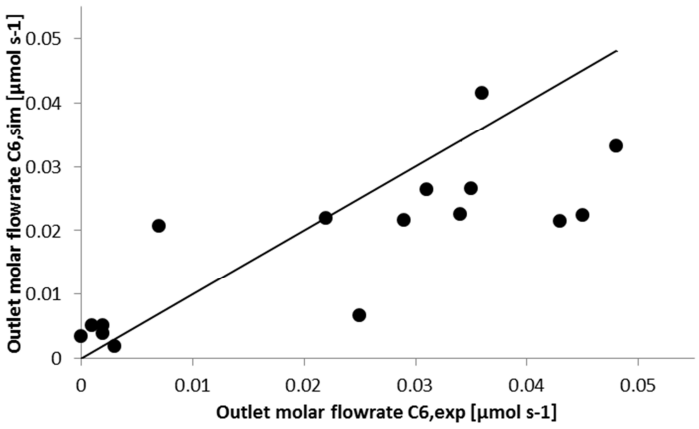

(D)

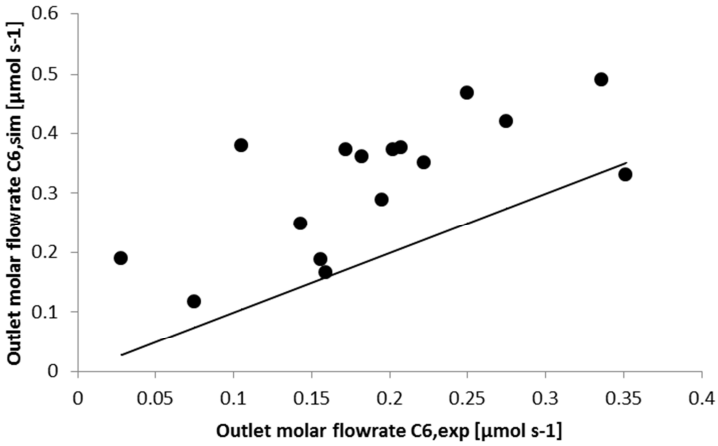

(E)

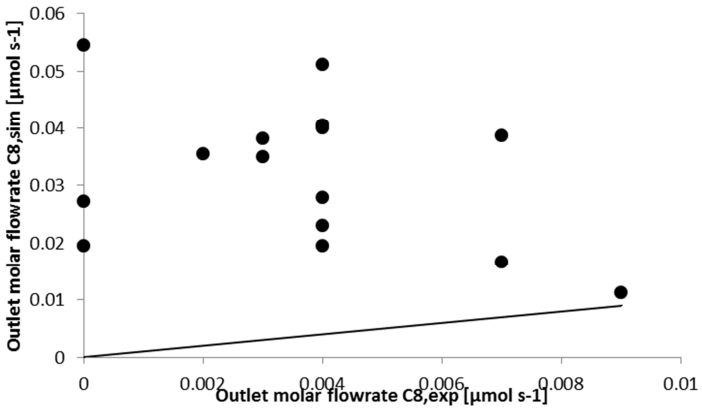

(F)

Figure 6-2: Parity plot obtained by simulation of ethylene oligomerization with the experimental dataset as given in Appendix B and the parameter values tabled in; (A) Parity diagram for the molar outlet flow rate of ethylene; (B) Parity diagram for the molar outlet flow rate of lumped propylene;(C) Parity diagram for the molar outlet flow rate of lumped butene; (D) Parity diagram for the molar outlet flow rate of lumped pentene;(E) Parity diagram for the molar outlet flow rate of lumped hexene; (F) Parity diagram for the molar outlet flow rate of lumped octene.

From the parity plots it can be concluded that a quite satisfactory agreement is obtained for ethylene and butene. However, how smaller the molar outlet flow rates become, the larger the relative error on the molar outlet flow rates. This indicates the existence of a relative big error on the experimental dataset, especially for the *cracking* products, and can also explain why the molar flow rate of octene is so difficult to determine accurately. As an example, the molar outlet flow rates of octene have a value around 10^{-3}µmol s^{-1}, and ethylene around 10^{2}µmol s^{-1}.

6.4.5 Residuals

The results of the simulation were given above in Figure 6-2. It has to be verified that no special effects or dependencies were introduced in the model. This can be verified by means of the residuals. Here, the residuals as function of temperature, pressure and space time will be discussed for the cracking products. Figure 6-3 ,Figure 6-4 and Figure 6-5 indicate that no dependencies were introduced into the model. This means that the error between the experimental value and the simulated value is independent of the reaction conditions and no systematical deviations are introduced.

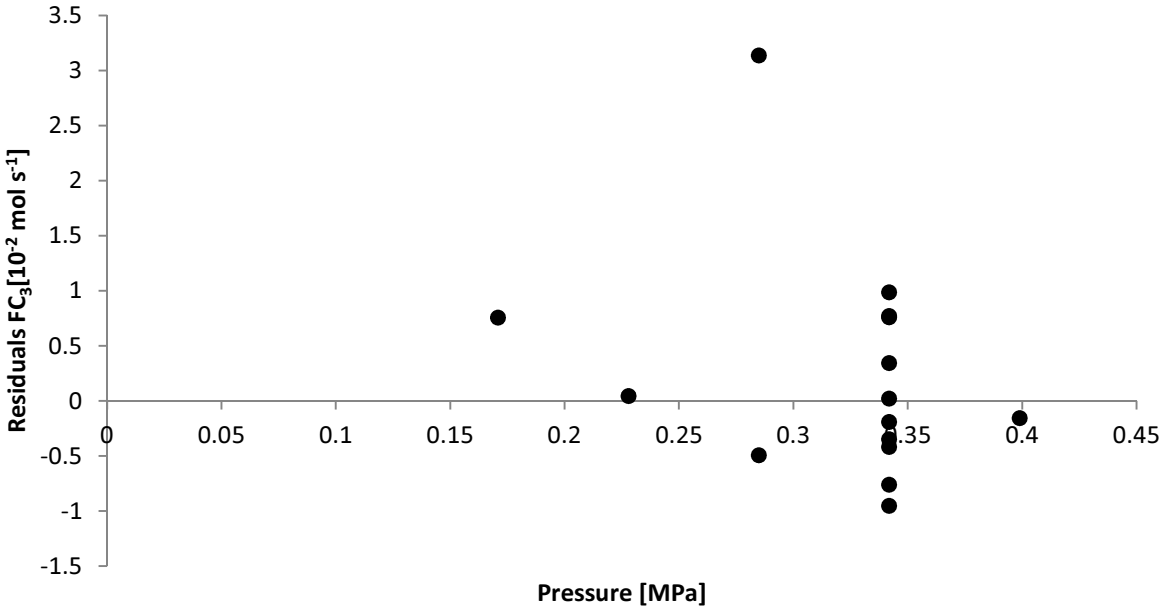

Figure 6-3: Residual figure of the molar outlet flow rate of propylene as function of partial pressure of ethylene

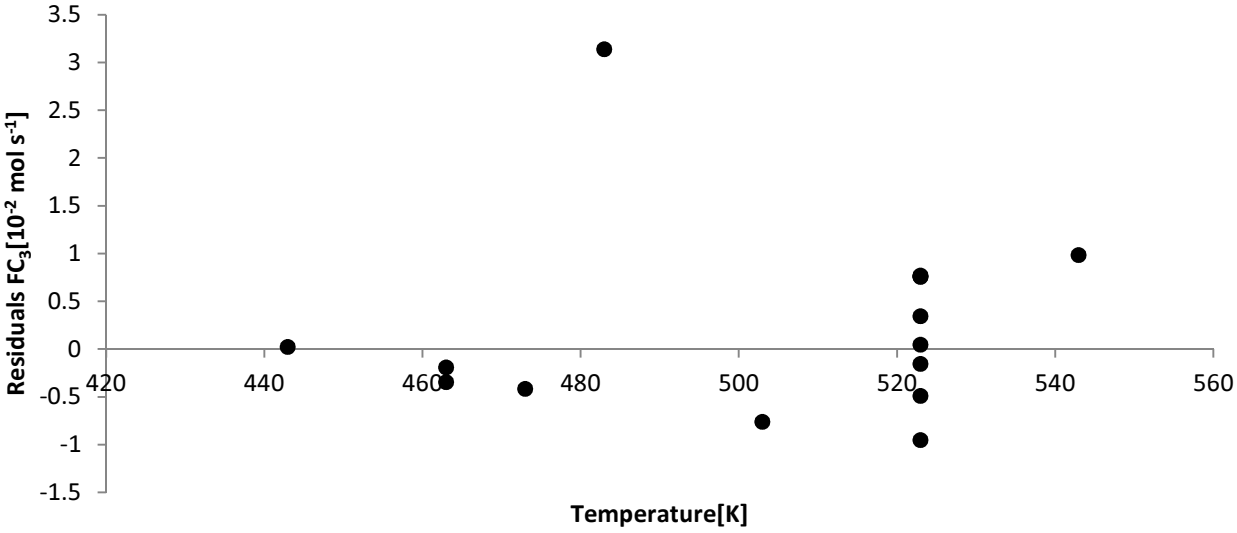

Figure 6-4: Residual figure of the molar outlet flow rate of propylene as function of temperature

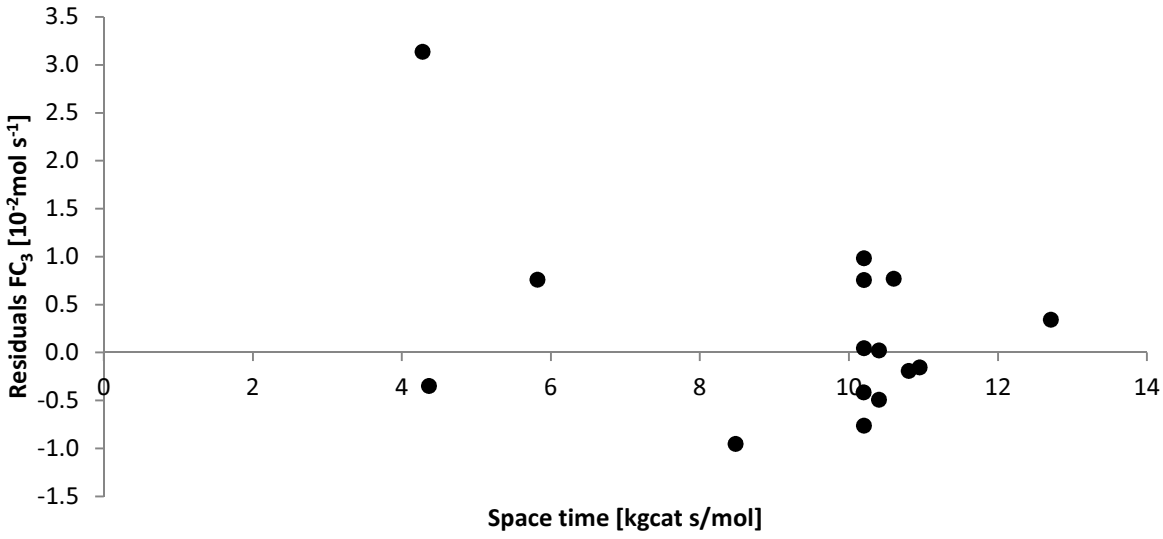

Figure 6-5: Residual figure of the molar outlet flow rate of propylene as function of space time

6.5 MODEL PERFORMANCE

In the previous paragraph, it became clear that a number of difficulties were accompanied with the regression of the data. Therefore, the performance of the model is investigated. First, the pressure is varied, see Figure 6-6. In this case, the pressure dependency on the ethylene conversion was not simulated adequately. When comparing this with the experimental data, it is clear that the pressure influence in the model is not corresponding with experiments. Therefore, more experimental data should be available, over a broader pressure range and with a more pronounced acidic behavior.

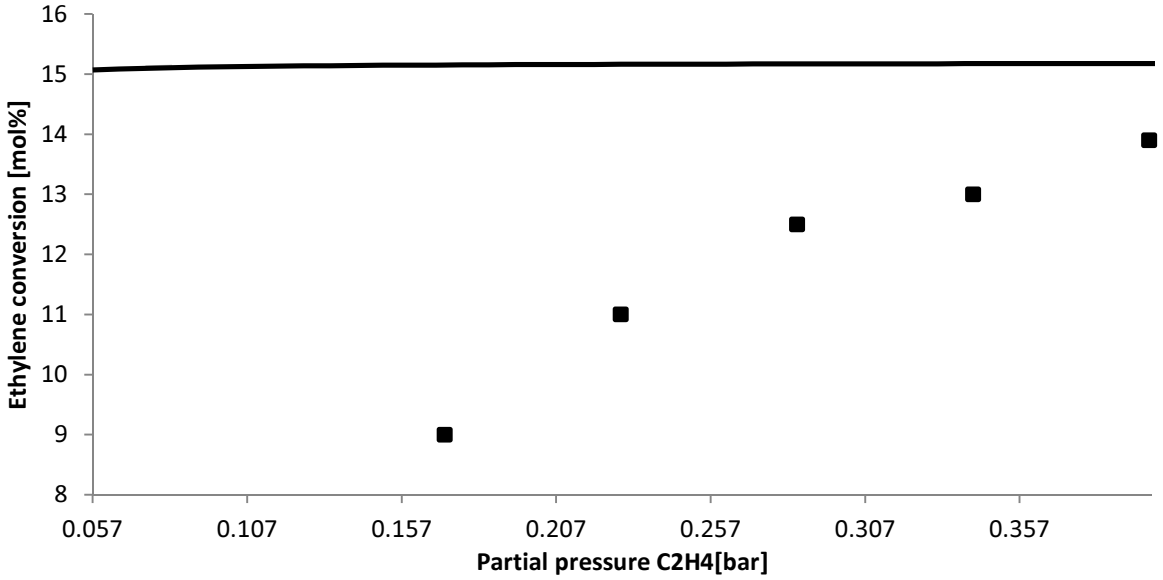

Figure 6-6: Conversion of ethylene oligomerization on 4.89wt%Ni-β as function of space time;(■) experiments; full line: simulation. Model simulations are obtained with the parameter values as reported in Table 6-4, a temperature of 523K and a space time of 10 $kg_{cat}s\ mol^{-1}$.

Concerning the temperature effect, the kinetic model together with the set of parameters corresponds rather good with the experimental data. On Figure 6-7 the same increasing trend for ethylene conversion is found. Looking at the simulated selectivities for propylene and lumped pentene, the experimental trend is also simulated. This indicates again the relative good implementation of the temperature effect in the model. However, the absolute experimental values do not correspond with the simulated ones. This can be attributed to the small molar flows detected during experiments.

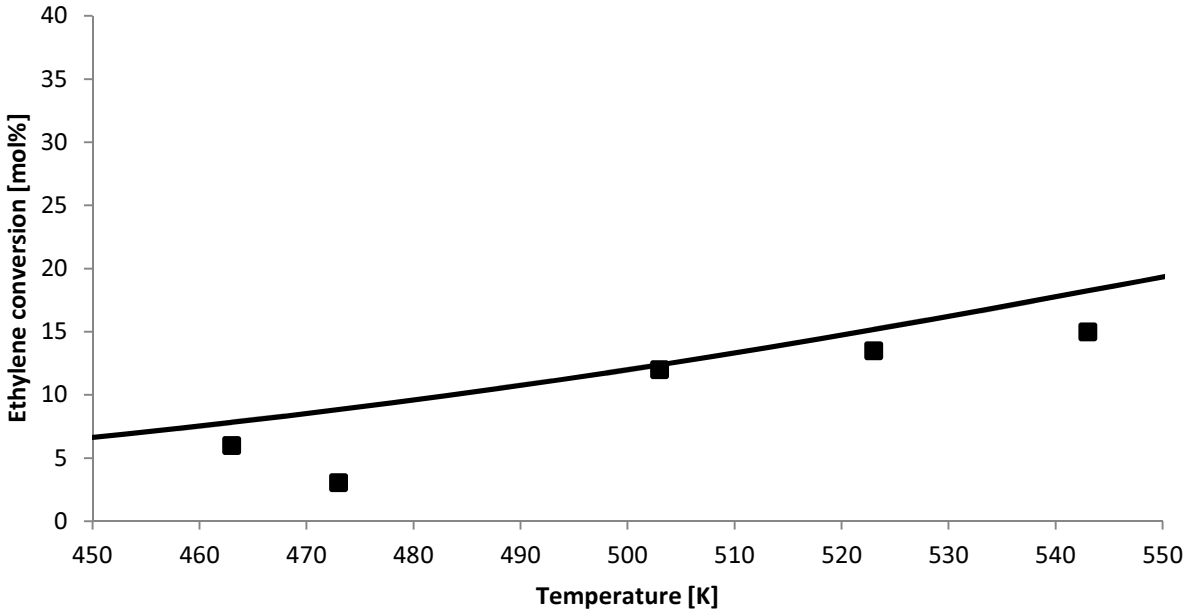

Figure 6-7: Conversion of ethylene oligomerization on 4.89wt%Ni-β as function of space time;(▪): experiments; full line: simulation. Model simulations are obtained with the parameter values as reported in Table 6-4, an ethylene partial pressure of 0.342MPa and a space time of 10 $kg_{cat}s\ mol^{-1}$.

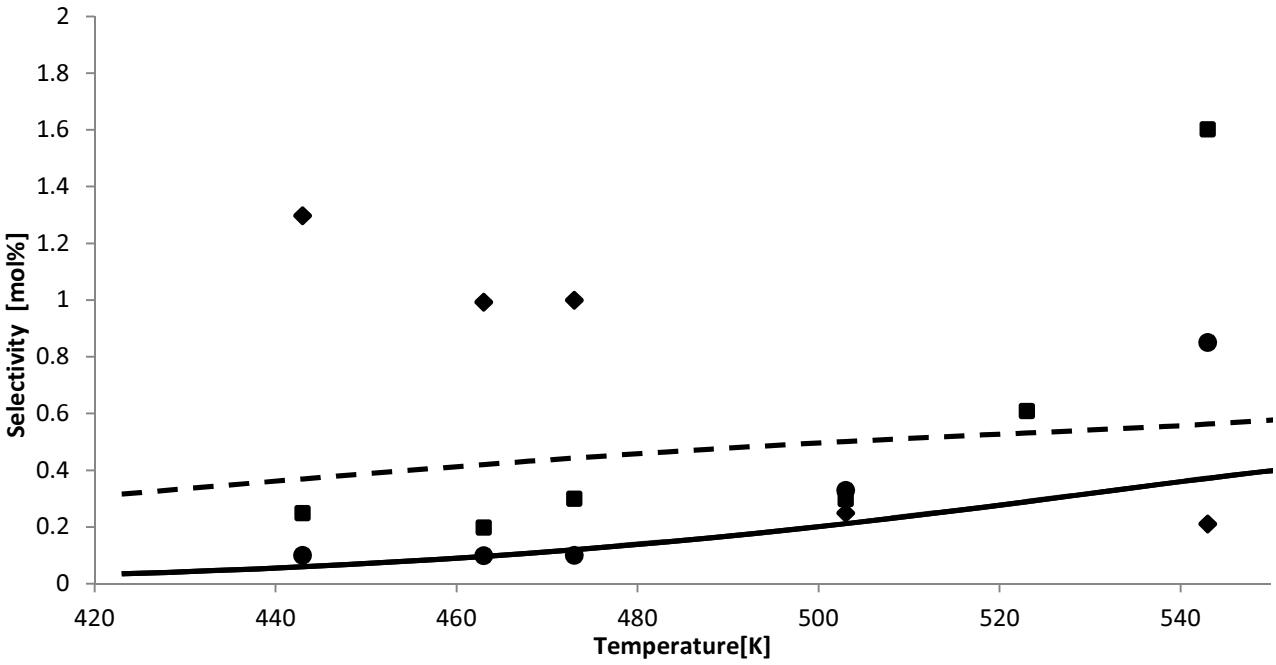

Figure 6-8: Selectivity of ethylene oligomerization on 4.89wt%Ni-β as function of temperature; experiments;(●): propylene; (■): lumped pentene; (◆): lumped octene; full line: simulation of propylene and lumped pentene, dashed line: simulation of octene. Model simulations are obtained with the parameter values as reported in Table 6-4 , an ethylene inlet partial pressure of 0.342MPa and a space time of 10 $kg_{cat}s\ mol^{-1}$.

Finally, the influence of the space time was verified by simulation. Figure 6-9 shows a good agreement between experiments and simulation, both in trend as in absolute conversion value. Concerning the selectivity values, the same trends occurs, i.e., octene is slowly increasing and pentene is decreasing, see Figure 6-10. However, to give an idea about the absolute values, the increase of octene is from 0.2mol% to 0.3mol% over the whole space time range. This shows that the absolute values of octene are very small and strengthen the idea that the absolute values of the cracking products are not high enough to make conclusions.

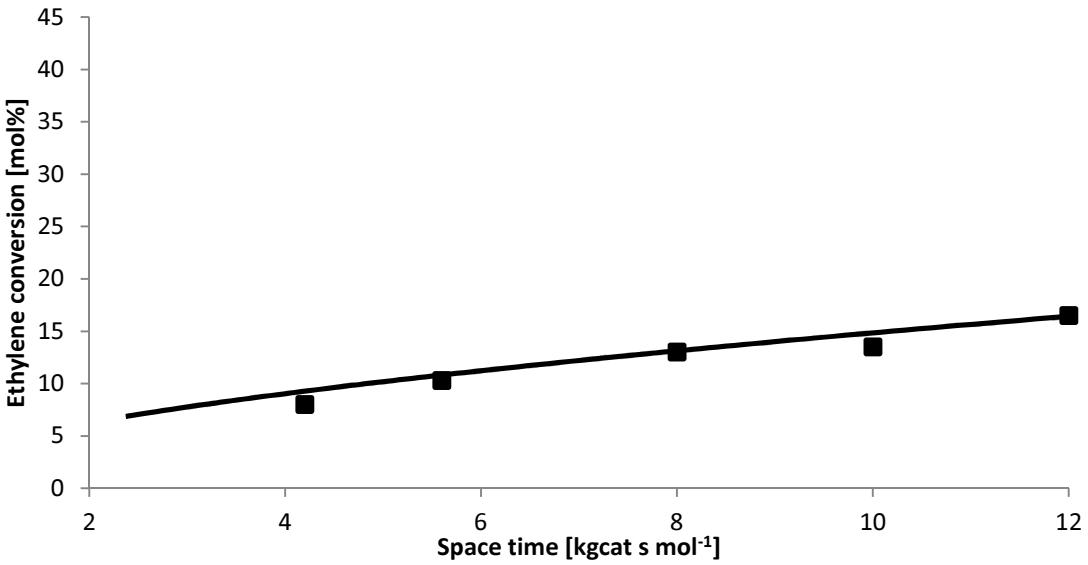

Figure 6-9:Conversion of ethylene oligomerization on 4.89wt%Ni-β as function of space time; (■) experiments; full line: simulation. Model simulations are obtained with the parameter values as reported in Table 6-4, a temperature of 523K and an ethylene inlet partial pressure of 0.342MPa.

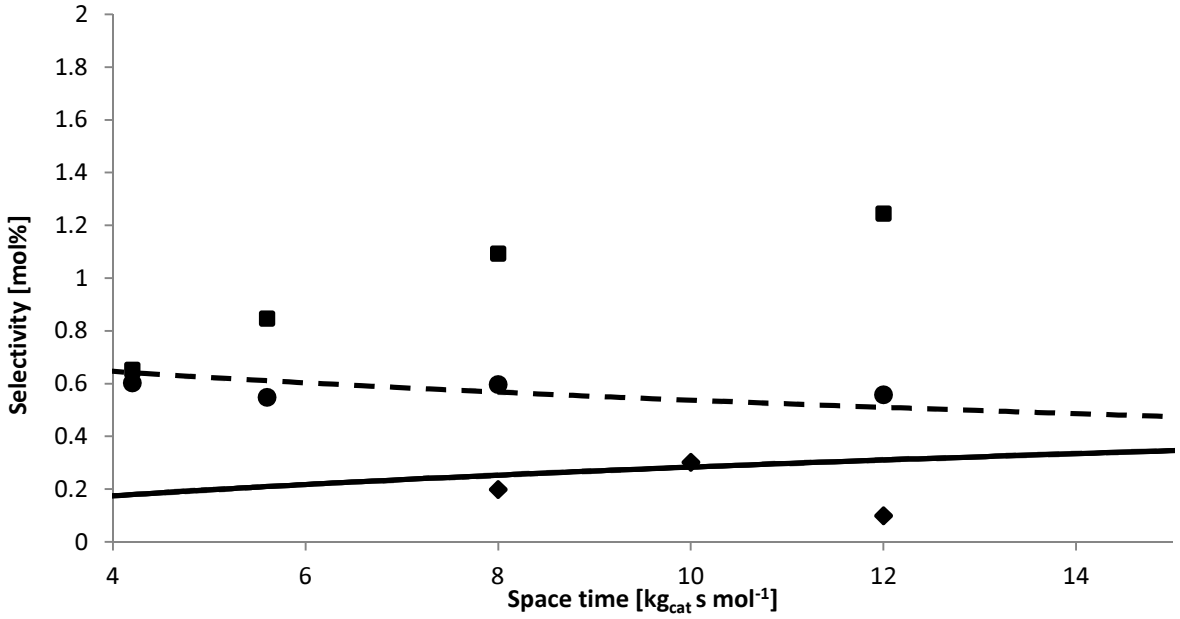

Figure 6-10: Selectivity of ethylene oligomerization on 4.89wt%Ni-β as function of space time; experiments;(●): propylene; (■): lumped pentene; (◆): lumped octene; full line: simulation of propylene and lumped pentene, dashed line: simulation of octene. Model simulations are obtained with the parameter values as reported in Table 6-4, a temperature of 523K and an ethylene inlet partial pressure of 0.342MPa.

6.6 REACTION PATH ANALYSIS

A reaction path analysis is performed to obtain insight in the production route for every compound. At a certain set of reaction conditions, the reaction path was defined by simulation. A schematic representation of this reaction path analysis is given in Figure 6-11. The olefins were grouped based on the carbon chain length and the number of branches. The arrows indicate the reaction path from

one compound to another and their colors correspond with the type of reaction, i.e., metal catalyzed oligomerization, alkylation, β-scission, PCP-branching and 1,2-alkyl shift.

The path starts with the conversion of ethylene through insertion to butene. All the butene that is then further converted will undergo another insertion towards linear hexene. 99.8% of all the hexene that reacts further will lead to linear alpha octene. The other 2% leads to branched hexene by PCP-branching. The linear octene will isomerize towards branched octene molecules, mainly secondary branched, i.e., 43.3%. The moment branched octene molecules are present in the mixture, β-scission can occur towards pentene and propylene. The relative importance of alkylation reactions is considered to be negligible, which is in agreement with the experimental results.

This reaction path shows that the linear olefins are exclusively produced through insertion of ethylene. Whereas, al the derivatives of these linear compounds are produced by carbenium ion chemistry.

On Figure 6-11, only the most important reactions are given. To reduce the complexity of the figure, the 1,2-alkyl shift reactions are not represented. These reactions take place between branched olefins with the same carbon length.

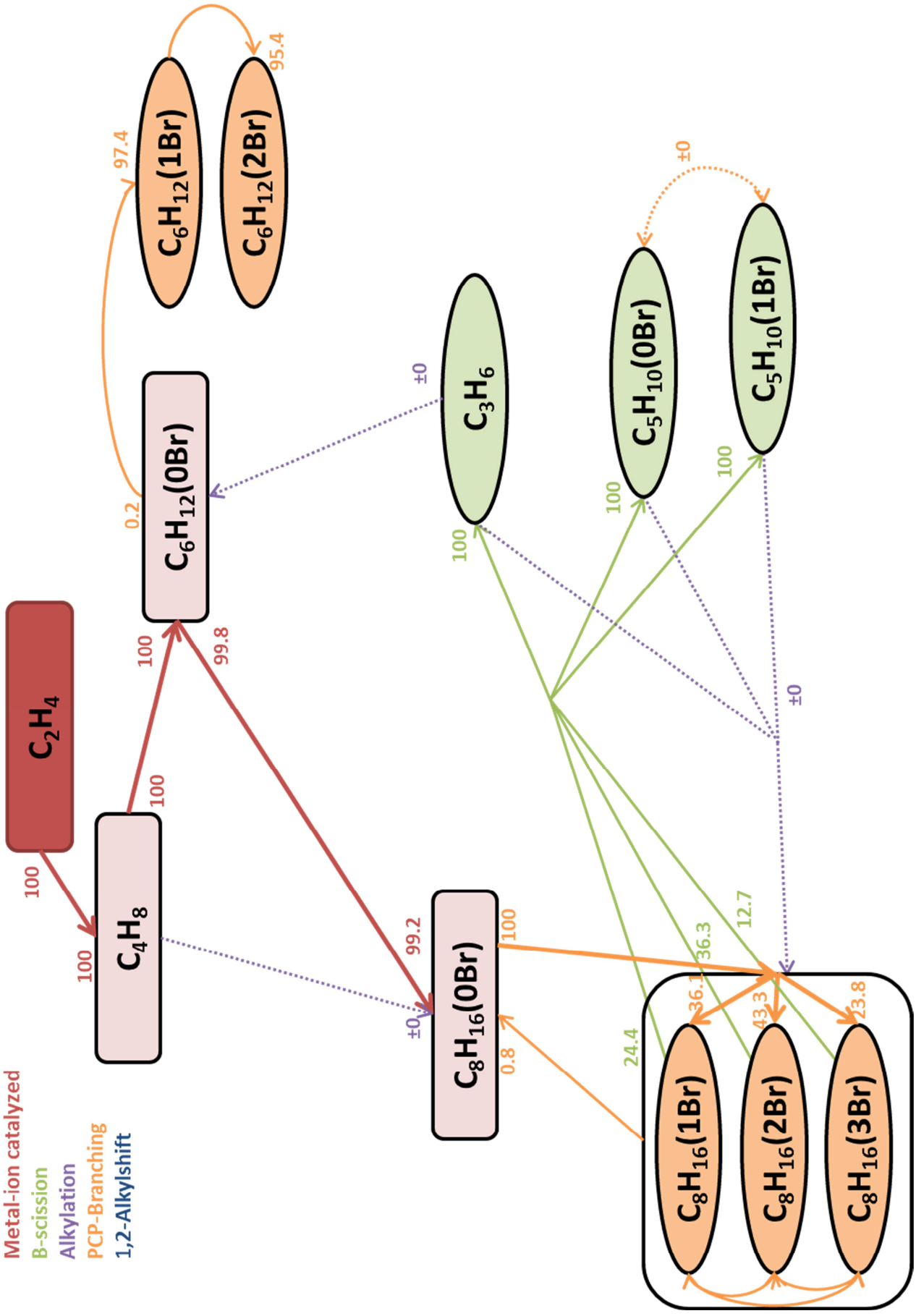

Figure 6-11: Reaction path analysis for a simulation at a temperature of 523K, an inlet partial pressure of ethylene of 0.342MPa and a space time of 10kg_{Cat}s mol^{-1}

6.7 CONCLUSION

In this chapter, the construction of the kinetic model for oligomerization of ethylene was discussed. Attention was put on the acid catalyzed reactions. For the different kind of carbenium ions, i.e., secondary and tertiary, stabilization effects were considered. These stabilization differences were introduced by accounting for differences within each reaction family based on the type of carbenium ions involved.

By using thermodynamic constraints, as discussed in Chapter 5, the number of parameters was successfully reduced. With this model, a regression was performed. More than half of the parameters were kinetic descriptors for which values were already reported in literature. The parameters estimated consisted of the catalyst descriptors, i.e., chemisorption enthalpy of ethylene on nickel ion, the physisorption enthalpies and protonation enthalpies, and some kinetic descriptors related to the acid catalyzed oligomerization. Some extra constraints were introduced to be able to estimate these parameters significantly due to limitations of the experimental dataset. From the regression, all parameters were estimated significantly and were not correlated with each other. In addition, the regression was tested to be significant. The model was able to describe the effect of temperature and space time on conversion and selectivity values satisfactory. However the description of the influence of the partial pressure of ethylene has room for improvement.

Finally, a reaction path analysis was performed to indicate the production routes for the different olefins. The two most pronounced routes were the metal ion kinetics and isomerization.

6.8 REFERENCES

1. Dewachtere, N.V., F. Santaella, and G.F. Froment, *Application of a single-event kinetic model in the simulation of an industrial riser reactor for the catalytic cracking of vacuum gas oil.* Chemical Engineering Science, 1999. **54**(15–16): p. 3653-3660.
2. Marin, G.B., *Chemische reactoren: principes en toepassingen.* Universiteit Gent, 2008.
3. Wilde, W.D., *Oligomerisatie van Ethyleen naar Vloeibare Brandstoffen en Chemicaliën*, in *Laboratory for Chemical Technology*, 2009-2010, University of Ghent. p. 155.
4. Toch, K., J.W. Thybaut, and G.B. Marin, *Ethylene oligomerization on amorphous Ni-SiO2-Al2O3: Experimental Investigation and Single-Event Kinetic Modeling*, 2012: Ghent University.
5. Nguyen, C.M., et al., *Physisorption and Chemisorption of Linear Alkenes in Zeolites: A Combined QM-Pot(MP2//B3LYP:GULP)–Statistical Thermodynamics Study.* The Journal of Physical Chemistry C, 2011. **115**(48): p. 23831-23847.
6. Vandegehuchte, B.D., et al., *n-Hexadecane hydrocracking Single-Event MicroKinetics on Pt/H-beta.* Applied Catalysis A: General, 2012. **441–442**(0): p. 10-20.
7. Toch, K., et al., *A Single-Event Micro Kinetic model for "ethylbenzene dealkylation/xylene isomerization" on Pt/H-ZSM-5 zeolite catalyst.* Applied Catalysis a-General, 2012. **425**: p. 130-144.

8. Fan, L., et al., *Theoretical Study of Ethylene Oligomerization by an Organometallic Nickel Catalyst.* Inorganic Chemistry, 1996. **35**(13): p. 4003-4006.

9. Toch, K., J. W. Thybaut, et al. (2013). Ethylene Oligomerization on Bifunctional Heterogeneous Catalysts: Model Development and Catalyst Optimization. Netherlands' Catalysis and Chemistry Conference (NCCC XIV).

Chapter 7

Conclusion and Future work

A literature review on oligomerization of ethylene was performed. Since ethylene oligomerization was investigated as part of the environmental friendly *OCMOL* process, a bifunctional heterogeneous catalyst was considered. The influences of the reaction conditions and the catalyst properties on the product distribution were discussed. A distinction was made between the conditions for production of diesel range and gasoline range products. Since zeolites are indicated as the most interesting acid carriers for oligomerization, some zeolite frameworks were discussed to conclude the literature review.

To obtain an insight in the reaction mechanism of oligomerization on a bifunctional catalyst, an experimental study is performed on the High-Throughput setup (HTK-1). The tested catalyst is a Ni-β catalyst. This catalyst consists of 4.89wt% Ni and a limited concentration of strong acid sites. These strong acid sites are responsible for the cracking behavior of the catalyst. During experiments, products containing up to 8 carbon atoms were produced. By insertion on the nickel ion complex, linear alpha-olefins were produced with a high selectivity towards butene. Once these linear olefins are generated, secondary reactions can occur through an acid site. Alkylation, i.e., acid catalyzed oligomerization, 1,2-alkyl shift, PCP-branching and β-scission were considered. These reactions led to a broad range of products, i.e., propylene, pentene and structural isomers of the lineair olefins. However, the selectivity towards these 'acid' products is very limited. The overall activity of the Ni-β catalyst can be considered rather low, i.e., in comparison with the reference catalyst 1.8wt%Ni-SiO_2-Al_2O_3. Additionally, the deactivation rate of the catalyst was high. In literature, the *'high'* acid concentration, together with the high nickel loading, is stated to be a reason why quick deactivation and low conversion is measured. Since the β-zeolite was loaded with a very high concentration of

nickel, no fine dispersion was obtained. As a result, NiO was found on the catalyst blocking the acid sites of the catalyst, which led to the low ethylene conversion.

By using the Single-Event MicroKinetic methodology (SEMK), the kinetic model of ethylene oligomerization was succesfully expanded. A preliminairy kinetic model describing the metal catalyzed reactions was available. To be able to describe the experimental observations, the acid catalyzed reactions were implemented. Since the ease of protonation is dependent of the type of carbenium ion formed, this will have its influence on the reaction rate and this is accounted for in the model. By using thermodynamic constraints, a reduction of the number of parameters that had to be estimated was succesfully executed. Taking into account the reverse reaction of the alkylation, i.e., the β-scission reaction, and determining the Born-haber cycle of this reaction system, the correlation between both reactions was determined.

With this expanded kinetic model and the obtained experimental dataset, a regression was performed. In this case, a good set of initial values was necessary, since a large number of estimated parameters was present in the model in comparison with the available experimental points. Some of these values were obtained from literature. With these values fixed, a regression was performed to obtain values for both kinetic, i.e., describing the β-scission, and catalytic descriptors, i.e., ΔH_{chem}, $\Delta H_{phys,}$ $\Delta\Delta H_{phys}$, $\Delta H_{pr}(s)$. However, since the low yield of cracked products, e.g., propylene, together with the limited number of experiments, the regression was rather difficult to perform. The results indicate the high affinity of the molecules to chemisorb on the nickel ions. Whereas, a very low $\Delta H_{pr}(s)$ shows the difficulties for protonation.

Some simulations were performed that indicated the good performance of the model. Concerning the pressure effect, there is still some room for improvement. Finally a reaction path analysis was done. By doing so, the significant paths to the different products were determined to be metal ion catalyzed oligomerization and isomerization.

Further investigation into the acidic behavior for oligomerization of ethylene should be done by performing experiments with a more active catalyst. In literature, the Ni-AlMCM-41 catalyst is suggested to be a very active and stable catalyst for the oligomerization of ethylene. Mainly the influence of the carbenium reactions should be more pronounced on this catalyst. The information, obtained from these experiments, can be used to estimate the acidic parameters more significant. This will lead to more accurate simulations and even optimization of the catalyst properties and reaction conditions.

Appendix A: Gas chromatograph method

Before any experiments could be analyzed, a proper GC-method had to be defined. This was done experimentally. Some aspects that had to be assured during analysis:

- Separation of the ethylene and methane peak, i.e., the internal standard
- Separation of the different isomers of butylene
- Detection of all the compounds. Assuring that the GC has time enough to elute all the products of the gas mixture. For example, the longer molecules will take a longer time to elute through the column

To obtain this proper method, several parameters could be varied:

- Analysis temperature and temperature program, i.e. rate of temperature increase during analysis
- The inlet flow of the mixture
- The dilution with nitrogen
- The split ratio of total inlet flow: ratio of helium inlet on gas inlet
- Initial flow

A proper method varies on the type of column that is used. In the first experiments, a small column was used and therefore another method had to be defined.

Table A-1 represents the properties of the second capillary column.

Table A-1: Property of the GC-column DB-1

Property	Value
Length [m]	30
Inside diameter [mm]	0.25
Film thickness [µm]	0.25

Table A-2: Oven Temperature program

Level	Rate [°C min^{-1}]	Next Temperature [°C]	Hold time [min]	Run time [min]
1	-	30	25	25
2	10	250	4	51

Table A-3: Zone temperatures

Zone	Set point [°C]
Inlet	275
Detector	325
Aux1	200

The determined oven temperature program is given in Table A-2, and the zone temperatures within the GC are given in Table A-3. Additionally, also an inlet split ratio of 60:1 was used and the inlet flow rate was 1.5ml min^{-1}.

Appendix B: Experimental dataset

Table B-1:Reaction conditions

Exp	Flow $C_{2,in}$	Flow $N_{2,in}$	T	P	W	τ
	[µmol s^{-1}]	[µmol s^{-1}]	[K]	[MPa]	[g]	[kg_{cat}s mol^{-1}]
1	50.000	385.965	473	3.000	0.510	10
2	49.974	385.658	523	3.500	0.520	10
3	49.974	385.658	523	2.500	0.510	10
4	49.974	385.658	523	2.000	0.510	10
5	49.974	385.658	523	1.500	0.530	10
6	49.974	385.658	443	3.000	0.520	10
7	119.120	919.520	463	3.000	0.520	4.2
8	89.284	689.471	523	3.000	0.520	5.6
9	62.499	482.382	523	3.000	0.530	8
10	41.692	321.832	523	3.000	0.530	12
11	49.974	385.658	503	3.000	0.510	10
12	49.974	385.658	543	3.000	0.510	10
13	49.97	385.658	463	3.000	0.540	10
14	119.120	919.520	483	3.000	0.510	4.2
15	49.974	385.658	473	2.500	0.510	10

Table B-2 Results experimental study

Exp	FlowC2,out [µmol s^{-1}]	FlowC3,out [µmol s^{-1}]	FlowC4,out [µmol s^{-1}]	FlowC5,out [µmol s^{-1}]	FlowC6,out [µmol s^{-1}]	FlowC7,out [µmol s^{-1}]	FlowC8,out [µmol s^{-1}]
1	48.475	0.001	0.709	0.002	0.028	0.000	0.004
2	43.028	0.017	3.114	0.022	0.207	0.000	0.004
3	43.727	0.027	2.750	0.035	0.202	0.000	0.003
4	44.477	0.029	2.406	0.043	0.172	0.000	0.004
5	45.477	0.030	2.004	0.045	0.105	0.000	0.004
6	47.076	0.002	1.313	0.003	0.075	0.000	0.009
7	114.355	0.000	2.168	0.000	0.143	0.000	0.000
8	80.088	0.034	4.030	0.031	0.336	0.000	0.000
9	54.374	0.032	3.574	0.036	0.275	0.000	0.004
10	34.813	0.026	3.042	0.034	0.222	0.000	0.002
11	43.977	0.013	2.679	0.007	0.195	0.000	0.004
12	42.478	0.043	3.273	0.048	0.250	0.000	0.004
13	46.976	0.002	1.242	0.002	0.159	0.000	0.007
14	109.590	0.038	4.164	0.025	0.351	0.000	0.007
15	46.351	0.002	1.574	0.001	0.156	0.000	0.000

Appendix C: XRD results

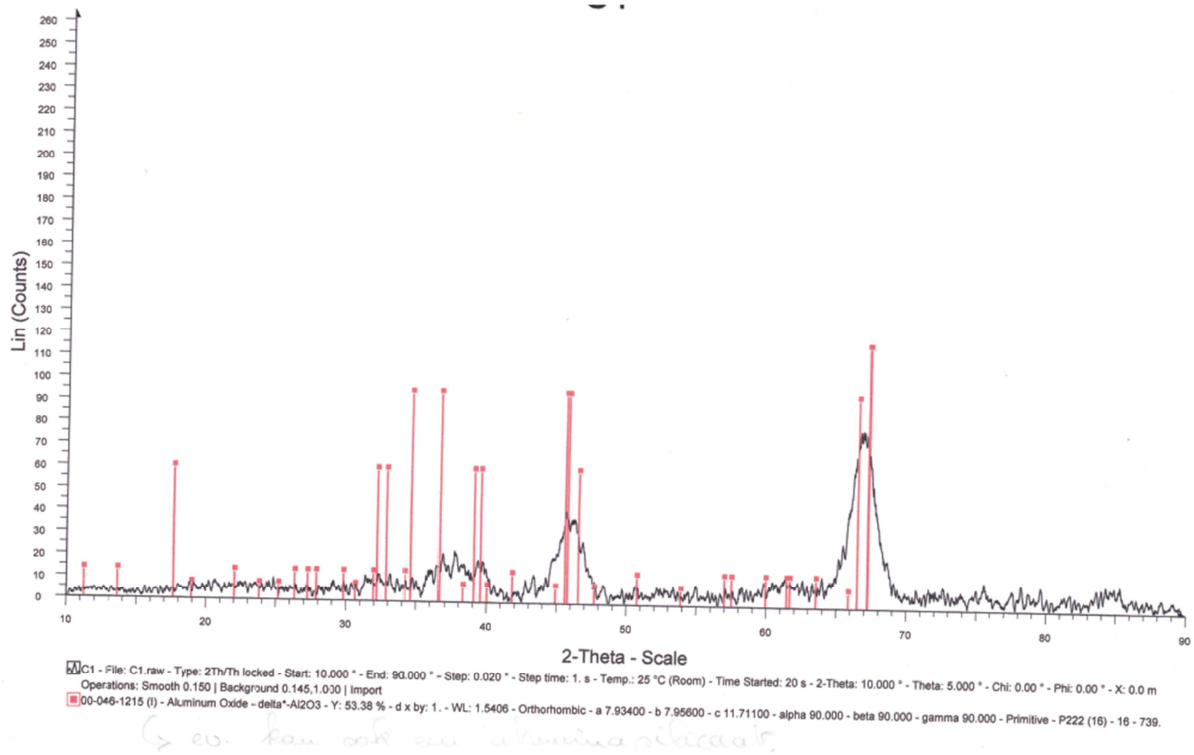

Figure C-1: XRD result of reference catalyst, i.e., 1.8wt%Ni-SiO_2-Al_2O_3

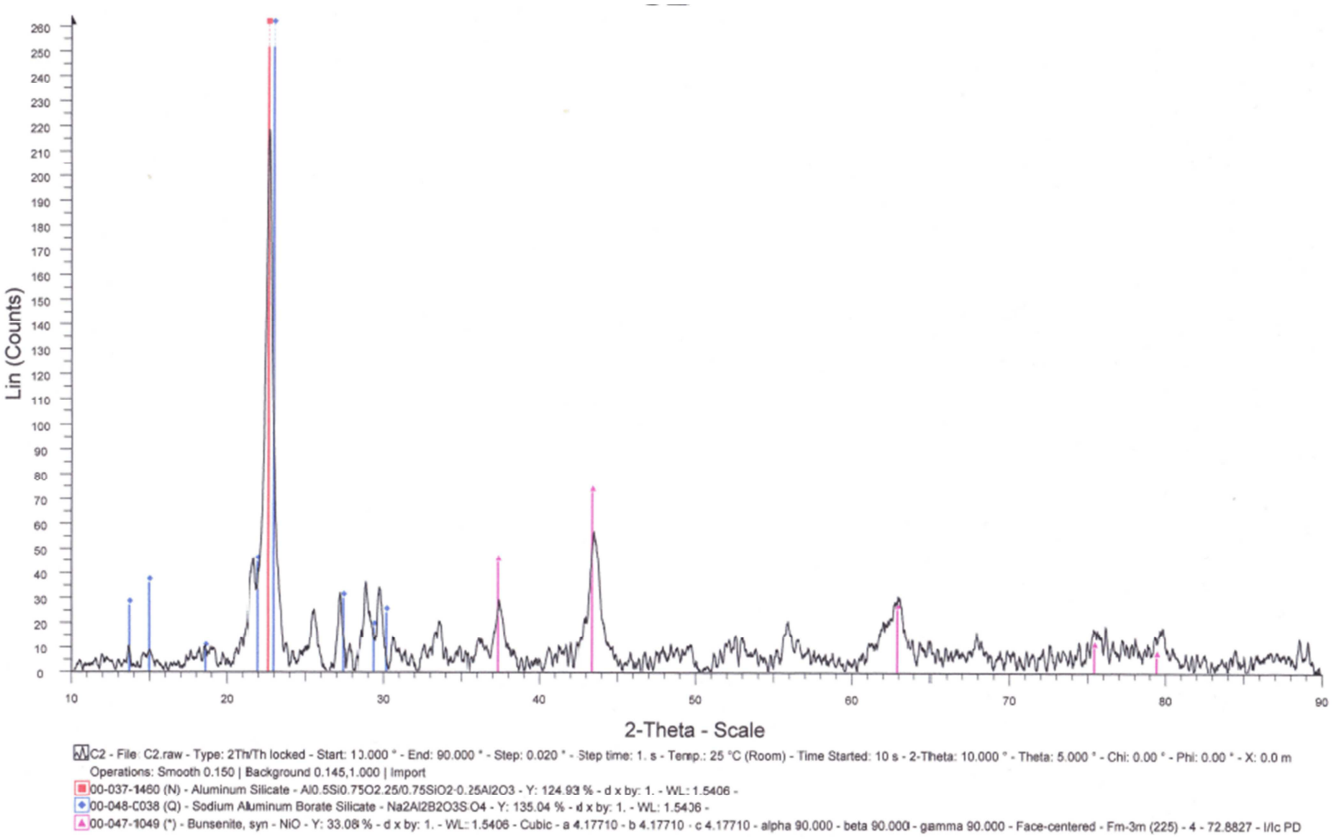

Figure C-2: XRD result of 4.98wt%Ni-β

Appendix D: Lab journal

Summary of the aspects discussed in the labjournal in order of appearance:

1. Notes concerning kinetic model
2. Design alkylation- β scission for adaptation kinetic model
3. Experimental startup
4. Determining GC-method
5. Experiments 1-9
6. Summary first experiments
7. Experiments 10-16
8. Setup Isotherm kinetic model
9. Experiments 17-25
10. Problems GC
11. Model: Implementation correlation entropy
12. Values alkylation- β-scission
13. Determining new GC-method
14. Results obtained during simulation
15. Reaction path analysis
16. Summary CD-rom

List of Figures

List of Tables